NASA CONTRACTOR REPORT

NASA CR-863

NASA CR-863

PROPAGATION OF MILLIMETER AND SUBMILLIMETER WAVES

by V. E. Derr

Prepared by
MARTIN MARIETTA CORPORATION
Orlando, Fla.
for Electronics Research Center

NATIONAL AERONAUTICS AND SPACE ADMINISTRATION • WASHINGTON, D. C. • AUGUST 1967

NASA CR-863

PROPAGATION OF MILLIMETER AND SUBMILLIMETER WAVES

By V. E. Derr

Issued by Originator as OR 8549

Prepared under Contract No. NAS 12-10 by
MARTIN MARIETTA CORPORATION
Orlando, Fla.

for Electronics Research Center

NATIONAL AERONAUTICS AND SPACE ADMINISTRATION

For sale by the Clearinghouse for Federal Scientific and Technical Information
Springfield, Virginia 22151 – CFSTI price $3.00

FOREWORD

The work described in this report was performed under the sponsorship of the National Aeronautics and Space Administration, Electronic Research Center, Cambridge, Massachusetts, under Contract NAS 12-10.

The work was performed at the Orlando Division of the Martin Marietta Corporation. From June 17, 1965 to August 12, 1966, the task was under the management of Dr. A. Ryan in the Physical Sciences Laboratory and from August 12, 1966, to October 16, 1966, under the management of W. Birge in the Electromagnetics Laboratory.

Personnel engaged in the major phases of the work were:

Dr. V. E. Derr, Task Leader
Dr. L. Frenkel*, Principal Investigator
M. Lichtenstein
D. Woods
G. T. McNice
E. Kelly
W. T. Smith
L. Boone

Mr. J. J. Gallagher gave valuable counseling and Miss F. Zlotshewer performed most of the manual calculations. Mr. F. Phillips and Mr. J. Borbely performed computer programming.

*Until May 27, 1966. Present address: NASA-ERC, 575 Technology Square, Cambridge, Massachusetts.

CONTENTS

Appendixes

ILLUSTRATIONS

TABLES

SUMMARY

The problems of communication in space and through planetary atmospheres, and the problem of electromagnetic exploration of the solar system and the cosmos require a knowledge of the spectral excitation, and absorption properties of the planetary atmospheres and the gases in the cosmos. The work under this program has begun the study of these properties with first attention to absorption measurements by coherent radiation methods. In this report, after an introduction to elementary line broadening theory, the instrumentation development for absorption measurements is discussed. Calculations and a search for O_2 submillimeter transitions are described in the next section. Spectroscopic investigations of the Stark effect in water have been used to confirm level assignment and to determine a new value of the dipole moment of water by a more accurate dc voltage method. D_2O, a chemical analog of water has been observed near 300 GHz. One of the major efforts has been to provide a better understanding of relaxation processes. A discussion of orientation relaxation theory is presented, as well as a consideration of quadrupole interaction in CO_2. A computer program that is suitable for computation of low J value transitions in asymmetric top molecules has been developed for the Kivelson-Wilson theory of centrifugal effects. Based on all available data from 100 to 1000 GHz, the absorption spectrum of water is computed by two methods with different form factors, in order to present a comparison.

I. INTRODUCTION

Under two consecutive contracts* the propagation of millimeter and submillimeter waves has been studied in those gases which are important absorbers of electromagnetic radiation in the earth's atmosphere. The overall objective of the program was, by experiment and theory, to determine the absorption by these gases in the 100 GHz to 1000 GHz frequency range, and by determination of the parameters, to allow the computation of the absorption due to water vapor, oxygen, or air. The program has been carried out so as to obtain the utmost generality, in order to be able to apply the results to the computation of absorptions of other gases when the necessary line locations and widths become available either through experiment or computation. In addition, an investigation of all current theories applicable to line broadening in the microwave and far infrared regions has resulted in the detailed consideration of two theories, those of Van Vleck-Weisskopf (Reference 2) and Zhevakin-Naumov (Reference 3). These theories are similar except for different line shapes. For low pressures these theories differ negligibly at the line peaks, but for low frequencies and even at atmospheric pressure, the theories may differ in the valleys. The comparison of these theories is presented under Conclusions, section IX.

As shown in section IV the oxygen molecule is a negligible absorber compared with water, everywhere except the many lines clustered around 56 GHz and the single line at 118 GHz. The other lines, near 400 GHz and 800 GHz, are of the same order of magnitude as the valleys in the water absorption. For this reason the principal effort in this task has been to put the theory of the broadening of the water molecule on a secure footing and to compare it with all known experimental facts, including those obtained in the literature and under this task.

The success of the task depends upon what use is made of the results. If a system design above 600 GHz had no margin for error in the absorption coefficient because of lack of power, the results could not be guaranteed. It is probable, given the consistency between theory and data becoming apparent from recent studies, that for fairly wide pressure ranges

*NASw-963 (July 1964-July 1965) and NAS 12-10 (July 1965-November 1966).

around the atmospheric there is probably no more than 15 percent to 20 percent error in the absorption curves. The effects of temperature are not as well understood and the data is estimated to be in good agreement only within 25 percent of T = 293°K.

Although it was not possible to obtain detailed data in the higher frequency range, the use of all available data has given a consistent picture for water. The energy level calculations under this task, the more accurate ones by Clough and Benedict* using a method of diagonalizing the whole secular equation, the theoretical studies of Benedict and Kaplan (Reference 4) on linewidth as a function of temperature and pressure, the data on linewidth, the accurate measurement of spectral line position and positive identification by Stark effects, the data obtained from lower resolution Michelson-Fourier spectrometer runs throughout the whole region, and the indirect data obtained from Gebbie's solar studies (Reference 5) have been welded together in this report to give a consistent picture of water from 100 GHz to 1000 GHz. In addition, the data and formulas have been presented in such a way as to enable the revision of the calculations whenever additional data is obtained or the theory of the linewidth parameter dependence on pressure and temperature becomes more precise. Curves are presented for a variety of conditions to allow the system designer daring to think in terms of this region, to find quick answers and if these do not cover the situation, to consult the formulas.

The report consists of a theoretical introduction, a description of experimental methods, and several sections dealing with the theory of the H_2O and O_2 molecules and the data obtained for each. Pertinent spectroscopic investigations are described and contributions to linewidth theory and symmetric top molecule theory are followed by a final compilation of data on water.

*S. A. Clough, Private Communication.

II. THEORY OF LINE BROADENING AT MILLIMETER WAVELENGTHS

It is not possible to review completely the theory of line broadening in this report, even if only millimeter spectra are considered. However, the theory is a framework on which our measurements are based and it is desirable to have a brief review in order to clarify the formulas used here. Of particular interest are the assumptions under which the theory is developed, and the limitations of applicability of the theory. The theory here developed is not able to stand the closest scrutiny, but is adequate in view of the accuracy desired in this study. More detailed studies of broadening would be very desirable from the point of view of molecular interaction studies, but would require greater accuracy than obtained in this task for experimental confirmation.

The most important gases of the earth's atmosphere in their effect on millimeter waves are water vapor and oxygen since these possess relatively large dipole moments. Other gases such as CO, NO, NO_2, and N_2O have some weak absorption lines in the millimeter region. Gases such as N_2 and CO_2 are nonpolar, having no permanent dipole moment, but their induced moments on collision can allow absorption which is only considerable at high pressures. The dipole moments of the gases are:

Gas		Dipole moment (μ)
H_2O		1.88 debye
O_2		1.854×10^{-20} erg/gauss
CO, NO, NO_2, N_2O	$\approx$	0.1 debye.

Further, the concentrations of the latter group of gases are less than 0.0001 percent in volume, hence make very little contribution to the absorption; thus for communication purposes, only water vapor and oxygen are significant.

In this section, after brief attention to natural, Doppler and saturation linewidths, the Lorentz-Van Vleck-Weisskopf theory and the Zhevakin and Naumov theory are reviewed, and the formulas adopted for use in this study are stated.

The natural linewidth of an absorption or emission line is related classically to the finite length of the wave train and the gradual decrease of the amplitude of the oscillator. Quantum mechanically natural linewidth is often described as a consequence of the Heisenberg uncertainty principle, $\Delta E \Delta t \geqq \hbar$ or $\Delta\omega\Delta t \geqq 1$. This relation means that, if a time of measurement Δt is available, the frequency can be measured at best with an accuracy $\Delta\omega$. The natural line shape and linewidth can also be attributed to the declining probability of initial atomic state. The expressions for the natural line shape can be derived from quantum mechanical radiation theory. According to Heitler (Reference 6) the absorption coefficient for a line in an unperturbed molecule is

$$\alpha(\omega) = N W_{ab} \frac{\pi^2 c^2}{\omega_o^2} \frac{\gamma}{2\pi} \frac{1}{(\omega-\omega_o)^2 + \gamma^2/4} .$$

Here N = number of atoms per cm^3 in absorbing state a

W_{ab} = transition probability for spontaneous emission b

ω = angular frequency, radians per second

γ = linewidth at half intensity

In this theory it is shown that γ, the linewidth, is just equal to W_{ab}, the total spontaneous transition probability per unit time. This transition probability is

$$W_{ab} = \frac{32\pi^3 e^2 \nu^3}{3hc^3} |< a | r | b >|^2$$

or

$$W_{ab} = \frac{32 \pi^3 \nu^3}{3hc^3} | \mu |^2$$

where $\mu = e < a \mid r \mid b >$ is the matrix element of the transition. Natural widths are thus much less than one Hz for frequencies in the range 10^{12} Hz $> \nu > 10^{11}$ Hz. Even thermal fields, stronger than the zero point field for room temperatures and frequencies, give a negligible width in comparison with that caused by other types of broadening, of the order of 10^{-5} Hz.

Likewise, although larger than the natural linewidth, the broadening due to the Doppler effect is small compared with pressure broadening, since the half width at half maximum is

$$\Delta\nu = 3.58 \times 10^{-7} \sqrt{\frac{T}{M}}\, \nu$$

where T = absolute temperature

M = molecular weight.

Then for room temperature and a molecular weight near thirty, $\Delta\nu/\nu \approx 10^{-6}$. Thus, for ν in the range $10^{11} < \nu < 10^{12}$, $10^5 < \Delta\nu < 10^6$. That is, in the range of interest in this report the half-width is less than 1 MHz.

Saturation broadening is generally of no importance in the frequency region of interest. In order to be significant the power generally must be higher than 1 mW/cm^2 (Reference 7) at pressures sufficiently low to produce linewidths less than 1 MHz. Saturation effects could be helpful for some communication problems if sufficiently high powers could be produced, since the effect of saturation is to decrease the absorption at all frequencies.

The principal absorption process for this report is absorption by uncooperating molecules, whose absorption linewidth is determined by collisions. Of the several approaches to this problem, interruption broadening is most applicable to the range of pressures, temperatures and frequencies under consideration. The principal applicable theories are by Lorentz, by Van Vleck and Weisskopf (Reference 2) and by Zhevakin and Naumov (Reference 3). We will review these theories and then indicate by a discussion of the data available which is the most reliable.

In their fundamental paper Van Vleck and Weisskopf determine the absorption coefficient for a single line to be

$$\alpha = \frac{8\pi^3 \nu N}{3hc} \mid \mu_{ij} \mid^2 \frac{\left| e^{-E_i/kT} - e^{-E_j/kT} \right|}{G} S(\nu, \nu_{ij}, \Delta\nu)$$

where ν = the frequency of the incident radiation

N = number of molecules per cubic centimeter

h = Planck's constant, erg-s

c = velocity of light, $cm\text{-}s^{-1}$

$|\mu_{ij}|^2$ = dipole moment of the transition (see section VIII)

E_i = energy of the molecular state i

T = absolute temperature

k = Boltzmann constant

$$\left[G = \sum_{j=o}^{\infty} \sum_{\tau=-J}^{J} \left[2 - (-1)^{|\tau|} \right] (2J + 1)\, e^{-E(J,\tau)/kT} \right]$$

where J, τ are the state designations of the rotational states, $E(J,\tau)$ are the same as E_i, with the state designations given specifically. This formula is derivable from the Einstein transition coefficients and hence must be universal. The problems arise however in the choice of the "shape factor" $S(\nu, \nu_{ij}, \Delta\nu)$ (where $\Delta\nu$ is the linewidth), and in the dependence of $\Delta\nu$ on pressure, temperature and composition.

The development of line width theory is well documented. However, it is useful to give a derivation of the formula for the absorption coefficient in order to note the fundamental factors which enter into it and to obtain a complete theory without some of the approximations indulged in by some writers. These approximations are normally accurate in the microwave range, but for frequencies in this report which range into the far infrared, it is necessary to present a theory as free of approximations as possible. This derivation will be partly quantum mechanical, correct to first order, but the line shape, dependent on a theory of collision broadening, will be obtained from either Van Vleck and Weisskopf or from Zhevakin and Naumov.

We consider a gas, N molecules per cc, traversed by radiation whose energy density at transition frequency ν_{nm} is $\rho(\nu_{nm})$, assumed for the moment to be isotropic. (If $E^2(\nu)$ is the average value of the square of

the electric field strength, $\rho(\nu) = 1/4\ \pi\ \ E^2(\nu)$ and $E^2(\nu) = E_x{}^2(\nu) + E_y{}^2(\nu) + E_z{}^2(\nu)$. Then the probability of a transition of a system originally in state n, to state m (Reference 8) is

$$\frac{8\ \pi^3}{3h^2} \qquad |(n\ |\ P\ |m)\ |^2 \quad \rho\ (\nu_{nm}) \tag{1}$$

where P is the dipole moment operator of the molecule. In this derivation no assumption was made nor required as to whether n or m was the state of higher energy. Thus the probability of induced emission and absorption are equal. It is here assumed that the probability of spontaneous emission for the frequencies and power levels is negligible. There may be situations where the effect of spontaneous emission is of comparative importance. The ratio (R) of spontaneous to induced emission is

$$\frac{N_m\ A_{m \to n}}{N_m\ B_{m \to n} \rho} = R$$

where N_m is the number of systems in m^{th} state, A, B are the Einstein coefficients. Then

$$R = \frac{8\ \pi h \nu^3_{mn}}{c^3 \rho} = \frac{2 \times 10^{-10}}{I}$$

for $\nu_{mn} = 10^{12}$ Hz, where I is the intensity (ergs per second) through an area of one square centimeter. Thus for $R = 1$, $I = 2 \times 10^{-10}$ erg/s or 2×10^{-3} watts. These power levels may occur. Since spontaneous emission is not coherent, it represents a loss mechanism. However, in this report we confine ourselves to absorption and collision processes.

Returning to expression (1) we write

$$\frac{8\ \pi^3}{3h^2} h\nu_{nm}\ N(n) - N(m)\ |(n\ |\ P\ |\ m)|^2\ \rho(\nu_{nm})$$

as the net number of transitions per second per cm^3 and finally,

$$\text{Net energy absorbed per } cm^3 \text{ at frequency } \nu_{nm} = \frac{8\ \pi^3}{3h^2} h\nu_{nm} \left[N(n) - n(m)\right] |(n|P|m)|^2\ \rho(\nu_{nm})$$

where N(n) = number of systems per cm^3 in state n. Since the transitions occur over a range of frequencies, (that is over the line shape) and since the lines are not perfectly narrow (due to collisions, ignoring natural width) this expression must be multiplied by a shape factor $S(\nu_{ij}, \nu, \Delta\nu_{ij})$. The shape factor will not be derived here, but can be found in the literature. The absorption coefficient is defined as $\alpha = 1/I\ dI/dx$ where I denotes the power (per cm^2) carried by the radiation, and dP/dx its rate of loss with distance. But $I = c\rho$ and $c = dx/dt$ is the velocity of the radiation, hence

$$\alpha = \frac{1}{c\rho}\frac{d\rho}{dt} = \frac{8\pi^3}{3hc}\ \nu\left[N(n) - N(m)\right]\ |(n|P|m)|^2\ S(\nu_{ij}, \nu, \Delta\nu).$$

The factor 3 in the denominator is retained from the assumption of isotropic radiation and should be removed for a plane wave. However it returns when one averages over all orientations of the atom with respect to radiation propagation vector, since $\overline{\cos^2\theta} = 1/3$.

The factor (N(n) - N(m)) is the excess of atoms in the lower level over those in the upper level per cm^3. We may assume thermal equilibrium and determine

$$N(i) = \frac{N\ g_i e^{-E_i/kT}}{G}$$

where N is the total number of systems per cm^3 and g_i is the total degeneracy of the i^{th} level whose energy is E_i. G is the partition function

$$G = \sum_{J=0}^{\infty}\ \sum_{\tau=-J}^{J}\left[2 - (-1)^{|\tau|}\right]\ (2J+1)\ e^{-E(J,\tau)/kT}.$$

The notation here and hereafter is the notation of the asymmetric top molecule (Reference 7); J and τ are the numbers designating the states. The degeneracy g must include both the Zeeman degeneracy and the nuclear degeneracy. The nuclear degeneracy arises from the nuclear spins of the protons in the water molecule and is either 3 or 1 as τ is respectively odd or even. This degeneracy must also appear in determining N(i), i.e.,

$$N(i) = \frac{N\left[2 - (-1)^{|\tau|}\right]\ (2J+1)e^{-E(J,\tau)/kT}}{G}.$$

However, in the computation of the effect of the Zeeman components of a level, line strength $S_{NM} = \sum_{n,m} |(n|P|m)|^2$ is often used; the factor (2J+1) is not used in the expression for N(i).

Thus far we have only considered the components of a line, However, since $S(\nu, \nu_{ij}, \Delta\nu_{ij})$ is a bell-shaped curve, the effects of absorption may, under the right conditions, extend far from the line center, hence it is necessary to sum over all transitions when determining the effective absorptions. It is customary also to put the results into units of decibels/kilometer (dB/km) by multiplying by $10^6 \log_{10} e$. With these changes, the absorption is

$$\alpha = 10^6 \log_{10} e \sum \frac{8\pi^3 \nu N}{3hc\, G} \left[\begin{Bmatrix} 3 \\ 1 \end{Bmatrix} e^{-E_\ell/kT} - \begin{Bmatrix} 1 \\ 3 \end{Bmatrix} e^{-E_u/kT} \right] |\mu|^2 S_{\ell u} S(\nu_{\ell u}, \nu, \Delta\nu_{\ell u}),$$

where $S_{\ell u}$ is the line strength connecting the lower and upper level, μ = permanent dipole moment of the molecule, and the summation is over all transitions in or sufficiently near the frequency of interest to contribute.

Because Lorentz' formulas did not fit the Debye theory at low frequencies, Van Vleck and Weisskopf justly critized his treatment; they substituted a line shape of the form

$$S(\nu_{ij}, \nu, \Delta\nu_{ij}) = \frac{\nu}{\pi \nu_{ij}} \left[\frac{\Delta\nu}{(\nu_{ij} - \nu)^2 + \Delta\nu^2} + \frac{\Delta\nu}{(\nu_{ij} + \nu)^2 + \Delta\nu^2} \right],$$

where ν_{ij} is the resonent frequency and $\Delta\nu$ is the half width of half height. This shape factor was derived under the assumption of "strong collisions". Strong collisions may be defined as those in which the impact is sufficiently strong so that no "memory" remains of the orientation or distribution after collisions. An additional assumption was that after collisions the electrons of the molecules were distributed in position and velocity according to the Boltzmann law rather than at random.

However, these assumptions, made for mathematical convenience, are surely not completely correct and it is possible to replace the assumption of Boltzmann distribution by a distribution function for the optical electron under collisions and an external sinusoidal magnetic field (Reference 9). This method has the advantage that it replaces an assumed distribution by a calculated one. Over a wide range of assumptions on the masses of the oscillator and molecular particles, both in quantum and classical theory, the same form of spectral line shape is obtained. Under the assumption that the time of collision is shorter than the period of the external field, the line shape (Reference 3) is

$$S(\nu, \nu_{ij}, \Delta\nu) = \frac{\nu \nu_{ij}}{\pi} \frac{4\Delta\nu}{(\nu_{ij}^2 - \nu^2)^2 + 4\nu^2(\Delta\nu)^2}$$

Thus, using the general form of the equation above we obtain (temporarily omitting the summation)

$$\alpha = 10^6 \log_{10} e \frac{8\pi^3 \nu N}{3hc} |\mu|^2 \frac{\left| e^{-E_\ell/kT} - e^{-E_u/kT} \right|}{G} \cdot \frac{S_{\ell u}\, \nu_{\ell u}\, \nu}{\pi} \cdot \frac{4\Delta\nu}{(\nu_{\ell u}^2 - \nu^2)^2 + 4\nu^2 \Delta\nu^2}.$$

(We will, in future writings of this equation, introduce the factor $10^6 \log_{10} e$ in order to express α in dB/km). We note that for $\nu = \nu_{\ell u}$, the Van Vleck-Weisskopf and Zhevakin-Naumov equations are substantially equal in the range where $(\nu_{\ell u})^2 >> \Delta\nu^2$ (true for the millimeter range):

$$\alpha = 10^6 \log_{10} e \frac{8\pi^2 \nu_{\ell u} N}{3hc\, G} |\mu_{\ell u}|^2 \left| e^{-E_\ell/kT} \right| \begin{cases} \frac{1}{\Delta\nu} & \text{(Zhevakin-Naumov)} \\ \left(\frac{1}{\Delta\nu} + \frac{\Delta\nu}{2(\nu_{\ell u})^2 + \Delta\nu^2}\right) & \text{(Van Vleck - Weisskopf)} \end{cases}$$

Further, it can be seen that the Zhevakin-Naumov form of α tends to zero for both $\nu \to 0$ and $\nu \to \infty$, whereas the Van Vleck-Weisskopf form tends to a constant for $\nu \to \infty$.

The broadening constant $\Delta\nu$ has a dependence on both temperature and pressure. In a single gas the dependence may be expressed as

$$(\Delta\nu)_{ij} = (\Delta\nu)_{\text{stand.}} \left(\frac{P}{P_s}\right)\left(\frac{T}{T_s}\right)^{-n_{ij}}$$

where $(\Delta\nu)_{\text{stand}}$ is the half width of the ij^{th} line at a pressure P_s and temperature T_s. In the case of mixtures

$$(\Delta\nu)_{ij}^{M} = C_{11} (\Delta\nu)_{ij}^{(c_2)} + C_{13} (\Delta\nu)_{ij}^{(c_3)} + \ldots\ldots$$

where $(\Delta\nu)_{ij}^{c_k}$ is the half width at standard temperature and pressure for self-broadening due to component k. The C_{mn} coefficients are the fractional composition of the mixture. For an average summer day when N_2 is 78 percent, O_2 21 percent, H_2O 1 percent (7.5 gm/m^3) and assuming that H_2O - H_2O collisions are approximately five times larger in cross section than the H_2O-N_2 collisions (Reference 3) and that H_2O-O_2 collisions are one third as effective, we may obtain with Zhevakin and Naumov that:

$$(\Delta\nu_{ij}) = 0.9(\Delta\nu)^{H_2O:N_2}_{ij} \left(\frac{P}{760}\right) \left(\frac{T}{300}\right)^{-n_{ij}}$$

where P is in millimeters of Hg.

A convenient form of this equation for a three component mixture, say N_2, O_2, H_2O, is:

$$\Delta\nu_{ij} = \left(R_e^{H_2O} \cdot f^{H_2O} + R_e^{N_2} \cdot f^{N_2} + R_e^{O_2} \cdot f^{O_2}\right) (\Delta_{ij})^{H_2O:N_2}_{ij} \left(\frac{P}{760}\right)\left(\frac{T}{300}\right)^{-n_{ij}}$$

where $R_e^{N_2}$ signifies the relative effectiveness of N_2 in collisions with water, etc., f^{N_2} is the fraction of N_2 molecules in the mixture. The formula may be easily varied to fit other mixtures.

III. INSTRUMENTATION AND MEASUREMENT

A. THE FABRY-PEROT INTERFEROMETER

1. Introduction

The use of resonant microwave cavities to observe molecular resonances in gases, and their absorption coefficients, is not of recent origin (References 10 through 12). Weidner (Reference 11), for example, used a resonant cavity at 6700 MHz to measure the loss of iodine monochloride with a sensitivity of 6×10^{-8} cm^{-1}. Since the method relies upon the reduction of cavity Q as a result of gas loss, the sensitivity of the instrument is proportional to the Q of the evacuated cavity. Therefore, it is desirable to design for maximum Q.

The low loss cylindrical cavity mode TE_{01} is usually employed for maximum Q. At submillimeter wavelengths, however, the wall losses of this mode become appreciable, and it becomes increasingly difficult to couple into the circular waveguide TE_{01} mode from the rectangular waveguide TE_{10} mode over a large range of frequencies.

These problems of loss, coupling efficiency, and tuning range have been greatly alleviated by the Fabry-Perot (F-P) interferometer (References 13 through 17). For example, the diffraction loss of a semiconfocal F-P interferometer, 61 cm in length and 12.1 cm in diameter, is 2.17×10^{-4} dB (Reference 18). The analogous wall loss of a cylindrical copper cavity of the same dimensions supporting the TE_{01} low loss mode is 7.68×10^{-4} dB.

The resonance spectroscopic technique also possesses the advantage of high resolution when compared to long waveguide absorption cells or grating spectrometers borrowed from the infrared. Molecular resonance lines can be examined in fine detail at pressures near atmospheric, or lower than 20 microns.

The F-P interferometer has been employed extensively as a resonant component in the microwave and millimeter wave region (References 13 through 17). Its application to the field of laser technology has also received extensive treatment (References 18 through 20).

2. Operating Principles and Fundamental Relationships

In its simplest form (Figure 1), the F-P interferometer consists of two partially reflecting mirrors separated by many wavelengths. When illuminated by a monochromatic plane wave, resonances occur at half-wavelength intervals in mirror separation. The shape of the transmission resonance curves (Reference 21), as a function of mirror separation d, is given by

$$I_T = \frac{(1-r^2)}{1-2r^2\cos\frac{4\pi d}{\lambda}+r^2} \tag{2a}$$

or

$$I_T = \frac{1}{1+\left[\frac{2r}{1-r^2}\right]^2 \sin^2\frac{2\pi d}{\lambda}} \tag{2b}$$

where r represents the reflectivity of the mirrors.

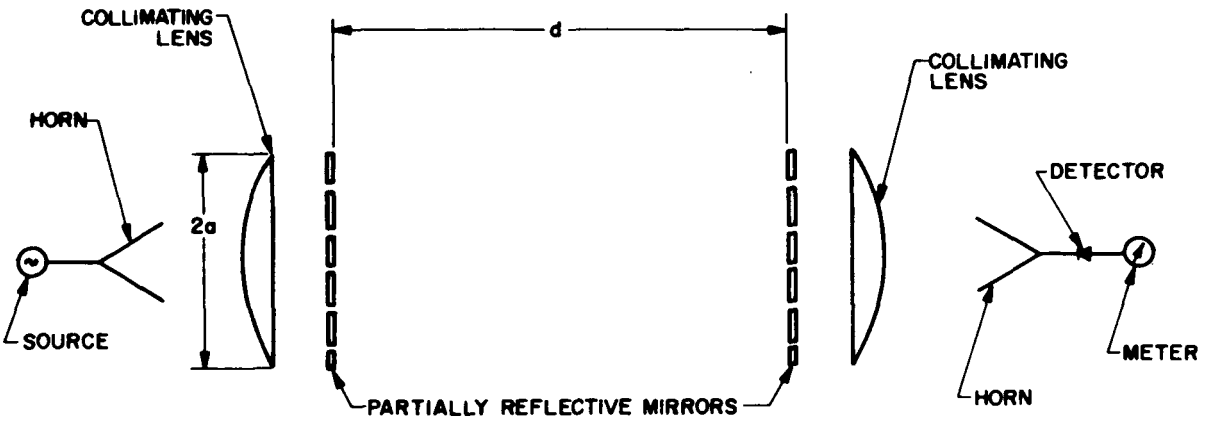

Figure 1. Flat Mirror Fabry-Perot Interferometer

The quality factor Q of a flat mirror F-P interferometer is given by

$$Q = \frac{f}{\Delta f} = \frac{2\pi}{\alpha\lambda} d \tag{3}$$

where

f = frequency of resonance

λ = wavelength of resonance

Δf = frequency separation of half-power points on response curve

α = losses of the resonator, per reflection.

For a given mirror spacing and wavelength, the Q is limited only by the loss α, consisting in vacuo of mirror conduction loss, mirror transmission loss, and diffraction loss.

Conduction loss is minimized by choosing a noncorrosive metal of high conductivity, which can be made to conform to a surface of maximum possible smoothness by plating, machining, and grinding processes.

Transmission loss is determined by considerations of output power of available sources and the sensitivity of the detector employed.

Diffraction loss is minimized by proper choice of mirror size for a given mirror separation. Mirror size should be limited to the point where diffraction losses have been reduced to be equal to other mirror losses. Further reduction of diffraction loss by increasing mirror size is not very effective since mirror loss will predominate.

Diffraction losses are most drastically increased by misalignment of the flat mirrors from true parallelism, destroying the high Q's of which the F-P interferometer is capable with large mirror separations.

Spherical mirrors may be employed to ease the mirror alignment problem as shown in Figure 2. The resonant modes which can be supported by the resulting confocal resonator (Reference 14) are commonly designated by the notation TEM_{qmn}, where

q = number of integral half wavelengths between spherical mirrors

m = number of field reversals in a direction transverse to the interferometer axis of symmetry

n = number of field reversals in a transverse direction which is orthogonal to the direction chosen for m and the interferometer axis of symmetry.

The index q is usually very large ($>10^3$) and, as a result, is omitted, resulting in the notation TEM_{mn}.

The conditions for resonance of the spherical mirror interferometer (Reference 14) for arbitrary mirror spacing d, and mirror radius of curvature b, are given by:

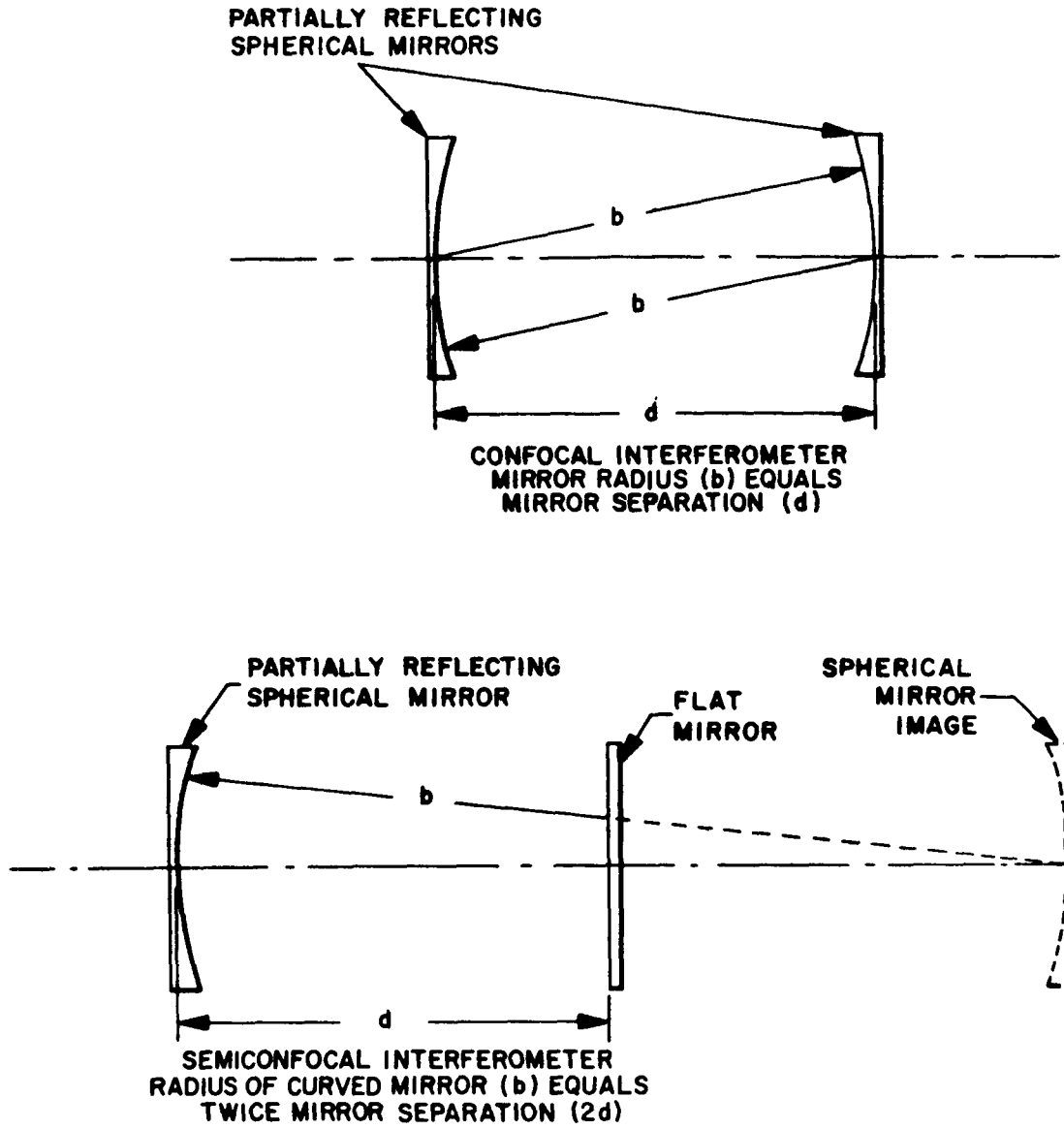

Figure 2. Confocal and Semi-Confocal Fabry-Perot Interferometers

$$\frac{4d}{\lambda} = 2q + (1+m+n)\left(1-\frac{4}{\pi}\tan^{-1}\frac{b-d}{b+d}\right) \qquad (4)$$

For the dominant mode, m=n=0(TEM_{00}).

When the mirrors are separated by their common radius of curvature d=b, the system is said to be confocal, and Equation (4) reduces to

$$\frac{4b}{\lambda} = 2q + (1+m+n) \qquad (5)$$

It should be noted that because of the boundary conditions imposed on the electric field by the flat mirror (tangential E=0), the index q is restricted to "even" integral values when applying Equation (4) to a semi-confocal interferometer such as the one outlined in Figure 2. The index q refers to the number of half wavelengths in a confocal system. Also, the quantity $4b/\lambda$ of Equation (5) must take on integral values. This requirement is not imposed on $4d/\lambda$ of Equation (4) as a condition for resonance of a nonconfocal system. In addition, the modes associated with a confocal system are degenerate in (m+n). This degeneracy is removed in the nonconfocal case.

In addition to making mirror alignment less critical, the use of spherical mirrors reduces diffraction losses for the dominant TEM_{00} mode, and permits the suppression of higher-order modes (m+n=0) by the proper choice of mirror radius. For the mirror losses usually encountered, the criterion for optimum mirror radius a in terms of confocal mirror spacing (b=d=radius of mirror curvature) and wavelength λ is

$$\frac{a^2}{b\lambda} \approx 1$$

Referred to as the Fresnel number, Equation (6) ensures that the diffraction losses associated with unwanted higher-order modes are significantly larger (>10 dB) than the diffraction losses associated with the TEM_{00} mode, serving as an effective means for suppression of higher-order modes.

Another concept useful in the design of the microwave feed system is the "spot size" defined as the radius at which the field distribution falls to 1/e of its peak value. From (Reference 19) it can be shown that the spot sizes at the mirrors of a semi-confocal F-P interferometer (Figure 2) are

$$r_s = \sqrt{\frac{d\lambda}{\pi}} \qquad \text{at the flat mirror}$$

$$r_s = \sqrt{\frac{2d\lambda}{\pi}} \qquad \text{at the spherical mirror}$$

The losses α of Equation (3) are additive. The loss of the propagating medium forms part of this loss when the system is not evacuated. Since

all other sources of loss remain unchanged, the loss of the propagating medium (gas or vapor) between the interferometer mirrors can be determined by measuring the Q of the interferometer with (Q_2) and without (Q_1) the absorbing gas, and subtracting to provide the following difference equation for the gas loss α:

$$\alpha = \frac{2\pi}{\lambda}\left(\frac{1}{Q_2} - \frac{1}{Q_1}\right) = \frac{2\pi}{\lambda} \tan \delta \text{ cm}^{-1} \tag{7}$$

Equation (7) can be written in a form which is more easily handled and less subject to the error associated with the difference between two large measured quantities such as Q_1 and Q_2. If A is the output of a loosely coupled square law detector at the output of the F-P resonator, then $Q_1/Q_2 = (A_1/A_2)^{\frac{1}{2}}$, and (7) becomes

$$\alpha = \frac{2\pi}{\lambda Q_1}\left[(A_1/A_2)^{\frac{1}{2}} - 1\right] \text{ cm}^{-1} \tag{8}$$

When expressed in terms of dB/km with λ in millimeters, Equation (8) becomes

$$\alpha = \frac{27.27 \times 10^6}{\lambda Q_1}\left[(A_1/A_2)^{\frac{1}{2}} - 1\right] \text{ dB/km} \tag{9}$$

Equation (8) implies that the F-P resonator possesses an "effective pathlength", given by

$$\text{EPL} = \frac{Q_1 \lambda}{2\pi} \tag{10}$$

Equation (10) makes the desirability of a very high Q system obvious since it implies a greater effective pathlength and, therefore, greater sensitivity. For example, a mirror separation of about 60 centimeters and a Q of 10^6 at 300 GHz will result in an effective pathlength equivalent to a waveguide absorption cell about 162 meters (530 feet) long.

The fractional change in detector output, A_1/A_2, is plotted as a function of α for a typical interferometer in Figure 3.

$$\frac{A_2}{A_1} = \frac{1}{\left[\frac{\alpha \lambda Q_1}{27.27 \times 10^6} + 1\right]^2} \quad \text{for } Q_1 = 2 \times 10^5$$

λ = 0.5 mm Case I
1.0 mm Case II

$1 \leqq \alpha \leqq 1000$

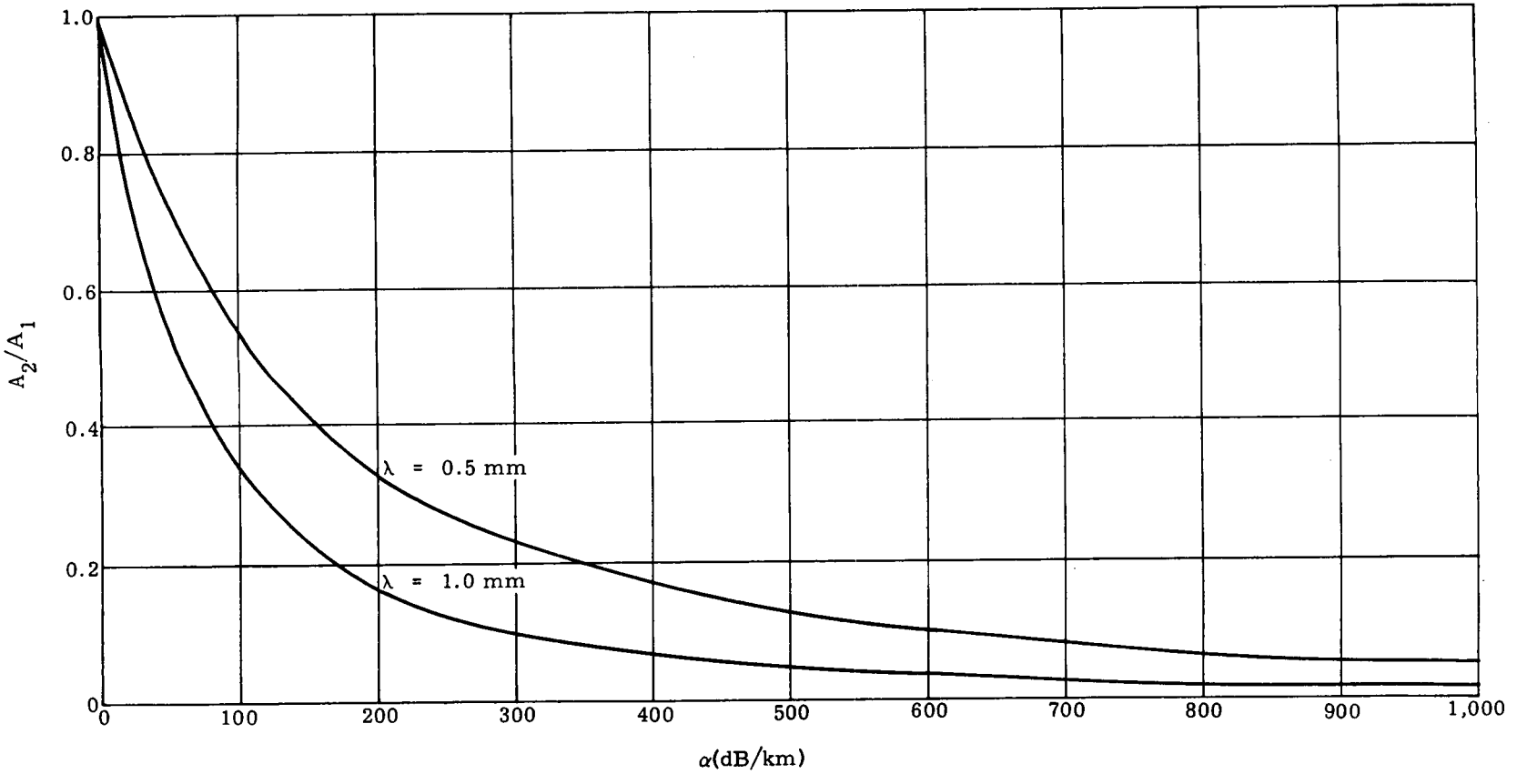

Figure 3. Variation of Interferometer Response with Absorption Coefficient

3. Design

The interferometer (Figure 4) was designed as a semiconfocal device with the following characteristics:

1. $Q = 10^6$
2. Mirror spacing, spherical to flat, 61 cm
3. Mirror radius of curvature = 122 cm
4. Mirror diameter = 22.86 cm.

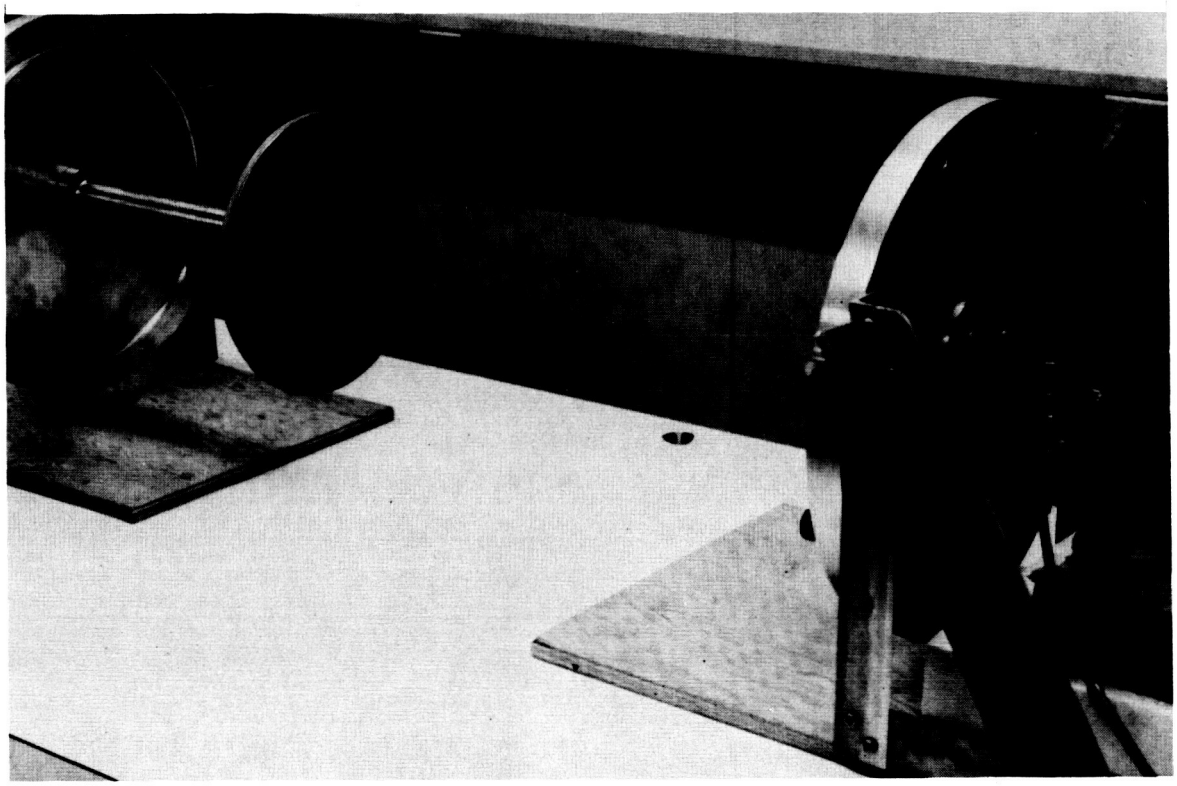

Figure 4. Photograph of Interferometer Removed from Vacuum Chamber

The spherical mirror is mounted to a threaded shaft (80 threads per inch) to permit tuning while the interferometer is mounted in a vacuum chamber. Electromagnetic energy coupling into and out of the interferometer is accomplished with two pieces of RG-135/W waveguide mounted symmetrically at the center of the flat mirror (Figure 5). The lateral position of the end of the waveguide relative to the mirror face is continuously adjustable, thus providing some tuning capability to reduce insertion losses.

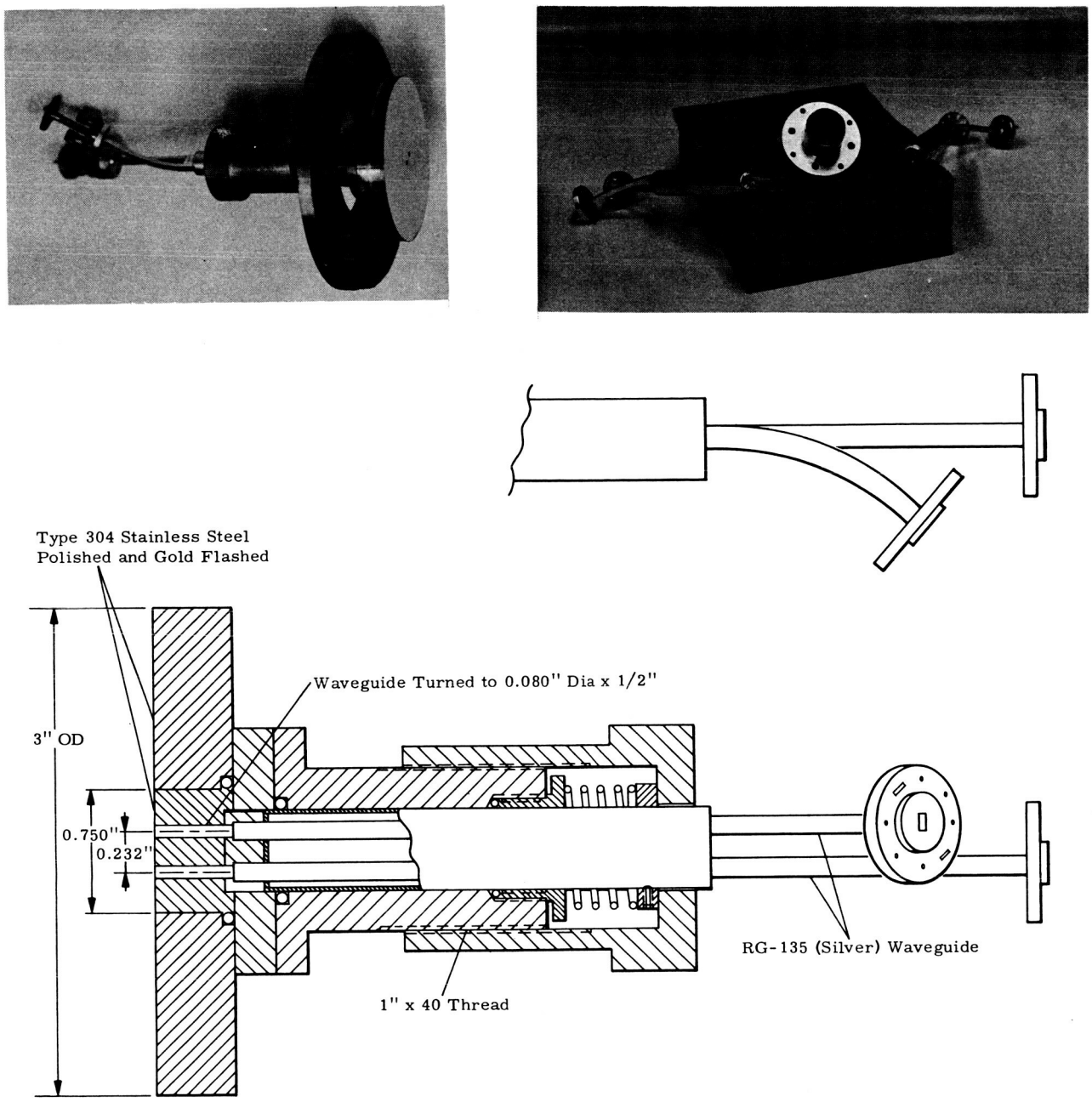

Figure 5. Microwave Feed Assembly and Components

It will be noted that the mirror diameter of 22.86 cm (9 inches) is much larger than required by Equation (6). This was done in order to accommodate the largest possible range of frequencies without the mirror size restrictions of Equation (5). Suppression of higher-order modes is accomplished by using a constricting iris of the aperture radius required. To minimize undesirable reflections within the vacuum chamber, the

chamber walls and iris were lined with sheets of black viton vacuum seal rubber, which proved to be an effective absorber of millimeter waves in the region of interest.

Mirrors were ground and polished from tool steel blanks to a surface tolerance of a few microns, copper plated, and gold flashed.

4. Instrumentation and Measurement Procedures

Figure 6 partially illustrates the instrumentation, showing the interferometer installed in the vacuum chamber, the gas manifold system, and vacuum gauges.

The basic measurement procedure consists of employing Equation (8) to determine the loss of water vapor as a function of water vapor density and pressure, using nitrogen, oxygen, and carbon dioxide as foreign gases.

Two basic systems were instrumented as shown in Figures 7 and 8. These two systems differ only in the method employed to generate frequency markers for the measurement of Q_1 of Equation (9).

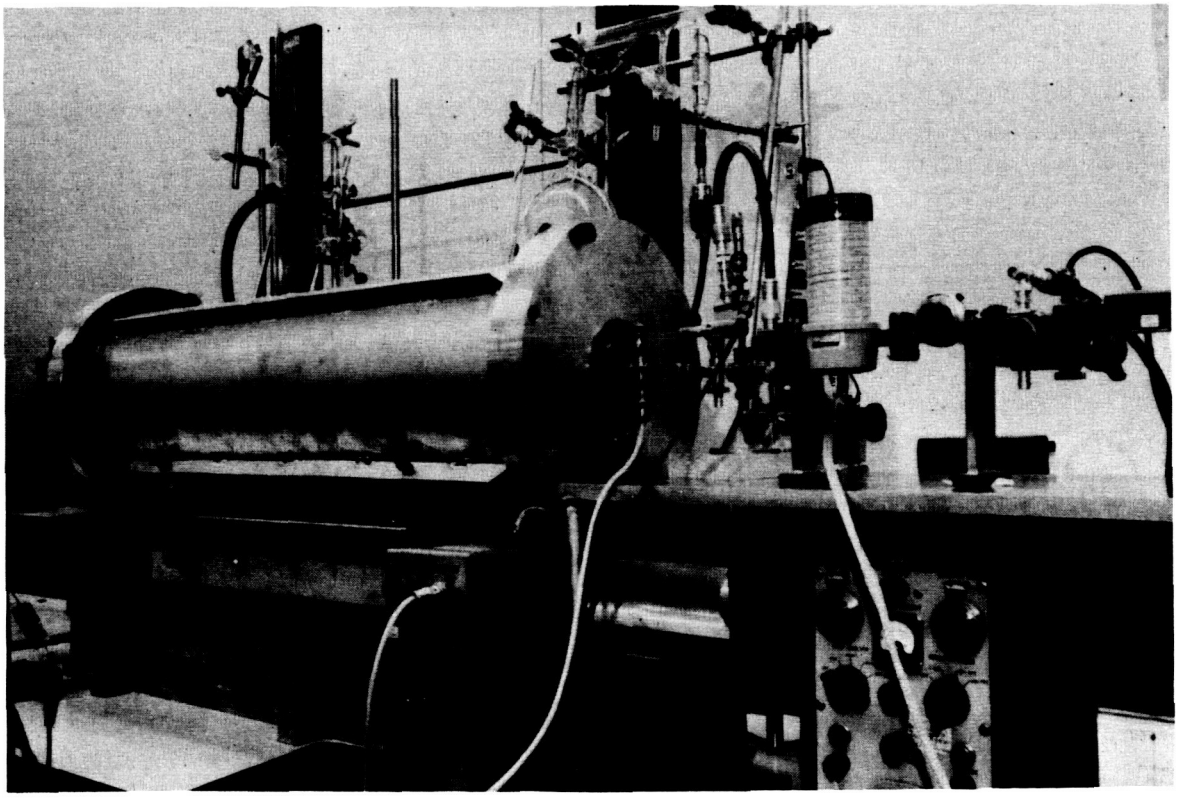

Figure 6. Complete Measurement System

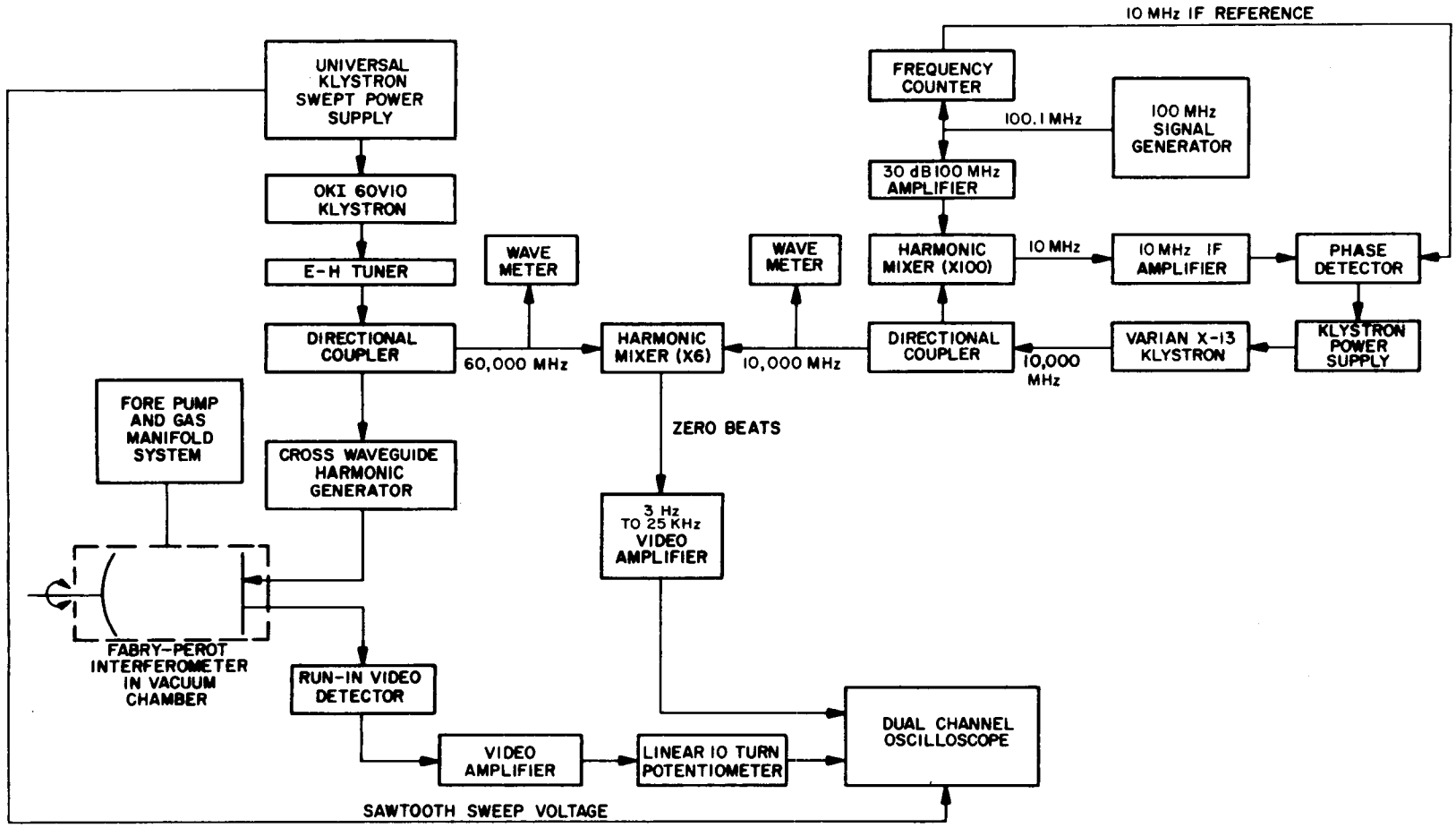

Figure 7. Block Diagram of Measurement System Using Single-Frequency Marker

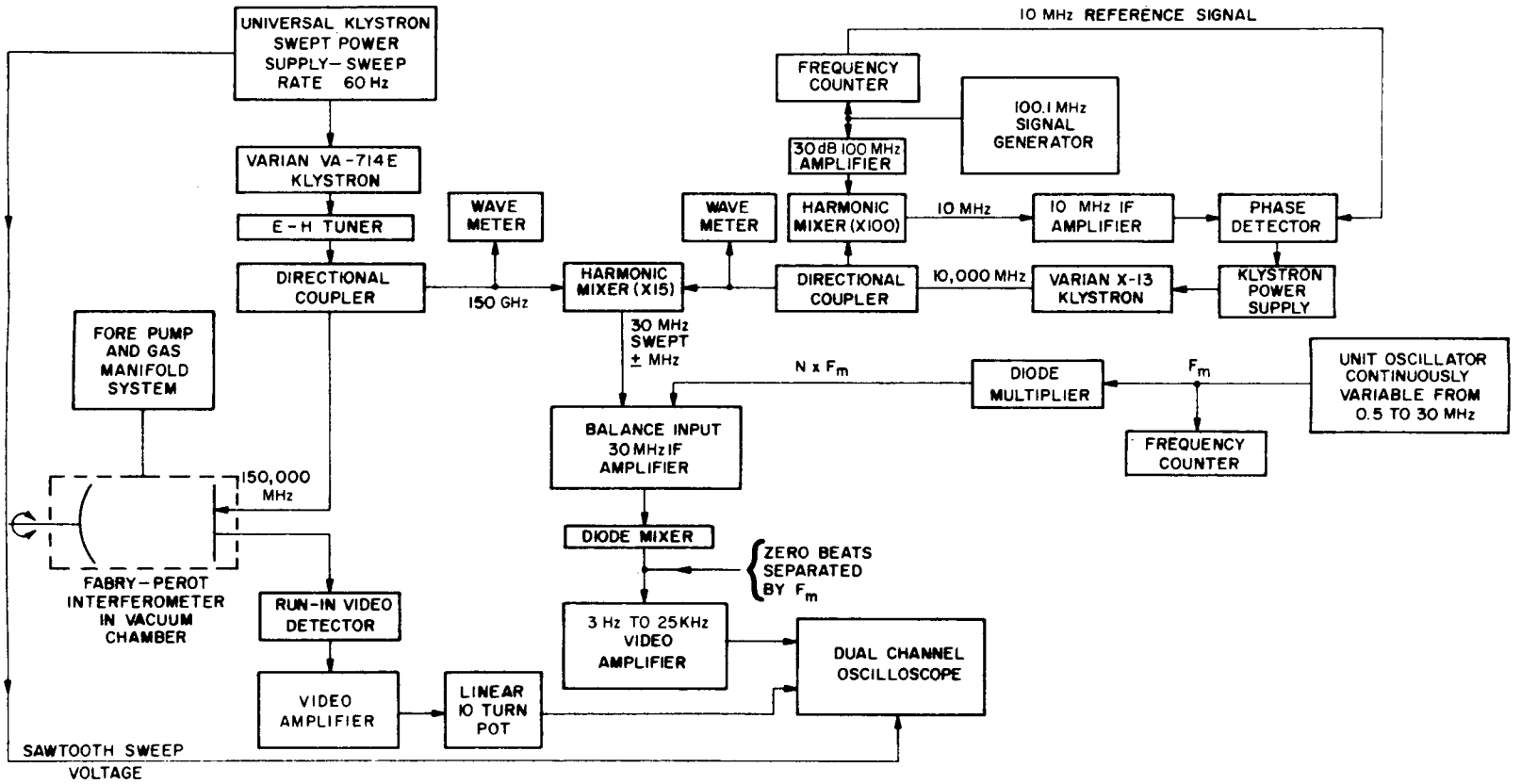

Figure 8. Block Diagram of Measurement System Using a Fence of Frequency Markers at 150 GHz

The vacuum chamber is first evacuated with the fore pump to a pressure of 25 to 30 microns of mercury. The evacuated Q of the interferometer is then measured by displaying frequency markers (zero beats) on the face of an oscilloscope along with the detected output of the interferometer.

As the 60V10 klystron is linearly swept with a sawtooth reflector voltage, the frequency response of the interferometer is displayed on the oscilloscope. As shown in Figure 7, the swept frequency output of the 60V10 klystron is sampled by a directional coupler, prior to multiplication from 60 GHz to 180 GHz in the crossed guide harmonic generator feeding the interferometer. A zero beat is then produced between the sampled 60 GHz GHz swept signal and the sixth harmonic of a phase-locked Varian X-13 klystron.

By adjusting the frequency of the 100 MHz signal generator in the phase-lock loop, the frequency of the X-13 klystron can be adjusted to place the zero beat at the maximum and the half-power points of the displayed interferometer response curve. The frequency of the 100 MHz signal generator is measured with a frequency counter, permitting the determination of the OKI 60V10 frequency to an accuracy of one part in 10^8. This data was used to determine Q_1 and λ. The interferometer response showing the zero-beat marker appears in Figure 9.

Once Q_1 and λ have been determined with the above procedure, water vapor is introduced into the vacuum chamber containing the interferometer by opening the water flask valve on the manifold until the desired partial pressure (density) is obtained. Therefore, the dielectric constant of the medium between the interferometer mirrors changes, and the interferometer tuning must be slightly adjusted by changing the mirror separation to maintain a resonant condition. As a result of water vapor loss,

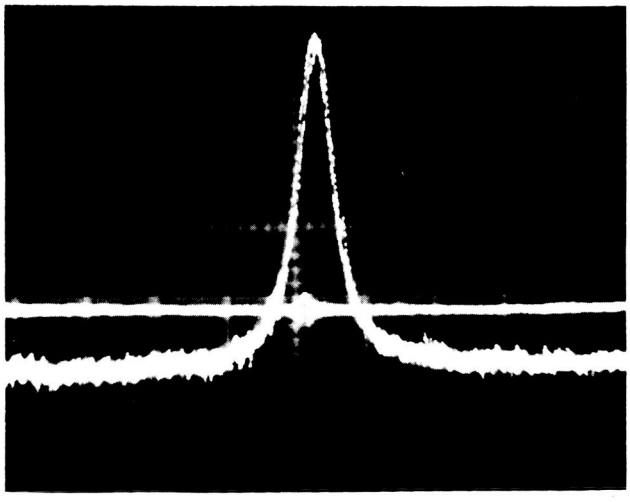

Figure 9. Oscilloscope Display of Interferometer Response Showing Zero-Beat Marker on Second Trace - Frequency 183.3 GHz

the detected output of the interferometer will be reduced from A_1, corresponding to an evacuated condition, to A_2, corresponding to the reduced system Q. The amount of this reduction is determined by removing video attenuation with the linear helipot to bring the output response back to its original level. The ratio of helipot settings then corresponds to the required ratio A_1/A_2 of Equation (9), and the loss α can be calculated.

It should be noted that retuning of the interferometer is required each time the pressure is changed. The tuning adjustments result in a total change in mirror separation of about 0.025 inch. Because of the large initial mirror separation, this retuning will produce a Q change less than 0.1 percent. The error can be ignored compared to the error in Q measurement inherent in the marker placement technique.

When using a Varian VA-714 klystron, operating from 137 to 155 GHz frequency marker (zero-beat) generation was not possible using the technique described above. This was due to the large multiplication (x15) required of the X-band phase-locked frequency.

As a result, the marker generator system shown in Figure 8 was employed as a unique method for producing a series or fence of zero beats of accurately known separation. These zero beats are obtained by mixing the harmonics of a stable unit oscillator with the swept 30 MHz IF signal derived from the VA-714 klystron, mixing with the fifteenth harmonic of the phase-locked X-13 klystron. By adjusting the unit oscillator frequency, a zero beat can be placed at each of the half-power points of the displayed resonance response of the interferometer. The width of the response curve is then given directly by the unit oscillator frequency as measured with a frequency counter.

The frequency of interferometer resonance is obtained by adjusting the unit oscillator to 30 MHz (or some known submultiple thereof) and adjusting the X-13 klystron frequency until a zero beat is superimposed on the peak of the response curve. With the aid of the wavemeters to obtain multiplication factors, the frequency of the VA-174 klystron can be determined to one part in 10^8 at the peak of the interferometer response curve. The oscilloscope trace of the interferometer response, at 150 GHz and the zero-beat markers are shown in Figure 10. The interferometer response at 300 GHz (second harmonic of VA-714 klystron) is shown in Figure 11. The measured Q of 0.33×10^5 at 300 GHz compares favorably with the design Q (unloaded) of 10^6. The difference is attributable to coupling and vacuum chamber loss not initially anticipated.

In conclusion, it has been demonstrated that Fabry-Perot interferometers are feasible as coherent spectrometers of quality factors

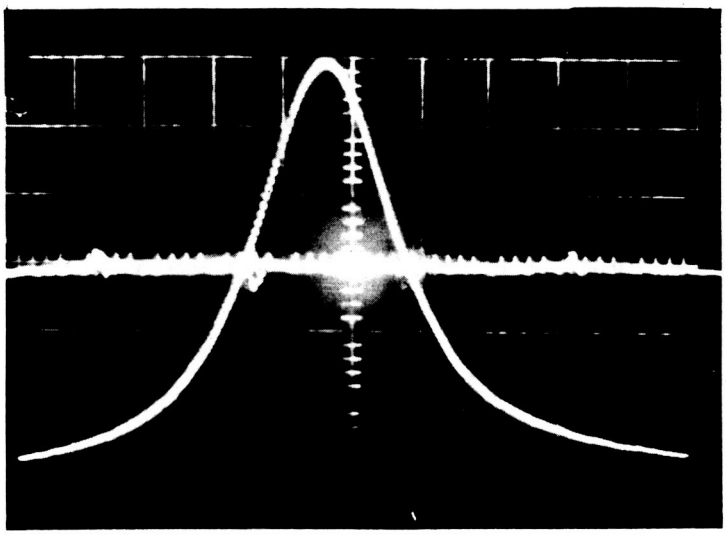

Figure 10. Oscilloscope Display of Interferometer Response Showing Zero-Beat Marker on Second Trace - Frequency 150 GHz

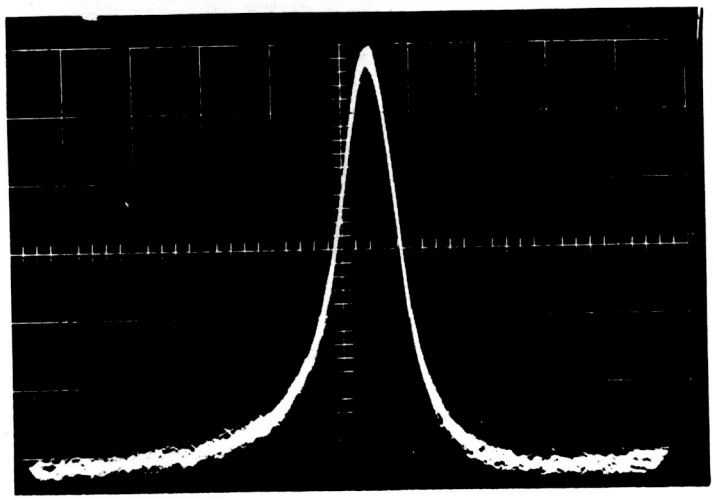

Figure 11. Oscilloscope Display of Interferometer Response at 300 GHz - Measured Q = 330,000

exceeding 3 x 10^5 at 300 GHz. The Q reduction technique of loss measurement has consistently provided a sensitivity on the order of 10^{-7} cm^{-1} at frequencies as high as 300 GHz using video detection methods. Heterdyne detection techniques will result in a further improvement in sensitivity.

In general, it was possible to measure Q repeatedly to about ±3 percent. However, the values obtained varied with coupling changes that occurred as a result of mechanical operations made on the cavity, either in intentional adjustments or during pressurization. These changes often amounted to ±15 percent of the initial set of readings. It is very doubtful that such large changes actually occurred during a given measurement series, or that they were systematic enough to affect the average results of repeated measurements by more than 5 percent. The origin of the Q sensitivity to mechanical influences lies primarily in the relatively tight coupling into and out of the interferometer. As more power becomes available, a higher insertion loss and less coupling are feasible.

The major benefits derived from using the Fabry-Perot interferometer are its long effective absorption path and its high resolving power Q. These qualities suggest other areas of application. Some of these areas, such as filtering applications, have been employed (Reference 22) in the far infrared. Another area, that of transform spectroscopy using incoherent sources suggests itself as worthy of investigation. The Michelson interferometer has been employed for this purpose in the past, providing a low Q dual beam device for which a Fourier transform exists to obtain by computer techniques the output spectrum of a "multiple bounce" long path cell.

In the event that an inverse transform can be obtained for a kernel of the type provided by a Fabry-Perot interferometer (Reference 10), other spectrometer components normally employed for long path cells or multiple filtering processes could be eliminated, resulting in a significant simplification of instrumentation normally employed in the far-infrared region.

B. FOURIER SPECTROMETER

The use of coherent radiation methods of attenuation measurement are superior in many ways to the incoherent optical sources previously used. However, in the present state of the art the production of sufficient power above 600 GHz to perform such measurements is very difficult unless sufficient funds to buy carcinotrons at 750 GHz are available (It is estimated that close to $40,000 would be necessary to put one carcinotron at that frequency into operation, counting the cost of the source and its power supply, and one source would cover only a very narrow range.) In order to provide a general coverage over the 600 to 1000 GHz range a Michelson-Fourier spectrometer was obtained. It has only sufficient resolution and accuracy to approximately confirm the location and shape of absorption lines, but it shows that oxygen is inconsiderable compared to water vapor in this frequency range. No evidence of the O_2 lines discussed in section IV was found.

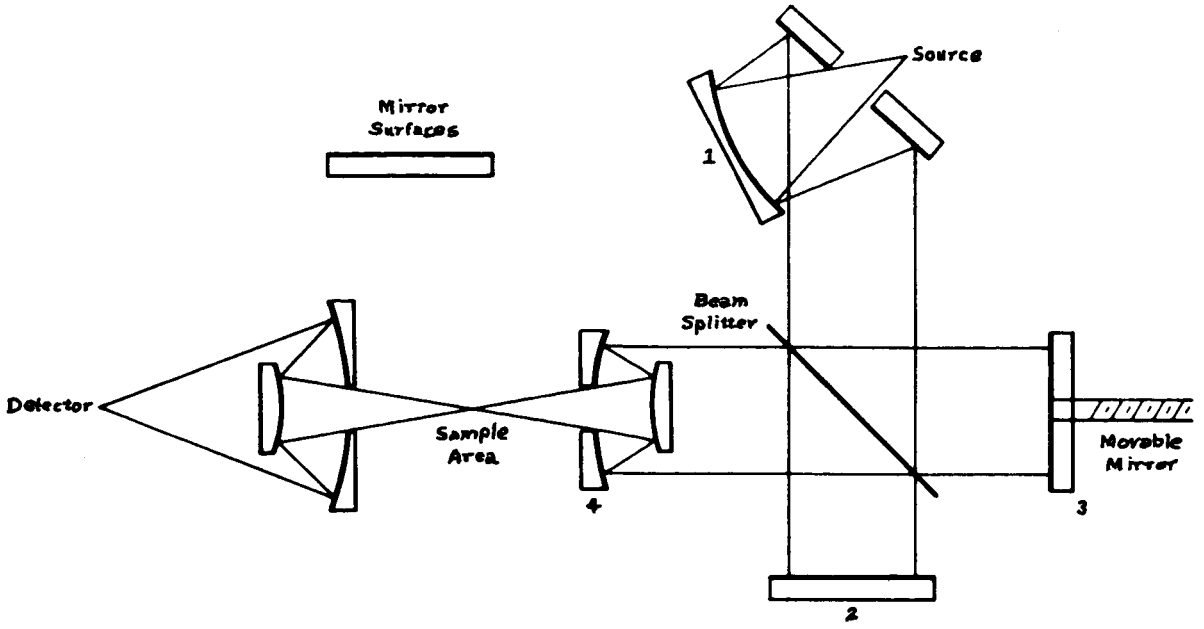

Figure 12. Optical Layout of Fourier Spectrometer

The Fourier spectrometer is a FS-520* far infrared interferometric spectrometer with a conventional Michelson interferometer. This type of spectrometer is superior to a dispersion type instrument due to the improved signal-to-noise ratio achieved by simultaneous measurement of the radiation throughout the spectrum and the absence of sorting problems.

Figure 12 shows the optical layout of the instrument. The source is a high pressure mercury lamp with a thin wall quartz envelope, mounted in a prefocused, water-cooled holder. The beam splitter consists of a sheet of polyethylene terephthalate (thickness chosen for wavelength region of operation) stretched in a precision spot ground circular frame. The detector is a diamond window Golay cell with a synchronous detection system.

In Figure 12, energy from the source is collimated by mirror 1 and reflected onto the beam splitter, from which it passes to the fixed mirror 2 and the driven mirror 3. The recombined beam is condensed by the concave mirror 4 and brought to focus at the detector through the Cassegranian system shown.

* RIIS, London, England

Mirror 3 is driven along the optical axis by a precision lapped piston and cylinder system. A grating attached to the piston, along with a grating which is fixed in position, make up a Moire fringe system which determines mirror movement to an accuracy on the order of 0.1 microns. The sampling interval is either 4 or 8 microns, and the mirror can be driven at speeds ranging from 1 micron per second to 250 microns per second.

A block diagram of the overall system is shown in Figure 13. The same chopper blade which modulates the source at 15 Hz, also provides a reference signal for the synchronous detector through the addition of a photovoltaic cell and lamp mounted on the chopper. The signal from the Golay cell is amplified, synchronously detected, integrated, and fed to the analog-to-digital (A/D) converter. Basically, the A/D converter is a summing ladder fed from eight bi-stable circuits. The current in the ladder is compared with the analog input and the required number of bi-stables set to balance the input.

The A/D converter is shown in detail in Figure 14. The eight bi-stable circuits are all set to zero by the start pulse, so that the current fed into the summing ladder is zero. After a short delay the first bi-stable is set to 1. This causes a constant current to be fed into the summing ladder, creating an output from the ladder equal to half the maximum analogue input. The output from the ladder is compared with the analogue input by a comparator. If the output from the ladder is greater than the analogue input, then the comparator output will cause all the gates it controls to open. The delayed output from the first bi-stable will then pass through the first gate and set itself to zero thereby removing its current feed from the ladder. Alternatively, if the output from the ladder is smaller than the analogue input, then the gates controlled by the comparator will remain closed and the current controlled by the first bi-stable will remain being fed into the ladder.

The delayed output from the first bi-stable also sets 1 on the second bi-stable, putting a current into the ladder which produces an output equal to one quarter of the maximum analogue input. The sequence of events described above is then repeated and so on down the ladder each feed giving a ladder output which is 2:1 down on the preceding one.

At the end, the output from the ladder will be within one digit of the analogue input, and the state of the bi-stable circuits, fed through buffer amplifiers reflects this in a straight digit reading.

The digital output is recorded on a standard Addo paper tape punch unit.

This data, the interferogram, is the Fourier transform of the required spectrum. That is:

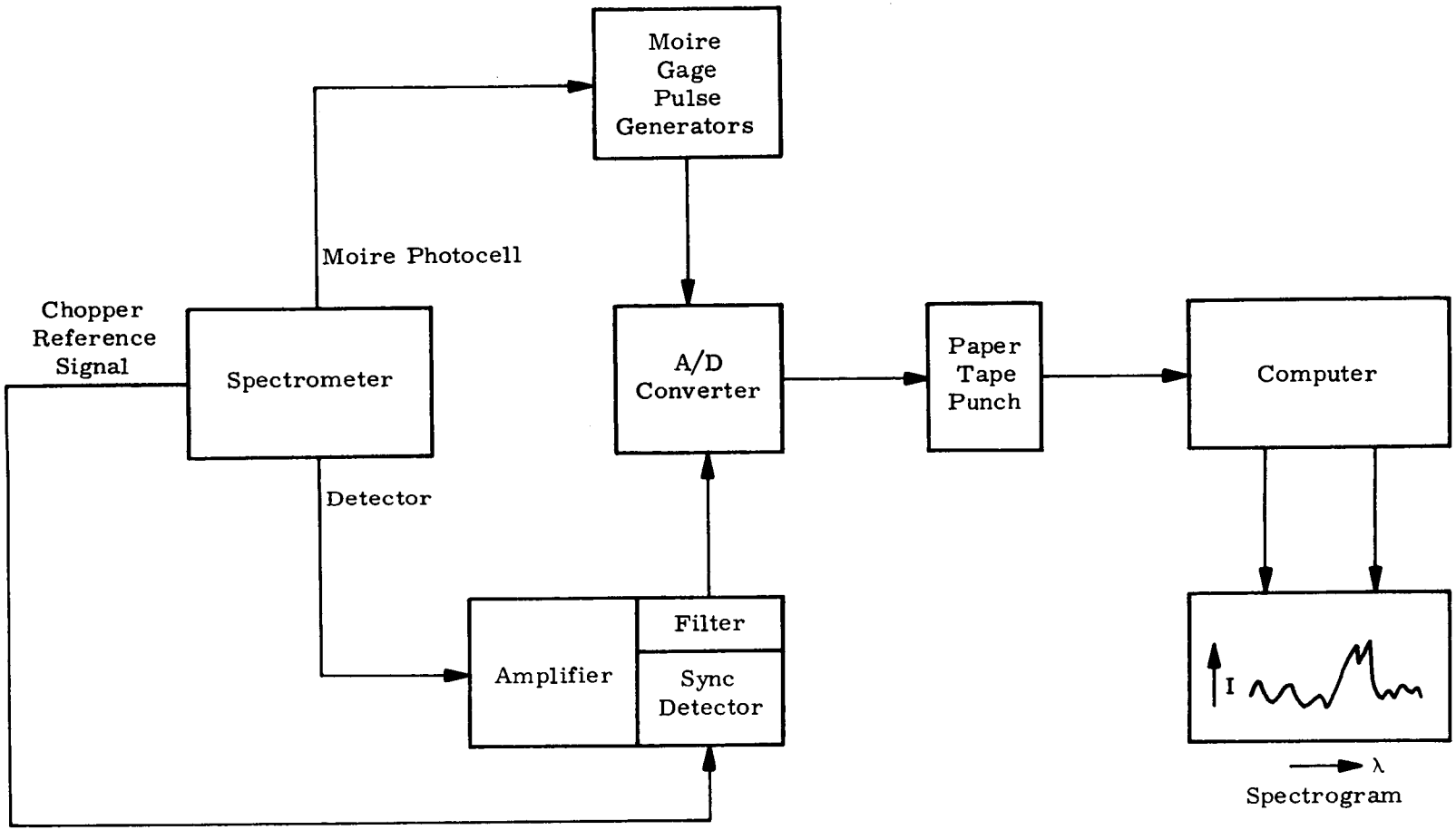

Figure 13. System Block Diagram

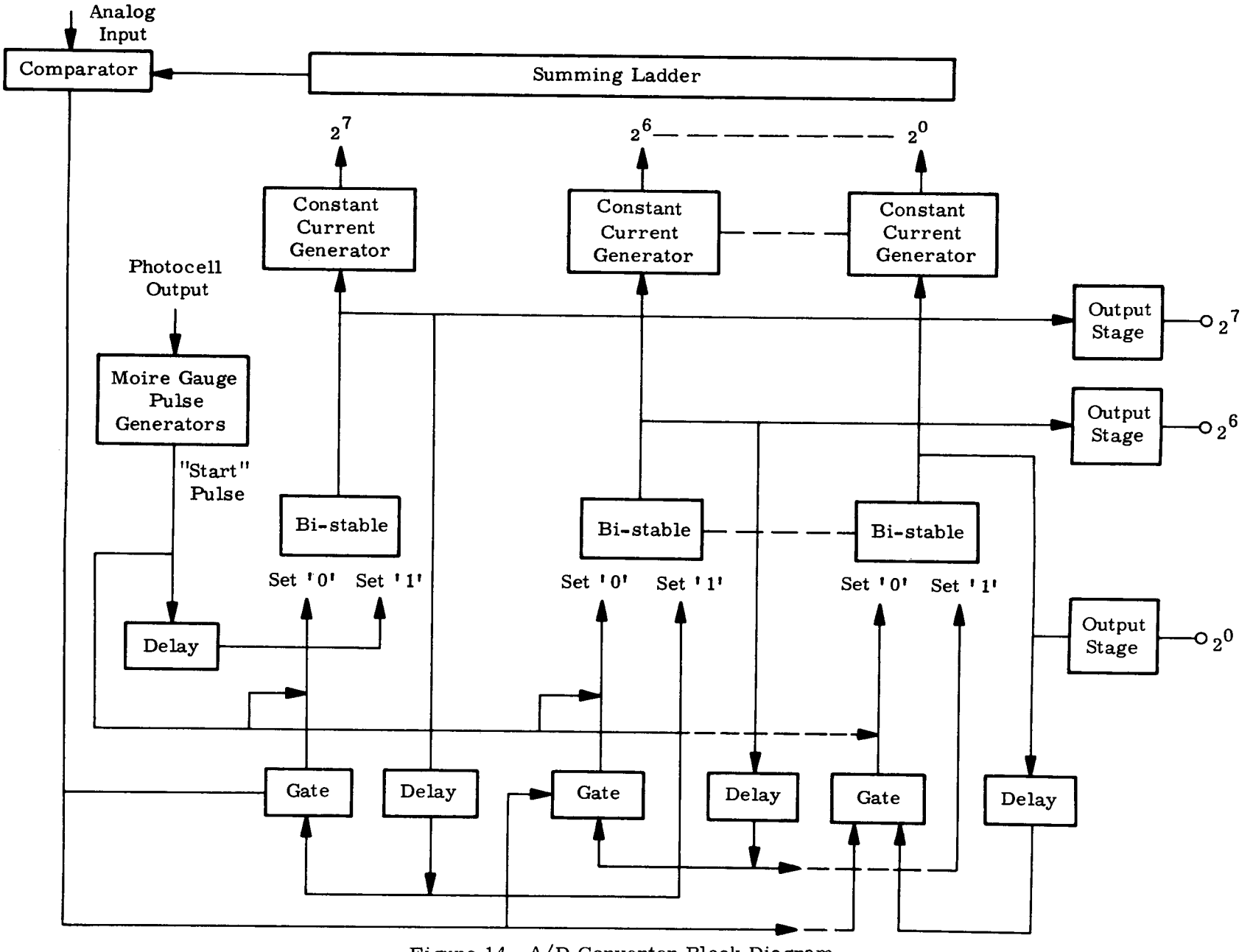

Figure 14. A/D Converter Block Diagram

$$I(\nu) = \int_0^{\alpha} F(x) \cos(2\pi\nu\, x)dx$$

where $I(\nu)$ is the spectral intensity at ν cm^{-1} and $F(x)$ the observed intensity at path difference x cm. The maximum theoretical resolution ($\Delta\nu$) is directly related to X, the maximum path difference by

$$\Delta\nu = \frac{1}{X}.$$

That is, if the actual mirror travel is 5 cm (x = 10 cm) then $\Delta\nu = 0.1$ cm^{-1}.

The transformation from interferograms to spectrograms performed by the computer is given by:

$$I(\nu) = \int_0^{\alpha} F(x) \cos(2\pi\, \nu\, x)dx$$

$$\cong 1/2\ F(0)\ \Delta x + \sum_i F(x_i) \cos(2\pi\, \nu\, x_i)\ \Delta x.$$

where Δx is the sampling rate chosen, either 4 or 8 microns.

C. 600 GHz SUPERHETERODYNE RECEIVER

The power available at frequencies over 500 GHz by harmonic generation has not been measured, but is estimated to be less than 10^{-9} watts. Such power has been observed by lock-in techniques and even by video detection, under the most favorable circumstance where the detector is connected directly to the harmonic generator. When it is considered that at least 20:1 signal to noise ratio is needed for accurate measurement and the Fabry-Perot insertion loss is between 20 and 30 dB, it is clear that a better detection method is necessary. Accordingly a program was begun to build a superheterodyne receiver. The gain in using a high intermediate frequency comes from the fact that most mixer and local oscillator noise is below 2 GHz. With the increase in signal-to-noise obtained by the superheterodyne receiver, the additional increase available with integration techniques, either lock-in, boxcar integrators, computers of average transients or waveform eductors should then make the measurement possible. Such methods, of course, require a very stable system, and power supplies must be of the highest quality, with stable mechanical or electrical sweep.

In order to improve the available signal-to-noise ratio the superheterodyne receiver shown in Figure 15 was designed and constructed by Martin Company for operation at 600 GHz. The system was designed to utilize harmonic mixing with the second harmonic of the 300 GHz local oscillator. The IF output frequency of the mixer was chosen to be as high as possible in order to reduce local oscillator noise. The specific frequency of 2.5 GHz was chosen because traveling wave tube (TWT) amplifiers in this range were available from previous programs.

The mixer (Figure 16) was, in principle, similar to the conventional crossed-guide harmonic generator described in Reference 10, however, several new and unique fabrication techniques were devised by E. Horvath and employed in its construction. The waveguides, complete with the crossover junction, crystal hole, and whisker hole were electroformed in one piece with 0.002 inch thickness of gold followed by approximately 0.020 inch thickness of copper, producing a precision seamless unit with all gold internal surfaces. The output (or IF) port was designed to match a 50-ohm line over a broad band centered at 2.5 GHz. Although no quantitative measurements have been made, it should be noted that the performance of this unit as a harmonic generator or as a detector of millimeter waves has been observed to be consistently superior to that of existing units specifically designed for these functions. It is concluded then that the use of this technique should be extended to other microwave components intended for operation at these frequencies.

The TWT amplifiers used were not the best available. Even so, the overall system consistently provided considerable improvement over a video detector or a 60 MHz IF amplifier. An increase in signal-to-noise ratio over video techniques of better than a factor of ten was observed at the OCS 291,839 MHz transition. Insufficient time remained in the task to couple the receiver with an integration system to perform the measurements.

D. MILLIMETER WAVE TUBES

Several new millimeter wave sources and power supplies were purchased by the Martin Company at a total expense of over $60,000 in an attempt to generate significant microwave power above 500 GHz. These consisted of a CSF COE-10 carcinotron and five of the Varian 714 series reflex klystrons.

The carcinotron generates up to 50 milliwatts from 275 to 315 GHz but is too unstable for most uses with a high Q interferometer due to its extreme sensitivity to power supply fluctuations.

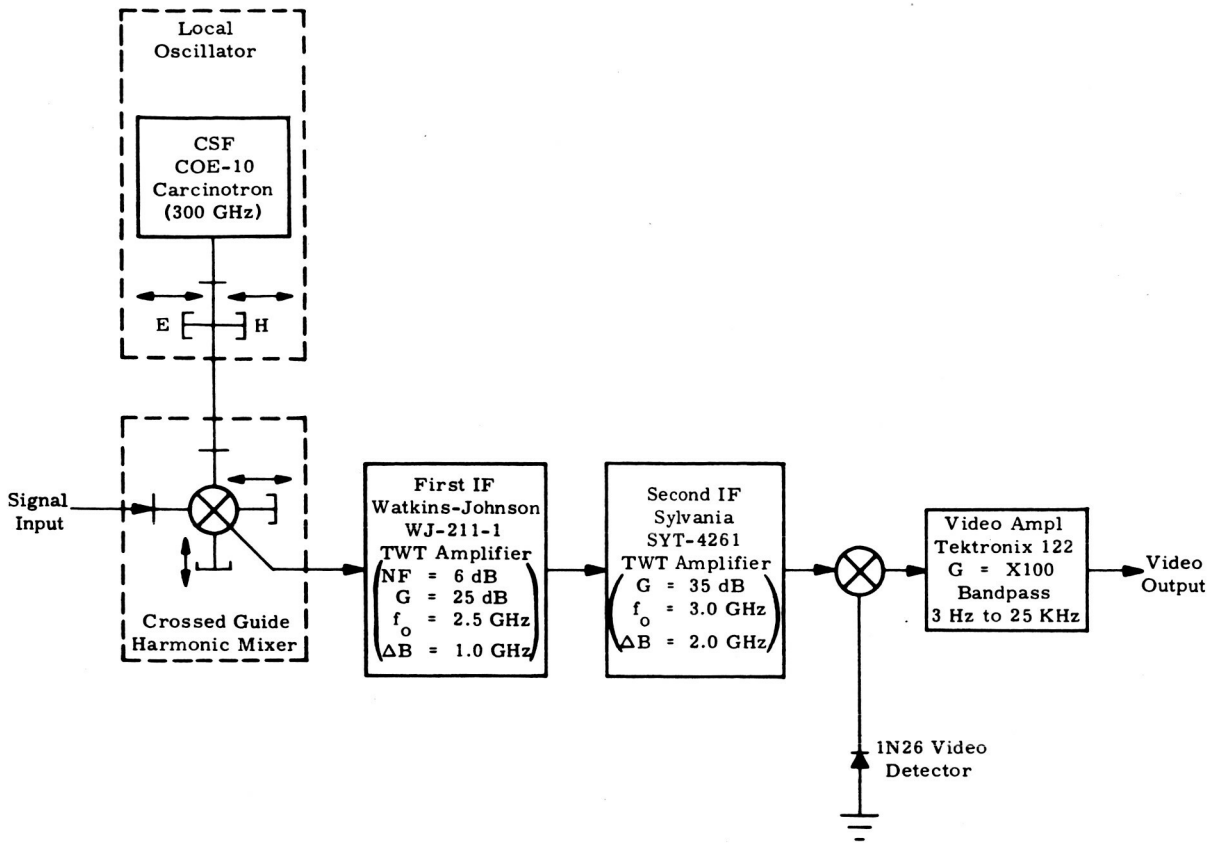

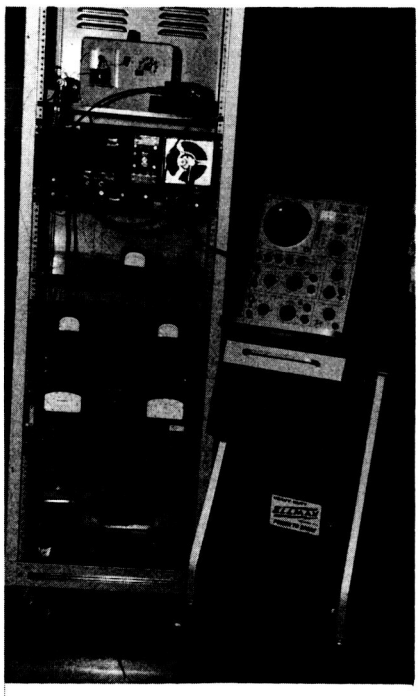

Figure 15. 600 GHz Superheterodyne Receiver

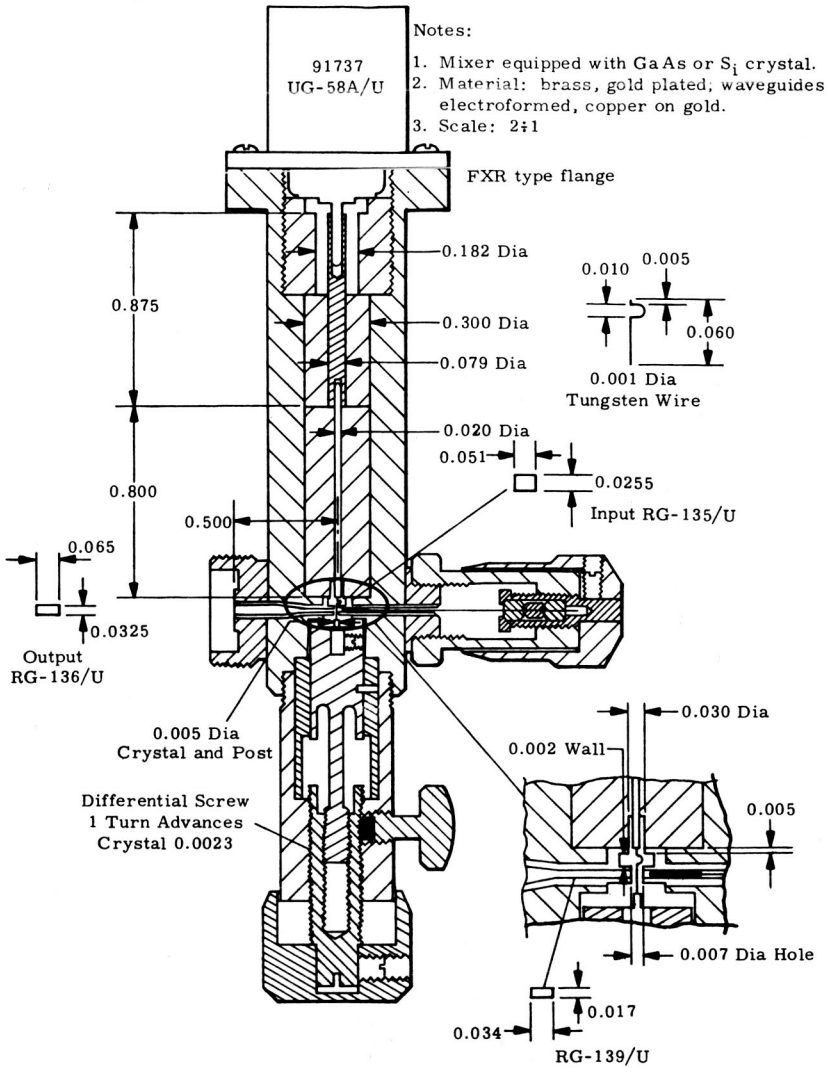

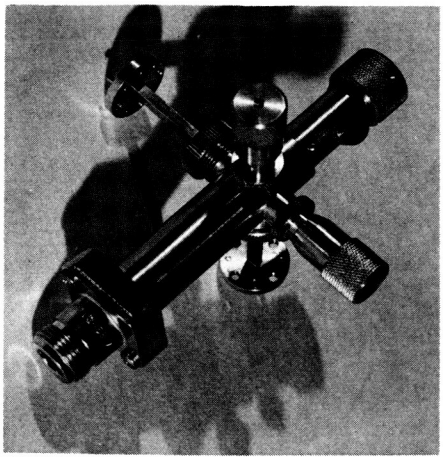

Figure 16. 600 GHz Mixer

The specifications on the Varian tubes are given in Table I. These devices are very stable but operate at about half the frequency of the carcinotron.

TABLE I

Available Varian Klystrons

Model	Frequency Range (GHz)	Power (mW)
VC 714D	134 - 142	80
VC 714D	137 - 145	150
VC 714D	137 - 145	110
VC 714E	142 - 150	80
VC 714F	149 - 157	150

A CSF COE-10-1D carcinotron which generates up to one watt of power at 300 GHz has also been obtained but has not yet been put into operation for lack of a suitable power supply. The power supply requirements for both carcinotrons are summarized in Table II.

TABLE II

Carcinotron Power Supply Requirements

	Model COE-10	Model COE-10-10
Electromagnet	None	0-70 Vdc at 12A
Heater	0-10 Vdc at 3A	0-10 Vdc at 3A
Collector	1-6 kV at 80 mA	0-3 kV at 50 mA
Anode	0-3 kV at 10 mA	0-3 kV at 10 mA
Delay line	None*	3-12 kV at 50 mA
Grid	0-100 Vdc at 10 mA	None
Insulation	13 kV	25 kV

* The delay line and collector are internally connected in the COE-10.

E. UP-CONVERSION TECHNIQUES

A technique showing some promise for generation of submillimeter waves is up-conversion from lower frequencies. Kempf, Cupp and Gallagher from this laboratory have mixed a 50 GHz signal and a 71.624 GHz signal to produce a sum output frequency of 121.624 GHz. This was accomplished through the use of the apparatus shown in Figure 17. The 70V11 klystron

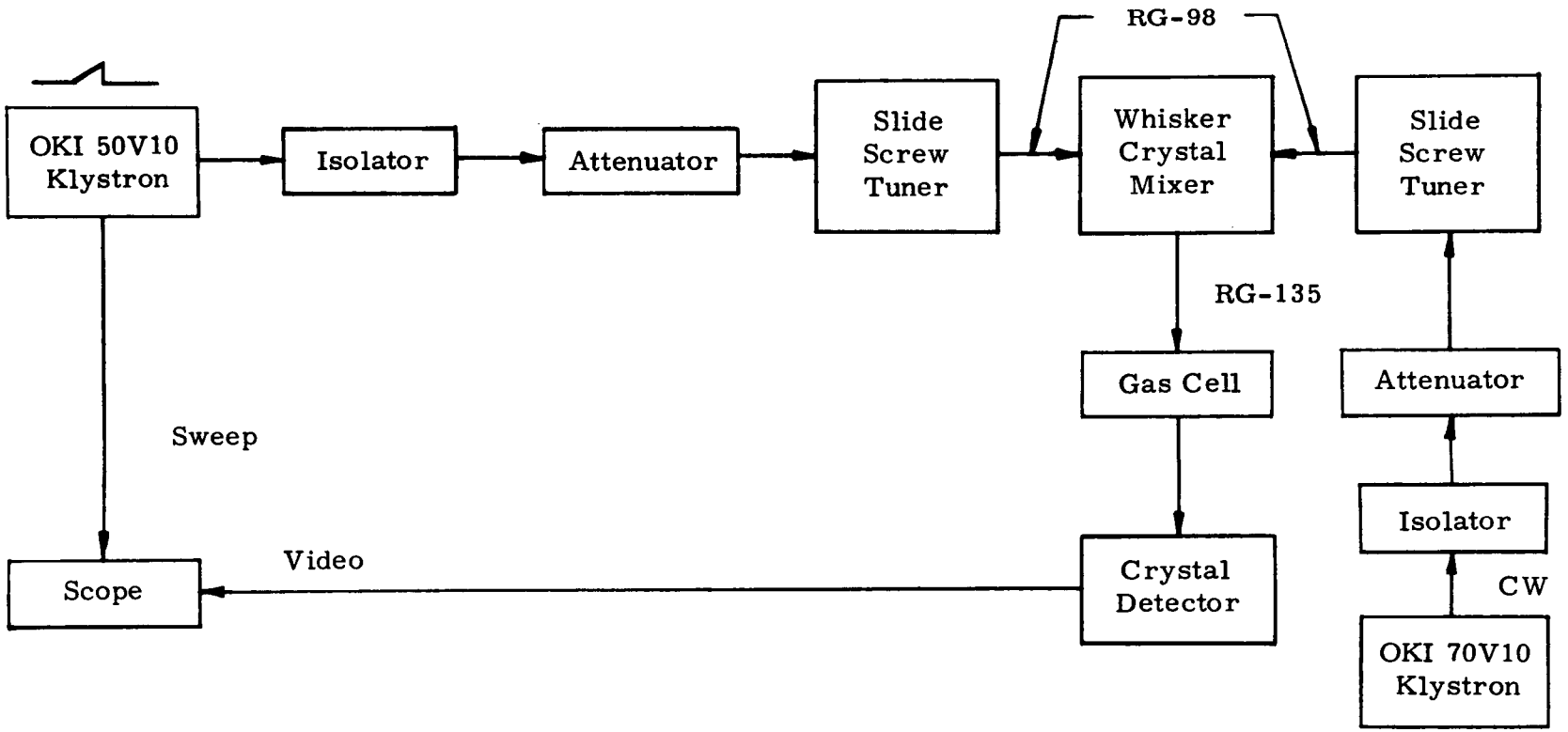

Figure 17. Schematic of Experimental Apparatus for Mixing 70 GHz and 50 GHz

was operated CW and the 50V10 klystron was driven by a sawtooth sweep. The mixer is an RG-98/U to RG-135U point contact run-in type, commonly used in the laboratory. The RG-98/U waveguide was flanged at both ends to accept the klystron inputs. The RG 135/U waveguide was flanged at one end with a tunable short on the other arm. A 0.001 inch tungsten whisker was used with P-type silicon crystals. Figure 18 is a view of the mixer assembly.

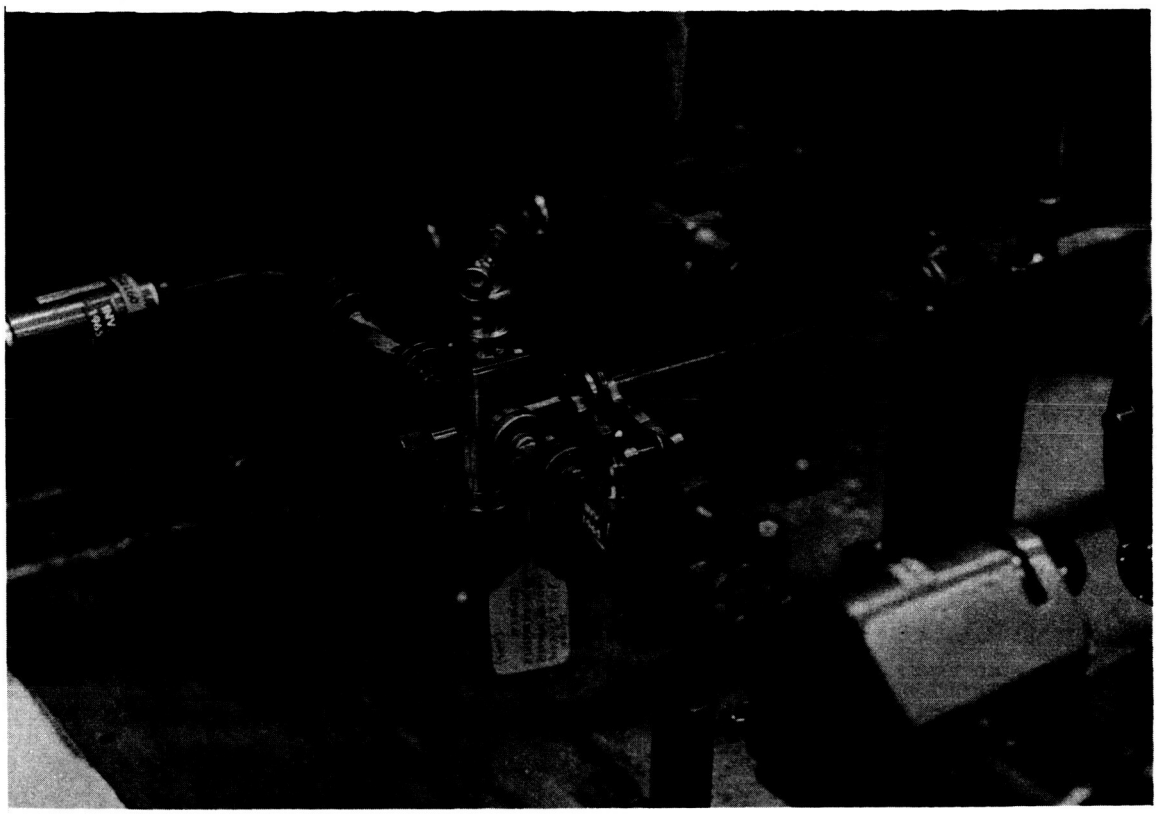

Figure 18. Close-Up of Millimeter Mixer

The 50 GHz oscillator was swept rather than the 70 GHz klystron in order to prevent the higher frequency mode from propagating in the harmonic waveguide (RG-135/U). In order to confirm that the mixing was occurring, a rotational absorption line of OCS was observed. The scope is externally swept by the 50 GHz klystron power supply and is on the 0.5 volt/cm gain setting with a times 100 external preamplifier. No attempt was made to optimize the equipment setup or the mixer run-in. Considering the possible combinations of the two fundamental signals, the observed line could only result at the sum frequency and not at a harmonic of one of the klystrons. The up-conversion action appears to be readily repeatable.

Power variation of either klystron alters the output signal in the same manner. By tuning the RG-135/U waveguide short, it was possible to obtain either the third harmonic of the 50V10 klystron or the sum of the two oscillators. This was observed to be dependent on the whisker point as well as on the mixer run-in.

In another experiment, two CW 70 GHz klystrons were mixed; the output transmitted from the mixer was detected by a superheterodyne receiver employing harmonic mixing and a swept local oscillator. The output mode then showed three zero beats; two of these beats could be identified as the harmonics of the two 70 GHz oscillators and the third as the sum of the two signals.

Subsequently, a 300 GHz CSF COE-10 carcinotron and a 70 GHz OKI klystron were mixed. The up-conversion action appeared to occur although the 369 GHz $4_0 \rightarrow 4_2$ rotational transition of H_2S was not observed in absorption. Instability in the carcinotron power supply caused an uncertainity in the results.

F. FAR INFRARED LASERS

A program was instituted to develop long wavelength lasers, because of the problems involved in instrumentation due to the lack of good sources above 600 GHz.

Operation was attained with H_2O at 118 and 220 microns after considerable problems involved with electrode heating. The unit developed is a tube with 2 1/2-inch diameter and 8-foot length. Fuzed quartz windows are used and one electrode has to be water-cooled. The power supply requirements are approximately 1100 volts at 1.0 ampere, after an ignition voltage on the order of 1500 volts. The detector used is a Golay cell with suitable filters.

Operation with CN (333 microns) is expected but cannot occur early enough to benefit the program.

G. FROOME GENERATOR

A Froome generator (Reference 42) has been under design in order to increase the amount of power available in the submillimeter range. After its completion, results will be reported in the literature.

IV. THE EFFECT OF OXYGEN ON ABSORPTION IN THE EARTH'S ATMOSPHERE

A diatomic molecule has its rotational energy given by $W = h^2/(8\pi^2 I)$ $J(J+1)$ and the frequency of rotational transitions by $\nu = 2B(J+1)$ unless the rotational motion interacts with the electronic motion. (Here J = rotational quantum number, $B = h/8\pi^2 I$ and the selection rule $\Delta J = \pm 1$ holds.) However, in the O_2 molecule the ground state is a $^3\Sigma$ state. Since the spin quantum S is 1 (two uncompensated spins), the molecule has a magnetic dipole of 2 Bohr magnetons. The spin angular momentum S combines with the rotational angular momentum J to give the total angular momentum N. By the vector coupling rules, a given value of N has three J values, J = N-1, N, N+1. The energy level for N = J is $W = B_o N(N+1) + B_1 N^2(N+1)^2$, where B_o and B_1 are the rotational and distortion constants respectively. The energy levels for the other cases given by Miller and Townes (Reference 23) are

$$W(J=N-1) = B_o N(N+1) - B_o(2N-1) - \lambda - \frac{\gamma}{2} + \left[\lambda^2 - 2\lambda\left(B_o - \frac{\gamma}{2}\right) + (2N-1)^2\left(B_o - \frac{\gamma}{2}\right)^2\right]^{\frac{1}{2}}$$

$$W(J=N+1) = B_o N(N+1) + B_o(2N+3) - \lambda - \frac{\gamma}{2} - \left[\lambda^2 - 2\lambda\left(B_o - \frac{\gamma}{2}\right) + (2N+3)^2\left(B_o - \frac{\gamma}{2}\right)^2\right]^{\frac{1}{2}}.$$

Values of the constants given by Miller and Townes and Mizushima and Hill are

B_o = 43,100 MHz λ = 59,501 MHz

B_1 = -0.141 MHz γ = -252 MHz

Figure 19 is the energy level diagram for the region of interest in this report.

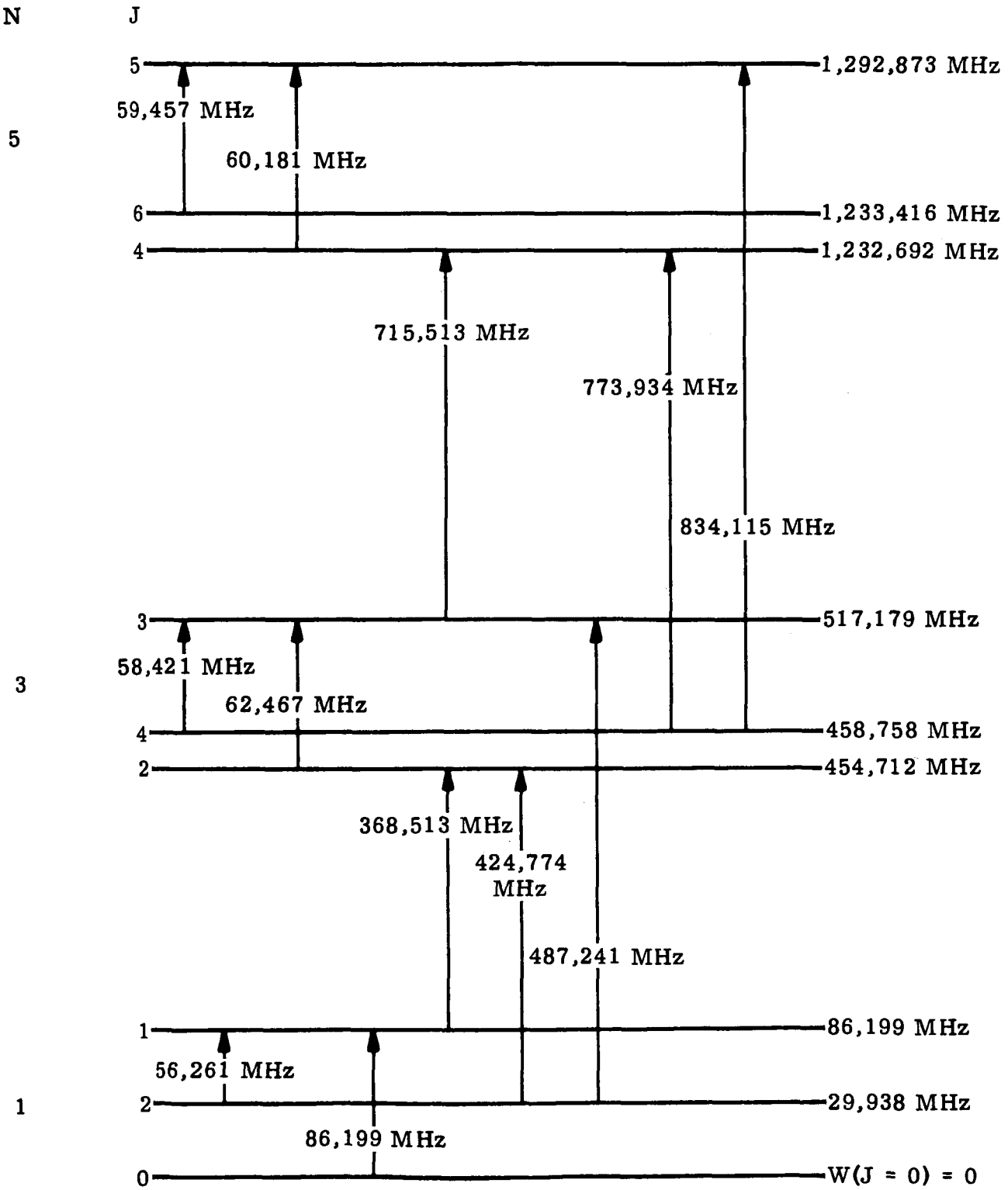

Figure 19. Energy Levels and Transitions in O_2

The lines near 56 GHz and that at 118 GHz are known experimentally (Reference 26). During both years of the contract the lines near 400 GHz were sought unsuccessfully. These lines and those near 800 GHz are weak, however, in the area near 400 GHz they are stronger than the 56 GHz group as shown by calculations by Mizushima (Reference 25). A search for these lines with a Zeeman spectrometer cooled to liquid nitrogen temperatures has been unsuccessful. It is certain that the region where the lines are, was covered. Very probably the best way to observe these lines will be with a Fabry-Perot absorption cell equipped for cooling. The long equivalent path length of the Fabry-Perot makes the observation of weak lines much easier than the conventional cell. It would not be difficult also to equip such a cell with a Zeeman modulation coil to improve the sensitivity since the splitting is 5.6 MHz/Gauss and even a weak uniform field would produce good modulation.

In addition to an experimental search, the literature was examined for evidence of oxygen absorption in the earth's atmosphere for the region above 200 GHz. The work of the far infrared spectroscopists on the observations of the sun through the earth's atmosphere has not revealed any evidence of oxygen absorption, probably because of the masking effects of water. For these reasons the investigation of oxygen was discontinued and the major effort was put into the water investigation.

V. SPECTROSCOPIC INVESTIGATIONS

A. STARK EFFECT OF THE WATER MOLECULE AND DETERMINATION OF THE DIPOLE MOMENT

The dipole moment of water has been previously measured by Birnbaum and Chattergee (Reference 27) and by Golden, et al (Reference 28). Birnbaum and Chattergee employed dielectric relaxation methods, measuring the dielectric constant as functions of temperature. Golden measured the Stark effect on the $5_{-1} - 6_{-5}$ transition near 22 GHz. The value obtained by Birnbaum was $\mu = 1.846 \pm 0.005$ debye; Golden obtained $\mu = 1.94 \pm 0.06$ debye. A third value of 1.884 ± 0.012 debye was obtained by Lichtenstein, Derr, and Gallagher (Reference 29), an average of measurements on the lines:

Transition	Frequency (MHz)
$5_{-1} - 6_{-5}$	22,235.1
$2_2 - 3_{-2}$	183,309.5
$3_1 - 4_{-3}$	380,196.8

The measurement of the dipole moment was motivated by the availability of phase stabilization equipment, by the accessibility of higher frequency lines than previously observed, and by the need for an accurate dipole moment for the calculation of line intensities for water. Previous work by Golden, et al, employed the energy levels of Randall, et al (Reference 30) and obtained the line strengths for H_2O from King, et al (Reference 31) to calculate the Stark coefficients. Better accuracy can be expected by using the energy levels given by Benedict, et al (Reference 32) and the line strength tables of West and Mizushima (Reference 33).

The region from 22 GHz to 520 GHz was searched systematically for water resonant transitions, using the frequencies computed from Benedict, et al, as a guide. His values were obtained from infrared measurements. They were presented with four to six significant figures, but as shown by Table IV, they are accurate to three or four significant figures. Location of lines so poorly known is a time consuming process in this frequency

region, but when they are located, the frequencies can be measured to between six and eight significant figures quite simply. Figure 20 shows the spectrometer.

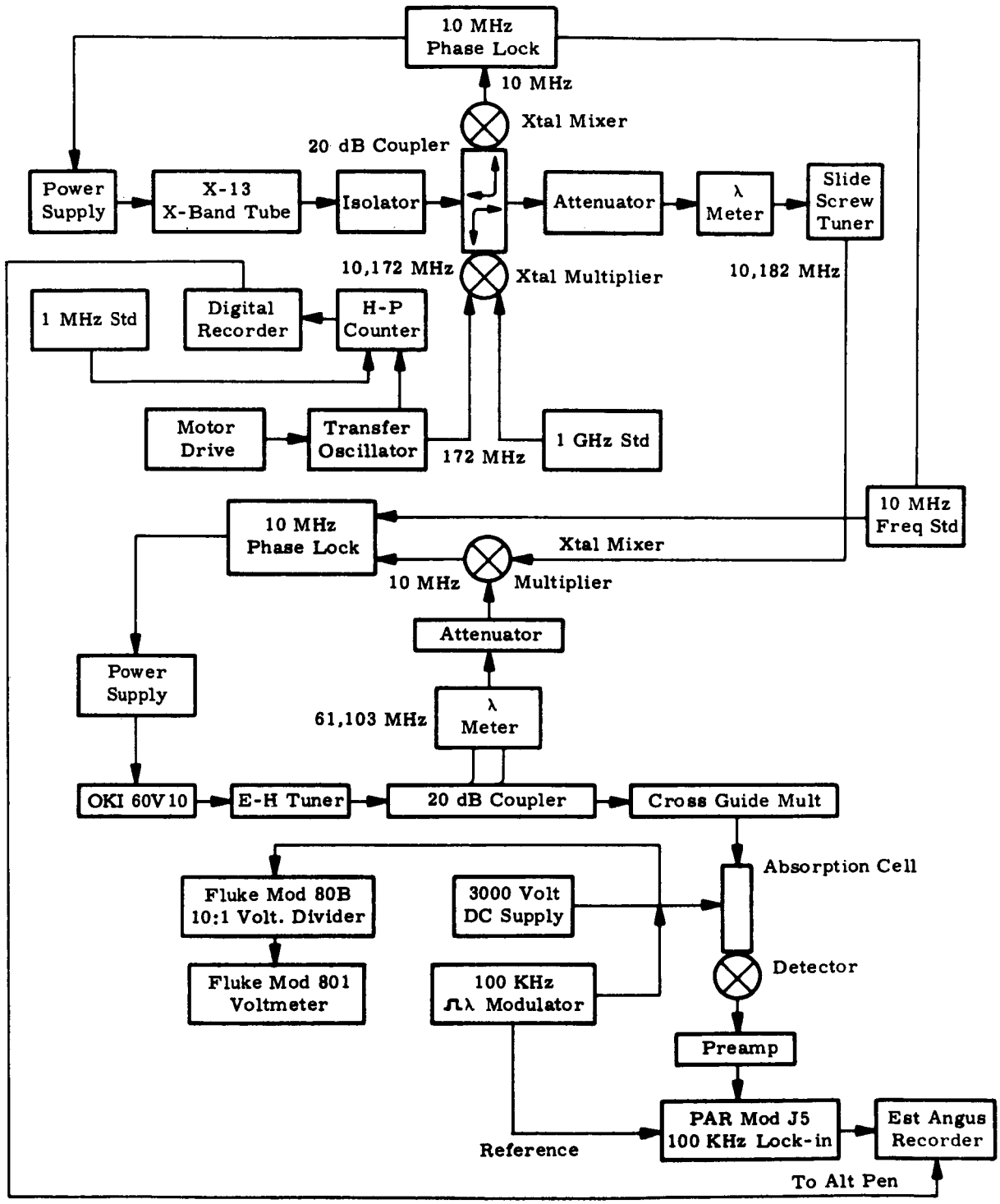

Figure 20. Diagram of Stark Spectrometer

The Stark cell, a conventional RG-96/U waveguide with a center septum for production of the electric field, was calibrated by observing the Stark effect on the OCS molecule and by using the dipole moment of μ = 0.7124 debye given by Marshall and Weber (Reference 47).

The Stark effect measurements were performed with the microwave sources phase-locked to a General Radio Type 1101A frequency standard. A 10 MHz phase-lock apparatus was employed (Figure 21). The outputs of the frequency standard at 1 GHz and 100 MHz were applied to a crystal to generate a frequency 10 GHz from an X-band klystron. A 10 MHz reference for the phase-lock was obtained from a James Knight frequency standard. The X-band radiation was then frequency multiplied from 12090 MHz to 24180 MHz (K-band). This K-band output was mixed with the output of the interpolation oscillator, a stable variable RF oscillator measured by a Hewlett-Packard counter (itself driven by the frequency standard). The output of the counter was recorded digitally by a printer that produced a marker on the recorder trace. The K-band klystron was then swept in the phase-locked condition by varying the interpolation oscillator. In this manner the frequency of the OCS Stark components could be determined.

A dc electric field was applied to the OCS molecule in the Stark cell and modulated for detection purposes with a small 100 kHz square wave. The results of these measurements yielded a septum-waveguide separation of d = 0.0185 cm, comparing favorably with the physical measurement of d = 0.187 cm. The dc field was measured by a calibrated voltage divider and a Leeds and Northrup potentiometer.

A similar phase-lock system was used to measure the Stark effect on the $2_3 \rightarrow 3_{-2}$ rotational transition of H_2O at 183,309.5 MHz, at room temperature (23°C) and 5 microns pressure. The main difference was that a 60V10 (OKI) was used instead of the K-band source, at a frequency equal to 1/3 of 183,309.5 MHz.

Measurement of the $5_{-1} - 6_{-5}$ water Stark transitions at 22,235.1 MHz was performed by using a signal of 22,205 MHz, which is the 233rd harmonic of 95.3 MHz obtained from a Hewlett-Packard 608C signal generator, varied by a motor drive. This frequency was mixed with the output of a K-band oscillator set at 22,234 MHz; the 30 MHz difference frequency was fed into a Dymec oscillator synchronizer unit controlling the K-band klystron. The reference frequency of 10 MHz was obtained from the frequency standard and multiplied by 3 in the Dymec unit. The 608C signal generator was measured by a Hewlett-Packard counter that obtained its 1 MHz reference signal from the frequency standard.

Stark measurements were also performed on the 380,196 GHz line in H_2O, but with less accuracy because the klystron was not phase locked.

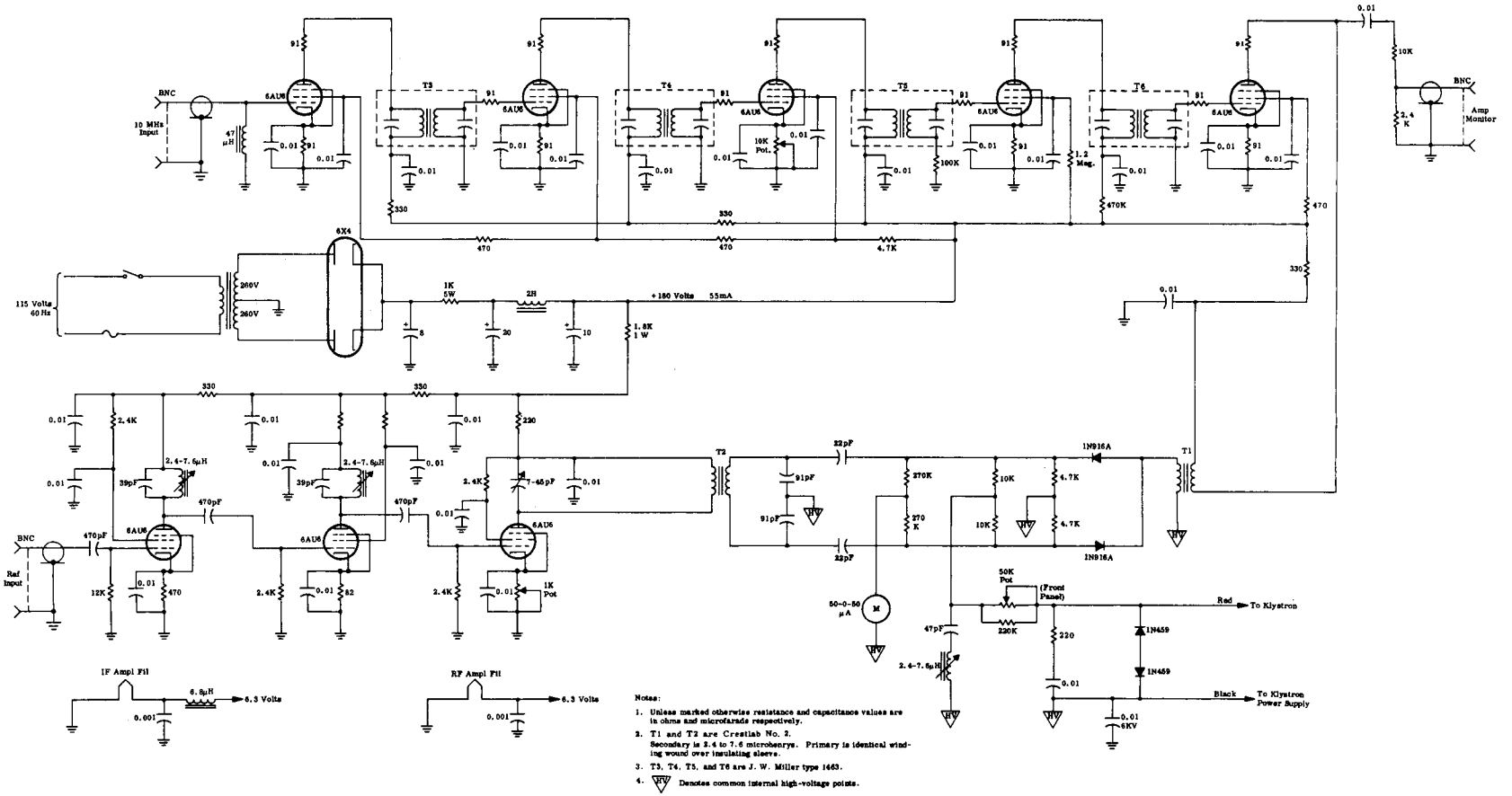

Figure 21. 10 MHz Phase Lock Circuit

However, the line was identified as the $3_1 \rightarrow 4_{-3}$ transition and the measurement of the dipole moment agreed well with the more accurate measurements of the low frequency lines.

The energy levels were obtained from Benedict, and the rotational constants were

$$A = 27.877\ cm^{-1} = 835{,}741\ MHz$$

$$B = 14.512\ cm^{-1} = 435{,}064\ MHz$$

$$C = 9.285\ cm^{-1} = 278{,}361\ MHz,$$

yielding an asymmetry parameter, $\kappa = -0.437715$.

Using the line strengths computed by polynomial interpolation and the energy level differences of Benedict, the Stark splittings may be computed from (Reference 1)

$$J_\tau = 4_{-3} \quad \Delta E_{4_{-3,M_J}} = \mu^2 E^2 \times 10^{-8} \quad (2.40988 - 0.68930 M_J)^2$$

$$J_\tau = 3_{-2} \quad \Delta E_{3_{-2,M_J}} = \mu^2 E^2 \times 10^{-8} \quad (5.02506 - 1.76539 M_J)^2$$

$$J_\tau = 3_{1} \quad \Delta E_{3_{1,M_J}} = \mu^2 E^2 \times 10^{-8} \quad (-2.92964 + 2.09564 M_J)^2$$

$$J_\tau = 2_{2} \quad \Delta E_{2_{2,M_J}} = \mu^2 E^2 \times 10^{-8} \quad (-3.75594 + 3.05474 M_J)^2$$

$$J_\tau = 5_{-1} \quad \Delta E_{5_{-1,M_J}} = \mu^2 E^2 \times 10^{-8} \quad (-10.6818 + 0.62880 M_J)^2$$

$$J_\tau = 6_{-5} \quad \Delta E_{6_{-5,M_J}} = \mu^2 E^2 \times 10^{-8} \quad (11.27364 - 0.45467 M_J)^2$$

These expressions were obtained from the general formula:

$$W_{J_\tau M} = \sum_{x = a,b,c} \frac{\mu_x^2 E^2}{(2J+1)} \sum_{\tau'}{}' \frac{J^2 - M^2}{J(2J-1)} \frac{{}^{x}S_{J_\tau, J-1_{\tau'}}}{W^o_{J_\tau} - W^o_{J-1_{\tau'}}}$$

$$+ \frac{M^2}{J(J+1)} \frac{{}^{x}S_{J_\tau J_{\tau'}}}{W^o_{J_\tau} - W^o_{J_{\tau'}}} + \frac{(J+1)^2 - M^2}{(J+1)(2J+3)} \frac{{}^{x}S_{J_\tau, J+1_{\tau'}}}{W^o_{J_\tau} - W^o_{J+1_{\tau'}}} .$$

For water the first summation is over b only, since the dipole moment of water lies along the b axis. For the summation Σ' is over all states except $J_\tau{}^o$. These are limited in number by the selection rules that allow transitions between states for which $\Delta J = \pm 1$ or 0, and for which $K_{-1}K_{-1}$ change by ee $\leftrightarrow$ oo or eo $\leftrightarrow$ oe. Here e designates even numbers, o, odd numbers.

As an example, the Stark splitting of the line at $J_\tau = 2_2 - 3_{-2}$ is given by

$$\Delta\nu = \mu^2E^2 \times 10^{-8}\left(8.78100 - 4.82013M_J{}^2\right).$$

The only transitions observed are for $\Delta M = 0$, since the radiative electric field is parallel to the dc Stark field. Figure 22 is a recording of the Stark spectrum of this transition. Since the dc is always applied in this measurement, the zero field line is not seen; the advantage of this method is that the Stark components are not obscured by the main line.

Combining the results of this measurement with those on the $5_{-1} - 6_{-5}$ transitions of 22,235 MHz, a value of $\mu = 1.884 \pm 0.012$ debye was obtained.

The measurements on the $3_1 - 4_{-3}$ transition at 380,196.8 MHz yield a dipole moment of $\mu = 1.882$ debye; with a nonstabilized source the rms deviation is $\pm$ 0.062 debye. These results serve to identify the transition, but have not been used in the computation of the dipole moment stated above.

This computation of the second order Stark effect has been performed on the basis of a rigid rotor molecule, without including centrifugal distortion effects. The line strengths have been calculated for $\kappa = -0.437715$. Future changes for the better in the rotational constants of water will be reflected in the evaluation of the dipole moment. Voltage measurements and voltage drifts were less than one part in 10^3. Frequency measurements were accurate to one part in 10^7. The effects of motion of the center septum under the influence of the applied modulation were negligible.

The value of $\mu = 1.884 \pm 0.012$ debye is higher than the value of $\mu = 1.846 \pm 0.005$ debye obtained by dielectric relaxation measurements. Here the molar polarization P is chosen as

$$P = A + \frac{B}{T}$$

However, when an additional temperature term (Van Vleck) is added, modifying the equation to

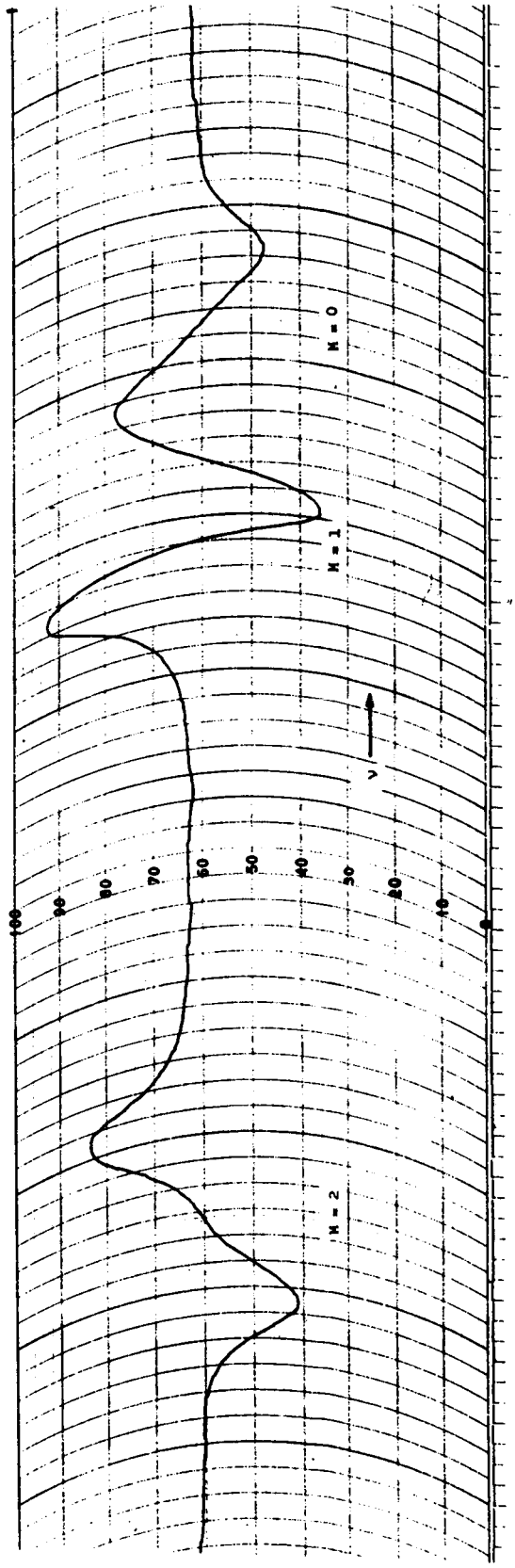

Figure 22. Stark Spectrum of H_2O, 183 GHz, dc Electric Field

$$P = A' + \left(\frac{4\pi N_o \mu^2}{9\ kt}\right)\left(1 - \frac{K}{T}\right),$$

the same dielectric relaxation measurements produce a $\mu = 1.889$ debye (Reference 27). It is suggested, therefore, that the calculation of the polarization requires the Van Vleck term.

It must be noted that the calculations of the dipole moment are strongly dependent on the energy levels and the line strengths, and any inaccuracy in their values can lead to unrealibility in the quoted value of the dipole moment. Recent calculations of the lines by S. A. Clough and W. Benedict have given better fits than previously obtained. There was not enough time to recalculate the dipole, but this will be done in the future and appropriately reported.

B. OBSERVATION OF D_2O

The D_2O molecule, chemically similar to water with the hydrogen replaced by deuterium offers an opportunity to study transitions which, in H_2O, would be at such a high frequency that the lack of power would make measurements difficult. Some of the transitions lie within the range of the carcinotron, 270 GHz to 315 GHz, and therefore can be observed with a good signal-to-noise ratio through the Fabry-Perot interferometer. Several lines have been calculated to lie in this region from constants of low accuracy by rigid rotor formulae. Table III shows the lines calculated. The following lines were observed:

GHz	Strong Medium, Weak
317.8	M
313.8	S
311.8	W
308.0	M
307.0	M
304.5	W

A = 461,284 MHz, B = 217,417 MHz, C = 145,048 MHz, $\kappa = -0.54232$ are the asymmetric rotor constants for D2O. It is not certain that all lines in the range were found, since the carcinotron has a variable power output spectrum, with many deep nulls. The identification of these lines is not complete; it is expected that future Stark effect studies will provide positive identification and will be published. The strongest line in the group, at

313.8 GHz, is strong enough to go to the baseline when displayed in the center of the Fabry-Perot mode. This makes it highly probable that this line is the $1_{-1} - 1_1$ transition calculated by rigid rotor formulae to be at 316 GHz.

TABLE III

Calculated D_2O Rotational Line Frequencies in MHz

$2_2 \rightarrow 3_{-2}$ 8,314	$4_2 \rightarrow 5_{-2}$ 327,575	$4_{-2} \rightarrow 4_0$ 692,267
$3_3 \rightarrow 4_{-1}$ 29,065	$5_2 \rightarrow 6_0$ 398,371	$3_{-1} \rightarrow 3_1$ 698,926
$4_3 \rightarrow 5_1$ 50,592	$2_{-2} \rightarrow 2_0$ 402,459	$6_0 \rightarrow 7_{-4}$ 707,555
$7_7 \rightarrow 8_3$ 65,615	$7_{-3} \rightarrow 8_{-7}$ 406,359	$4_1 \rightarrow 5_{-1}$ 712,726
$7_5 \rightarrow 8_1$ 69,861	$2_1 \rightarrow 3_{-1}$ 454,683	$7_{-1} \rightarrow 8_{-5}$ 731,831
$5_{-1} \rightarrow 6_{-5}$ 91,855	$6_5 \rightarrow 7_3$ 459,708	$2_0 \rightarrow 2_2$ 745,549
$4_4 \rightarrow 5_0$ 95,166	$6_6 \rightarrow 7_2$ 460,712	$5_{-3} \rightarrow 5_{-1}$ 750,913
$6_{-2} \rightarrow 7_{-6}$ 110,270	$1_0 \rightarrow 2_{-2}$ 467,208	$4_{-4} \rightarrow 4_{-2}$ 781,034
$6_3 \rightarrow 7_1$ 117,237	$7_3 \rightarrow 8_{-1}$ 508,014	$2_{-1} \rightarrow 3_{-3}$ 849,682
$3_1 \rightarrow 4_{-3}$ 150,328	$3_{-3} \rightarrow 3_{-1}$ 553,710	$6_{-4} \rightarrow 6_{-2}$ 892,024
$4_0 \rightarrow 5_{-4}$ 181,266	$5_1 \rightarrow 6_{-3}$ 563,845	$1_{-1} \rightarrow 2_{-1}$ 896,430
$3_2 \rightarrow 4_0$ 212,657	$7_2 \rightarrow 8_0$ 582,151	$6_1 \rightarrow 7_{-1}$ 901,545
$5_4 \rightarrow 6_2$ 264,598	$0_0 \rightarrow 1_0$ 606,333	$3_0 \rightarrow 4_{-2}$ 928,617
$5_5 \rightarrow 6_1$ 272,025	$6_2 \rightarrow 7_2$ 623,231	$7_1 \rightarrow 8_{-3}$ 932,851
$5_3 \rightarrow 6_{-1}$ 273,908	$7_6 \rightarrow 8_4$ 650,528	$2_{-1} \rightarrow 2_1$ 948,709
$1_{-1} \rightarrow 1_1$ 316,236	$7_7 \rightarrow 8_3$ 650,648	

TABLE IV

Parameters of H_2O for Transitions from 22 to 1200 GHz

Transition Low to High	Δcm^{-1} (Benedict by diff.)	ν Benedict by diff.	ν Observed	$\lvert\mu_{ij}\rvert^2$ x 10^{-38}	$e^{-W_l/kT}$ T = 295°K	$e^{-W_u/kT}$ T = 295°K	Linestrengths x 10^{-6}	Linewidth Δij Benedict (GHz)	Linewidth Δij Observed (GHz)	Temp. Coeff. n	ν (computed) Clough and Benedict
$5_{-1} - 6_{-5}$	0.74	22,183	22,235	1.78	$5_{-1} = 0.11327$	$6_{-5} = 0.11286$	55,217	2.70	2.61*	0.626	22,235.21
$15_{-9} - 14_{-3}$	3.8	113,914			$15_{-9} = 2.9687 \times 10^{-7}$	$14_{-3} = 2.9157 \times 10^{-7}$			H_2O:H_2O 16.7 ‡		
$2_2 - 3_{-2}$	6.12	183,462	183,310	7.218	$2_2 = 0.51474$	$3_{-2} = 0.49957$	101,702	2.877	H_2O:N_2 3.19 ‡	0.649	183,307.76
$14_{-8} - 13_{-2}$	7.9	236,823			$14_{-8} = 1.5641 \times 10^{-6}$	$13_{-2} = 1.5048 \times 10^{-6}$					
$16_{-10} - 15_{-4}$	8.3	248,814			$16_{-10} = 5.215 \times 10^{-8}$	$15_{-4} = 5.008 \times 10^{-8}$					
$15_{-10} - 14_{-6}$	10.6	317,762			$15_{-10} = 8.199 \times 10^{-7}$	$14_{-6} = 7.786 \times 10^{-7}$					247,872.60
$9_{-3} - 10_{-7}$	10.78	323,159		1.505	$9_{-3} = 0.001914$	$10_{-7} = 0.0018158$	80,582.825	2.29		0.420	321,205.76
$4_0 - 5_{-4}$	10.86	325,557	325,153	3.531	$4_0 = 0.21438$	$5_{-4} = 0.20329$	89,540.433	2.785		0.619	325,148.63
$15_{-7} - 14_{-1}$	12.2	365,727			$15_{-7} = 1.2907 \times 10^{-7}$	$14_{-1} = 1.2157 \times 10^{-7}$					
$15_{-3} - 14_3$	12.6	377,718			$15_{-3} = 4.390 \times 10^{-8}$	$14_3 = 4.2242 \times 10^{-8}$					
$3_1 - 4_{-3}$	12.67	379,816	380,196	6.229	$3_1 = 0.35526$	$4_{-3} = 0.33397$	122,878	2.84		0.630	380,193.91
$11_{-8} - 10_{-4}$	13.00	389,709		0.9795	$11_{-8} = 5.870 \times 10^{-4}$	$10_{-4} = 5.5095 \times 10^{-4}$	57,959.569				390,699.51
$6_6 - 7_{-2}$	14.53	435,574		2.315	$6_6 = 0.006108$	$7_2 = 0.005690$	84,821.756	1.498		0.290	438,400.39
$5_5 - 6_1$	14.66	439,472		3.183	$5_5 = 0.026783$	$6_1 = 0.02494$	98,658.045				439,774.39
$6_5 - 7_3$	14.74	441,870		2.316	$6_5 = 0.006108$	$7_3 = 0.005684$	84,843.807				444,052.15
$3_3 - 4_{-1}$	14.98	449,064	448,000	6.673	$3_3 = 0.24855$	$4_{-1} = 0.23103$	131,627.00	2.47		0.510	447,995.23
$5_4 - 6_2$	15.60	467,651		3.191	$5_4 = 0.026783$	$6_2 = 0.024823$	98,906.370	1.885		0.380	471,479.16
$4_4 - 5_0$	15.83	474,545		4.591	$4_4 = 0.09243$	$5_0 = 0.085564$	116,428.71	2.068		0.380	474,875.00
$7_{-6} - 6_{-2}$	16.29	486,836		0.9378	$7_{-6} = 0.057237$	$6_{-2} = 0.052877$	34,353.424				488,490.65
$15_{-2} - 16_{-8}$	16.30	488,635			$15_{-2} = 2.1016 \times 10^{-8}$	$16_{-8} = 1.941 \times 10^{-8}$					
$7_7 - 8_3$	16.74	501,825		1.757	$7_7 = 0.0011092$	$8_3 = 0.0010228$	74,276.854	1.27		0.320	504,474.53
$7_6 - 8_4$	16.74	501,825		1.757	$7_6 = 0.0011092$	$8_4 = 0.0010228$	74,279.539	1.27		0.340	505,380.19
$13_{-5} - 14_{-9}$	17.36	520,411			$13_{-5} = 4.280 \times 10^{-6}$	$14_{-9} = 3.9323 \times 10^{-6}$					532,564.22
$13_{-7} - 12_{-1}$	18.19	545,293			$13_{-7} = 7.6175 \times 10^{-6}$	$12_{-1} = 6.9707 \times 10^{-6}$		1.649		0.071	
$1_{-1} - 1_1$	18.58	556,984		177.45	$1_{-1} = 0.8905$	$1_1 = 0.81336$	1,500,000	3.33		0.645	556,937.36
$14_2 - 14_4$	20.20	605,548			$14_2 = 4.556 \times 10^{-8}$	$14_4 = 4.128 \times 10^{-8}$					
$14_1 - 14_3$	20.42	612,143			$14_1 = 4.556 \times 10^{-8}$	$14_3 = 4.128 \times 10^{-8}$					
$4_3 - 5_1$	20.63	618,438		4.703	$4_3 = 0.9244$	$5_1 = 0.083586$	119,263.31	2.28		0.600	620,862.06
$8_7 - 9_5$	21.67	650,100		1.378	$8_7 = 0.00016212$	$9_5 = 0.00014585$	66,041.922	1.139		0.400	645,788.16
$8_8 - 9_4$	21.67	650,100		1.378	$8_8 = 0.00016212$	$9_4 = 0.00014585$	66,041.974	1.139		0.400	645,651.03
$2_{-2} - 2_0$	25.11	753,300		14.728	$2_{-2} = 0.71058$	$2_0 = 0.62865$	2,075,019.4	3.129		0.690	752,034.36
$11_{-7} - 10_{-1}$	28.51	855,300		1.258	$11_{-7} = 0.00026179$	$10_{-1} = 0.0002278$	74,488.050	1.96		0.180	
$13_{-9} - 12_{-3}$	28.65	859,500			$13_{-9} = 1.7368 \times 10^{-5}$	$12_{-3} = 1.5104 \times 10^{-5}$		2.00		0.200	
$9_8 - 10_6$	28.99	869,700		1.1103	$9_8 = 1.9282 \times 10^{-5}$	$10_6 = 1.6738 \times 10^{-5}$	59,443.715				862,771.06
$9_9 - 10_5$	28.99	869,700		1.1103	$9_9 = 1.9282 \times 10^{-5}$	$10_5 = 1.6738 \times 10^{-5}$	59,443.646				862,753.67
$8_{-2} - 9_{-6}$	30.31	909,300		9.588	$8_{-2} = 0.005959$	$9_{-6} = 0.005140$	459,305.15	2.39		0.510	906,292.44
$3_2 - 4_0$	30.48	916,400		8.171	$3_2 = 0.24873$	$4_0 = 0.21438$	161,165.71	2.589		0.676	916,180.27
$4_2 - 5_{-2}$	32.26	967,800		10.348	$4_2 = 0.15375$	$5_{-2} = 0.13135$	262,442.00	2.476		0.560	970,283.10
$1_0 - 2_{-2}$	32.93	987,900		89.315	$1_0 = 0.83436$	$2_{-2} = 0.71058$	754,987.05	3.09		0.660	987,946.88
$14_{-10} - 13_{-4}$	35.50	1,065,000			$14_{-10} = 3.9416 \times 10^{-6}$	$13_{-4} = 3.3153 \times 10^{-6}$					

TABLE IV (Cont)

Transition Low to High	Δcm^{-1} (Benedict by diff.)	ν Benedict by diff.	ν Observed	$\lvert\mu_{ij}\rvert^2$ x 10^{-38}	$e^{-W_\ell/kT}$ T = 295°F	$e^{-W_u/kT}$ T = 295°F	Linestrengths x 10^{-6}	Linewidth Δij Benedict (GHz)	Linewidth Δij Observed (GHz)	Temp. Coeff. n	ν (computed) Clough and Benedict
$12_{-6} - 11_0$	36.31	1,089,300			$12_{-6} = 3.4433 \times 10^{-5}$	$11_0 = 2.8842 \times 10^{-5}$		1.80		0.180	
$3_{-3} - 3_{-1}$	36.59	1,097,700		110.7137	$3_{-3} = 0.5132$	$3_{-1} = 0.42931$	2,183,703.5	2.98		0.701	1,097,364.89
$10_{-6} - 9_0$	36.95	1,108,500		1.025	$10_{-6} = 0.0008979$	$9_0 = 0.00074976$	54,878.021	1.95		0.202	
$0_0 - 1_0$	37.13	1,113,900		354.9	$0_0 = 1$	$1_0 = 0.83436$	1,000,000	3.008		0.689	
$8_{-7} - 7_{-3}$	38.27	1,148,100		0.5539	$8_{-7} = 0.02652$	$7_{-3} = 0.022003$	23,415.684				1,146,669.82
$2_1 - 3_{-1}$	38.45	1,153,500		21.2861	$2_1 = 0.51784$	$3_{-1} = 0.42931$	299,889.95	2.85		0.610	1,153,135.15
$12_{-9} - 11_{-5}$	38.59	1,157,700			$12_{-9} = 1.7375 \times 10^{-4}$	$11_{-5} = 1.4395 \times 10^{-4}$					1,155,256.32
$5_3 - 6_{-1}$	38.63	1,158,900		8.9822	$5_3 = 0.050935$	$6_{-1} = 0.042185$	278,403.79	2.137		0.399	
$10_9 - 11_7$	38.64	1,159,200		0.9132	$10_9 = 1.8863 \times 10^{-6}$	$11_7 = 1.5623 \times 10^{-6}$	54,040.436				1,155,953.51
$10_{10} - 11_6$	38.64	1,159,200		0.9132	$10_{10} = 1.8863 \times 10^{-6}$	$11_6 = 1.5623 \times 10^{-6}$	54,040.531				1,155,954.41
$7_5 - 8_1$	38.80	1,164,000		5.2488	$7_5 = 0.002649$	$8_1 = 0.0021923$	221,845.03	1.546		0.290	
$3_{-1} - 3_1$	38.80	1,164,000		128.853	$3_{-1} = 0.42931$	$3_1 = 0.35526$	2,541,485	2.84		0.682	
$6_4 - 7_0$	39.05	1,171,500		6.8502	$6_4 = 0.013101$	$7_0 = 0.010828$	250,924.07	1.94		0.360	
$7_4 - 8_2$	39.59	1,187,700		5.255	$7_4 = 0.002649$	$8_2 = 0.0021838$	222,109.59	1.62		0.300	
$15_{-4} - 14_4$	39.60	1,188,000			$15_{-4} = 5.008 \times 10^{-8}$	$14_4 = 4.1376 \times 10^{-8}$					
$4_{-2} - 4_0$	40.25	1,207,500		144.1005	$4_{-2} = 0.26086$	$4_0 = 0.21437$	3,654,283.2	2.85		0.720	1,207,650.11
$16_{-11} - 15_{-7}$	40.50	1,215,000			$16_{-11} = 1.572 \times 10^{-7}$	$15_{-7} = 1.2901 \times 10^{-7}$					
$8_6 - 9_2$	40.74	1,222,200		4.1283	$8_6 = 0.00042668$	$9_2 = 0.0003498$	197,749.99	1.33		0.320	1,216,195.29
$8_5 - 9_3$	40.88	1,226,400		4.1288	$8_5 = 0.00042668$	$9_3 = 0.00034954$	197,777.25	1.34		0.340	1,220,304.21
$2_0 - 2_2$	40.98	1,229,400		89.3151	$2_0 = 0.62865$	$2_2 = 0.51471$	1,258,314.4	2.935		0.670	1,228,801.82

*Becker and Autler

‡This task

VI. CONTRIBUTIONS TO THE DEVELOPMENT OF THE THEORY OF SPECTRAL LINE WIDTHS

A. ORIENTATION RELAXATION IN SYMMETRICAL-TOP GASES AND BINARY GAS MIXTURES

A theory of orientation relaxation has been developed which will be summarized in this report. Details may be found in an article by L. Frenkel (Reference 34). The frequency dependence of the absorption coefficient in the dielectric behavior of gases is governed by

$$\alpha = \frac{C\omega^2 \Gamma}{1 + \omega^2 \Gamma^2} \tag{11}$$

where C is a constant and Γ is a measure of the average time between collisions which randomly reorient the dipole (Reference 2). By kinetic theory Γ may be determined if each collision can take a molecule from any populated initial state to any final state. Under this assumption of strong collisions the parameter Γ is given by kinetic theory as

$$\Gamma^{-1} = \pi\, b_{eff}^2\, \bar{v}\, N, \tag{12}$$

where b_{eff} is the effective collision diameter, $\bar{v}$ is the average velocity, and N the number of molecules in a unit volume. However, Equation (11) is still correct for the case of weak collisions, where the initial orientation is remembered through many successive collisions if the probability of a reorientation of the dipole moment from solid angle element $d\Omega$ to $d\Omega'$ depends only on the angle between the elements i.e., $A_{\Omega,\Omega}\, d\Omega\, d\Omega' = f(\theta)\, d\theta$ and if Γ is replaced by Γ',

$$\Gamma' = (\gamma - \delta)^{-1}$$

where

$$\gamma = \iint d\Omega\, d(\theta) \text{ and } \delta = \iint d\Omega\, f(\theta) \cos\theta.$$

Thus calculation of $(\Gamma')^{-1} = \int\int f(\theta)\,(1 - \cos\theta)\,d\theta$ will allow calculation of Γ'. Calculation of this quantity is difficult because of the form of $f(\theta)$, and it is normally best found by the measurement of the nonresonant absorption of microwaves in symmetric top gases (Reference 35). However, a macroscopic phenomenalogical model may be devised which will permit a calculation of the cross sections and shed some light on intermolecules interactions.

The colliding molecules are divided into groups according to the internal angular momentum $\hbar J$ of the top, the relative velocity of approach v and the impact parameter b. The plan is to determine the equivalent number of strong collisions in order to determine the parameters of Equation (12). The first assumption is that only those collisions are considered strong in a given partial cross section $2\pi b\,db$ for which $m_r vb/\hbar J \geq \phi$ where ϕ is a constant assumed the same for all gases. m_r is the mass of the rotor. Its value is to be determined from experimental data. An alternative way of stating this assumption is; only those collisions are to be counted for which the input parameter is larger than $b_{min}(J,v) = \phi\,(\hbar J/m_r v)$.

By defining a maximum impact parameter

$$b_{max}(v) = b_o\left[1+(2\epsilon/v^2 m_r)\right]^{\frac{1}{2}}$$

where b_o is the hard core impact parameter and ϵ is the potential energy at b_o we may state the second assumption; count only those binary collisions in the velocity range (v,v + dv) which actually result in a collision within the hard core b_o for which it is less than b_{max}. The factor $[1 + (2\epsilon/mv^2)]$ may be interpreted as the contribution to the effective collision cross section arising from the bending of the path as encounter nears. The total number of equivalent strong collisions per unit time and volume in the range (v,v + dv;J) is

$$\eta(v,J,K) = \frac{N}{2}\left\{\frac{Ndv}{P_{JK}P_v}\left[(2J+1)\exp\left(-\frac{\alpha J^2+\beta K^2}{kT}\right)\right]\right.$$

$$\left.\left[4\pi v^3\exp\left(-\frac{v^2 m}{2kT}\right)\right]\right\}\int_{b_{min}}^{b_{max}} 2\pi b\,db, \qquad (13)$$

where P_v and P_{JK} are partition functions, J and K are symmetric top quantum numbers, $\alpha = \hbar^2/2I_B$, $\beta = \hbar^2\,[1/2I_A - 1/2I_B]$, N = number molecules per unit volume, and k = Boltzmann constant and T = absolute temperature.

The total number of equivalent strong collisions is then obtained by summing Equation (13) over J and K and integrating over velocity. By proper attention to the limits of integration, affected by the values of b_{min} and b_{max}, by replacing the symmetric top by an equivalent spherical top of effective moment of inertia $I = 1/2\ (I_A + I_B)$, thus eliminating K from the summation, and replacing the summations by integrations we may obtain a value for η_{eff}. Then a quantity $Z = \eta_{tot}/\eta_{eff}$

where

$$\eta_{tot} = \frac{\pi b_o^2}{2P_v} N^2 \int 4\pi v^3 \exp\left(\frac{-v^2 m}{kT}\right)$$

may be defined which is the ratio of all collisions occurring per unit time to the equivalent strong collisions. The result of the calculation is:

$$Z = \left\{ \frac{F(1+3F)\exp(-FT^*)^{-1}}{(\pi FT^*)^{\frac{1}{2}}(1+F)} + \exp\left(\frac{1}{T^*}\right)(1+F)\,\Phi\left[\frac{2(1+F)}{FT^*}\right]^{\frac{1}{2}} + \left(1 + T^{*-1} - \frac{3F}{2}\right)\left[1 - \Phi\left(\frac{2}{FT^*}\right)^{\frac{1}{2}}\right] \right\}^{-1}$$

where

Φ is the standard error function and $F = \frac{\phi^2 I}{m b_o^2}$ and $T^* = \left(\frac{\epsilon}{kT}\right)^{-1}$.

The general agreement between the model presented and experiment lends some plausibility to the basic assumption that the ratio of internal angular momentum to orbital angular momentum is an important quantity in deciding the efficiency of a collision. Further discussion and details may be found in the article by L. Frenkel (Reference 34).

B. MICROWAVE ABSORPTION IN CO_2

As part of the effort to develop the theory of absorption in gases, experiments were performed on carbon dioxide CO_2 (Reference 36). Carbon dioxide is of only small importance in the atmosphere of the earth as far as absorption of radiation in the region 100 to 1000 GHz is concerned, but it may be of great importance on Venus.

Since carbon dioxide has no permanent dipole moment, the unperturbed molecule does not absorb in the microwave region. Non-resonant absorption of radiation has been detected by A. A. Maryott and G. Birnbaum (Reference 37) in compressed CO_2 near 9 and 22 GHz, and H. A. Gebbie and W. B. Stone (Reference 38) observed a broad resonant absorption region in the far infrared. This absorption is probably due to the quadruple moments of induced dipoles which develop during collisions. Measurement of the loss at points between these can give an indication of the frequency dependence of the effect.

The measurements were made at 800 torr and room temperature and 150 and 300 GHz. At 300 GHz a loss tangent of 1.2×10^{-7} was measured, while at 150 GHz no losses were noted. The instrumental loss tangent sensitivity was approximately 5×10^{-8}.

Tentatively, there is a minimum loss between the centimeter and far infrared regions, especially between the centimeter region and one millimeter wavelength. The losses detected at 300 GHz were probably due to the low frequency wing of the far infrared bands.

VII. DEVELOPMENTAL COMPUTATIONAL METHODS FOR ASYMMETRIC TOP MOLECULES

A. CALCULATION OF ASYMMETRIC RIGID ROTOR ENERGY LEVELS

The water molecule is the particularly complex type known as asymmetrical, characterized by the inequality of its principal moments of inertia. Standard methods of computation for the rigid rotor asymmetric top molecules exist and are summarized here. However when it is necessary to take into account the stretching of the molecule under the centrifugal forces of rotation, one must employ approximations such as the Kivelson-Wilson method or diagonalize the secular equation. It is here that economics enters the picture, since the extensive computations of the more accurate method require much computing machine time and the Kivelson-Wilson method is a considerably cheaper operation. However, for such a molecule as water which is very asymmetrical, the Kivelson-Wilson method does not give very good prediction and computing costs must be balanced against the time spent searching in the laboratory.

The energy levels of an asymmetric rigid rotor may be determined through the solution of the operator equation (References 7 and 39)

$$\overline{H}\psi = (a\overline{P}_x^{\,2} + b\overline{P}_y^{\,2} + c\overline{P}_z^{\,2})\,\psi = w_o\psi$$

where

$\overline{H}$	=	Hamiltonian operator
$\overline{P}_x$, $\overline{P}_y$, $\overline{P}_z$	=	angular momentum operators in a body-fixed principal axis coordinate system
a, b, c	=	molecular constants associated with the moments of inertia of the molecule and chosen so that $a \geq b \geq c$
w_o	=	energy of the rigid rotor
ψ	=	wave function of the rigid rotor

A direct solution to this equation is not possible unless b = a (the oblate symmetric rotor). In these cases the energy is:

$$w_o = aJ(J+1) - (a-c)\,K^2 \qquad \text{for the oblate rotor,}$$

$$w_o = cJ(J+1) + (a-c)\,K^2 \qquad \text{for the prolate rotor,}$$

where

$J = 0, 1, 2, \ldots$

$K = 0, 1, 2, \ldots, J - 1, J$.

In all other cases the Hamiltonian matrix must be diagonalized.

An asymmetry parameter useful in the solution of this problem is

$$\kappa = \frac{2b - a - c}{a - c}$$

Since $a \geq b \geq c$ it is seen that $-1 \leq \kappa \leq 1$, and that $\kappa = 1$ corresponds to the oblate symmetric rotor ($b = a$) while $\kappa = -1$ corresponds to the prolate symmetric rotor ($b = c$).

It is apparent that, for a given J value, a general asymmetric rigid rotor state may be specified by the K values of the limiting oblate and prolate symmetric rotors. Denoting the value of K in the oblate symmetric rotor limit ($\kappa = 1$) by K_1 and in the prolate limit ($\kappa = -1$) by K_{-1}, the energy levels are specified by the notation JK_{-1}, K_1. Another useful notation is obtained through the use of an index, τ, which assumes the $2J + 1$ integral values $-J \leq \tau \leq J$ such that $\tau = J$ identifies the level of highest energy and $\tau = -J$ identifies the level of lowest energy for a given value of J. $\tau = K_{-1} - K_1$. Asymmetric rigid rotor levels may also be specified by the notation J_τ.

The use of these quantities generates a considerable reduction in the labor required to diagonalize the Hamiltonian matrix. It is found that the energy may be written in the form:

$$w_o = \frac{a + c}{2} J(J + 1) + \frac{a - c}{2} E_\tau^J(\kappa)$$

where the quantity $E_\tau^J(\kappa)$, called the reduced energy, is found by diagonalization of the one of four matrices, designated as E^+, E^-, O^+, and O^-. These matrices have the form:

$$\begin{pmatrix} k_o & 1 & 0 & 0 & 0 & \cdots \\ b_1 & k_1 & 1 & 0 & 0 & \cdots \\ 0 & b_2 & k_2 & 1 & 0 & \cdots \\ 0 & 0 & b_3 & k_3 & 1 & \cdots \\ & & & & & \\ \cdots & \cdots & \cdots & \cdots & \cdots & \cdots \\ \cdots & \cdots & \cdots & \cdots & \cdots & \cdots \end{pmatrix}$$

the matrix elements being

$$E^+: k_m = FJ(J+1) + (G-F)(2m)^2$$
$$b_1 = 2H^2 f(J, 1)$$
$$b_m = H^2 f(J, 2m - 1) \qquad (m \neq 1)$$

where

$m = 0, 1, 2, \ldots, J/2$ for J even $\qquad (k = 2m)$

$= 0, 1, 2, \ldots, (J-1)/2$ for J odd

$$E^-: k_m = FJ(J+1) + (G-F)\left[2(m+1)\right]^2$$
$$b_m = H^2 f(J, 2m+1)$$

where

$m = 0, 1, 2, \ldots, (J-2)/2$ for J even, $\qquad \left[k = 2(m+1)\right]$

$= 0, 1, 2, \ldots, (J-3)/2$ for J odd

$$O^{\pm}: k_o = FJ(J+1) + (G-F) \pm H\sqrt{f(J, 0)}$$
$$k_m = FJ(J+1) + (G-F)(2m+1)^2 \qquad m \neq 0$$
$$b_m = H^2 f(J, 2m)$$

where

$m = 0, 1, 2, \ldots, (J-2)/2$ for J even

$= 0, 1, 2, \ldots, (J-1)/2$ for J odd.

The proper matrix and the values of F, G, H, and K are determined by the parity (even or odd) of J, K_{-1}, and K_1 and the polarity of κ(positive or negative) in accordance with the following tables.

and

$$f(J,K) = 1/4\left[(J-K)(J-K+1)(J+K)(J+K+1)\right] .$$

A polynomial solution to the secular equation produces the correct eigenvalues but does not identify the energy states to which they belong. One diagonalization process which retains this information is the continued fraction approach. The eigenvalue associated with the level $J_{K_{-1}}, K_1$ is found by

1 Choosing the proper matrix from Table V

2 Choosing the proper identification of K with K_{-1} or K_1 from Table VI

3 Calculating the value of m

4 Expanding the matrix about the chosen m value as shown below

$$\lambda_m = k_m - \cfrac{b_m}{k_{m-1} - \lambda_m - \cfrac{b_{m-1}}{k_{m-2} - \lambda_m - \cdots}} - \cfrac{b_{m+1}}{k_{m+1} - \lambda_m - \cfrac{b_{m+2}}{k_{m+2} - \lambda_m - \cdots}}$$

where $\lambda_m = E_\tau^J(\kappa)$ for the energy state associated with the chosen value of m.

TABLE V

Reduced Energy Matrix Selection

		Polarity of κ			
		Negative		Positive	
K_{-1}	K_1	J Even	J Odd	J Even	J Odd
Even	Even	E^+	E^-	E^+	E^-
Even	Odd	E^-	E^+	O^-	O^+
Odd	Even	O^+	O^-	E^-	E^+
Odd	Odd	O^-	O^+	O^+	O^-

TABLE VI

Matrix Constants

	Polarity of K	
	Negative	Positive
F	$\frac{\kappa - 1}{2}$	$\frac{\kappa + 1}{2}$
G - F	$-\frac{\kappa - 3}{2}$	$-\frac{\kappa + 3}{2}$
H	$-\frac{\kappa + 1}{2}$	$\frac{\kappa - 1}{2}$
K	K_{-1}	K_1

B. KIVELSON - WILSON THEORY OF CENTRIFUGAL EFFECTS

The rigid rotor solution does not account for the effects of centrifugal stretching of the chemical bonds of the molecule as it rotates at different angular rates. It can be shown (Reference 40) that such effects may be included in the Hamiltonian by an expansion of the form

$$\overline{H} = \sum_{\alpha\beta} \phi_{\alpha\beta} \overline{P}_\alpha \overline{P}_\beta + \sum_{\mu\nu\xi\zeta} \tau_{\mu\nu\xi\zeta} \overline{P}_\mu \overline{P}_\nu \overline{P}_\xi \overline{P}_\zeta + O(\overline{P}^6) + \ldots .$$

where each of the indices are summed over the three space coordinates. The first term is the rigid rotor Hamiltonian, while the second introduces the effects of centrifugal distortion. The Kivelson-Wilson theory (Reference 41) consists of an approximate calculation of the energy levels due to the first two terms through the use of first order perturbation theory.

If the rigid rotor term is taken to be the zero order approximation and the centrifugal distortion term is taken to be the perturbation Hamiltonian, then the Hamiltonian becomes

$$\overline{H} = \overline{H}_o + \overline{H}_1$$

where

$\overline{H}_o$ = rigid rotor term

$\overline{H}_1$ = centrifugal distortion term

and the energy of the system is

$$w = w_o + \left\langle \overline{\overline{H}}_1 \right\rangle . \tag{14}$$

Here, the brackets indicate the diagonal terms (average values) of the enclosed quantity in a basis which diagonalizes $\overline{\overline{H}}_o$.

Since this calculation is based on first order perturbation only the diagonal elements of $\overline{\overline{H}}_1$ are required, and in most cases of interest many of these terms are zero. It can be shown that the only distortion terms which enter into the calculation are those with coefficients of the form

$$\tau_{\mu\mu\mu\mu}$$

$$\tau_{\mu\mu\nu\nu} = \tau_{\nu\nu\mu\mu}$$

$$\tau_{\mu\nu\mu\nu} = \tau_{\mu\nu\nu\mu} = \tau_{\nu\mu\nu\mu}.$$

Combining these terms with the commutation rules for angular momentum, the Hamiltonian may be reduced from the form

$$\overline{\overline{H}} = H_o' + \overline{\overline{H}}_1'$$

$$\overline{\overline{H}}_o' = a\overline{P}_x^{\,2} + b\overline{P}_y^{\,2} + c\overline{P}_z^{\,2}$$

$$\overline{\overline{H}}_1' = \frac{1}{4} \sum_{\mu\nu\xi\zeta} \tau_{\mu\nu\xi\zeta}\, \overline{P}_\mu\, \overline{P}_\nu\, \overline{P}_\xi\, \overline{P}_\zeta$$

to the form

$$\overline{\overline{H}} = \overline{\overline{H}}_o + \overline{\overline{H}}_1$$

$$\overline{\overline{H}}_o = \beta\overline{P}_x^{\,2} + \gamma\overline{P}_y^{\,2} + \alpha\overline{P}_z^{\,2}$$

$$\overline{\overline{H}}_1 = \frac{1}{4} \sum_{\mu\nu} \tau'_{\mu\mu\nu\nu}\, \overline{P}_\mu^{\,2}\, \overline{P}_\nu^{\,2}$$

where

$$\alpha = c + 3\tau_{xyxy} - 2\tau_{xzxz} - 2\tau_{yzyz}$$

$$\beta = a + 3\tau_{yzyz} - 2\tau_{xyxy} - 2\tau_{xzxz}$$

$$\gamma = b + 3\tau_{xzxz} - 2\tau_{yzyz} - 2\tau_{xyxy}$$

$$\tau'_{\mu\mu\mu\mu} = \tau_{\mu\mu\mu\mu}$$

$$\tau'_{\mu\mu\nu\nu} = \tau_{\mu\mu\nu\nu} + 2\tau_{\mu\nu\mu\nu}.$$

The problem reduces to one of computing the value of

$$\langle \bar{H}_1 \rangle = \left\langle \frac{1}{4} \sum_{\mu\nu} \tau'_{\mu\mu\nu\nu} \bar{P}_\mu^2 \bar{P}_\nu^2 \right\rangle$$

$$= \frac{1}{4} \Big[\tau'_{xxxx} \langle \bar{P}_x^4 \rangle + \tau'_{yyyy} \langle \bar{P}_y^4 \rangle + \tau'_{zzzz} \langle \bar{P}_z^4 \rangle$$

$$+ \tau'_{xxyy} \langle \bar{P}_x^2 \bar{P}_y^2 + \bar{P}_y^2 \bar{P}_x^2 \rangle + \tau'_{xxzz} \langle \bar{P}_x^2 \bar{P}_z^2 + \bar{P}_z^2 \bar{P}_x^2 \rangle$$

$$+ \tau'_{yyzz} \langle \bar{P}_y^2 \bar{P}_z^2 + \bar{P}_z^2 \bar{P}_y^2 \rangle \Big]. \qquad (15)$$

The technique to be employed consists of computing these averages in terms of $\langle \bar{P}_z^2 \rangle$, $\langle \bar{P}_z^4 \rangle$, w_o, and the molecular constants. $\langle \bar{P}_z^2 \rangle$ and $\langle \bar{P}_z^4 \rangle$ will then be computed by a technique similar to that of computing w_o. The computation is started by considering the total angular momentum operator

$$\bar{P}^2 = \bar{P}_x^2 + \bar{P}_y^2 + \bar{P}_z^2 . \qquad (16)$$

Operating successively with $\bar{P}^2$ and $\bar{P}_x^2$ we have

$$\bar{P}_x^2 \bar{P}^2 \psi = \bar{P}_x^2 (\bar{P}^2 \psi) = \bar{P}_x^2 [J(J+1)\psi] = J(J+1) \bar{P}_x^2 \psi$$

$$\langle \bar{P}_x^2 \bar{P}^2 \rangle = J(J+1) \langle \bar{P}_x^2 \rangle$$

$\bar{P}^2$ commutes with $\bar{P}_x^2$ and $\bar{P}_y^2$ so that

$$< \bar{P}_x^2 \bar{P}^2 + \bar{P}^2 \bar{P}_x^2 > = 2 < \bar{P}_x^2 \bar{P}^2 > = 2J(J+1) < \bar{P}_x^2 >$$

$$= 2 < \bar{P}_x^4 > + < \bar{P}_x^2 \bar{P}_y^2 + \bar{P}_y^2 \bar{P}_x^2 >$$

$$+ < \bar{P}_z^2 \bar{P}_x^2 + \bar{P}_x^2 \bar{P}_z^2 > \qquad (17)$$

and

$$< \bar{P}_y^2 \bar{P}^2 + \bar{P}^2 \bar{P}_y^2 > = 2 < \bar{P}_y^2 \bar{P}^2 > = 2J(J+1) < \bar{P}_y^2 >$$

$$= 2 < \bar{P}_y^4 > + < \bar{P}_y^2 \bar{P}_x^2 + \bar{P}_x^2 \bar{P}_y^2 >$$

$$+ < \bar{P}_z^2 \bar{P}_y^2 + \bar{P}_y^2 \bar{P}_z^2 > . \qquad (18)$$

Squaring $\bar{H}_o$ and averaging we have

$$< \bar{H}_o^2 > = \alpha^2 < \bar{P}_z^4 > + \beta^2 < \bar{P}_x^4 > + \gamma^2 < \bar{P}_y^4 > + \alpha\beta < \bar{P}_z^2 \bar{P}_x^2 + \bar{P}_x^2 \bar{P}_z^2 >$$

$$+ \beta\gamma < \bar{P}_x^2 \bar{P}_y^2 + \bar{P}_y^2 \bar{P}_x^2 > + \gamma\alpha < \bar{P}_y^2 \bar{P}_z^2 + \bar{P}_z^2 \bar{P}_y^2 > . \qquad (19)$$

Eliminating $< \bar{P}_y^2 >$ by substitution of Equation (16) into Equation (17) and differentiating with respect to α

$$\frac{\partial < \bar{H}_o^2 >}{\partial \alpha} = 2(\alpha - \gamma) < \bar{P}_z^4 > + (\beta - \gamma) < \bar{P}_x^2 \bar{P}_z^2 + \bar{P}_z^2 \bar{P}_x^2 > + 2\gamma J(J+1) < \bar{P}_z^2 > . \qquad (20)$$

Similarly eliminating $< \bar{P}_x^2 >$

$$\frac{\partial < \bar{H}_o^2 >}{\partial \alpha} = 2(\alpha - \beta) < \bar{P}_z^4 > + (\gamma - \beta) < \bar{P}_y^2 \bar{P}_z^2 - \bar{P}_z^2 \bar{P}_y^2 > + 2\beta J(J+1) < \bar{P}_z^2 > . \qquad (21)$$

But

$$< \bar{H}_o^2 > = w_o^2$$

and

$$\frac{\partial < \bar{H}_o^2 >}{\partial \alpha} = 2 w_o \frac{\partial w_o}{\partial \alpha} . \qquad (22)$$

Differentiating $\overline{H}_o$ with respect to α and averaging

$$\frac{\partial \overline{H}_o}{\partial \alpha} = \overline{P}_z^{\,2}$$

$$\langle \overline{P}_z^{\,2} \rangle = \langle \frac{\partial \overline{H}_o}{\partial \alpha} \rangle = \frac{\partial w_o}{\partial \alpha} . \tag{23}$$

Then substituting Equation (10) into Equation (22)

$$\frac{\partial \langle \overline{H}_o^{\,2} \rangle}{\partial \alpha} = 2w_o \langle \overline{P}_z^{\,2} \rangle .$$

Substituting Equation (23) into Equations (20) and (21) and rearranging we have obtained two of the terms required in Equation (1):

$$\langle \overline{P}_x^{\,2} \overline{P}_z^{\,2} + \overline{P}_z^{\,2} \overline{P}_x^{\,2} \rangle = \frac{1}{\beta - \gamma} \left[2w_o \langle \overline{P}_z^{\,2} \rangle - 2(\alpha - \gamma) \langle \overline{P}_z^{\,4} \rangle - 2\gamma J(J+1) \langle \overline{P}_z^{\,2} \rangle \right] \tag{24}$$

$$\langle \overline{P}_y^{\,2} \overline{P}_z^{\,2} + \overline{P}_z^{\,2} \overline{P}_y^{\,2} \rangle = \frac{1}{\beta - \gamma} \left[-2w_o \langle \overline{P}_z^{\,2} \rangle + 2(\alpha - \beta) \langle \overline{P}_z^{\,4} \rangle + 2\beta J(J+1) \langle \overline{P}_z^{\,2} \rangle \right] . \tag{25}$$

Returning to the definitions of $\overline{H}_o$ and $\overline{P}^2$

$$\beta \overline{P}_x^{\,2} = \overline{H}_o - \alpha \overline{P}_z^{\,2} - \gamma \overline{P}_y^{\,2} = \overline{H}_o - \alpha \overline{P}_z^{\,2} - \gamma (P^2 - \overline{P}_x^{\,2} - \overline{P}_z^{\,2})$$

$$\langle \overline{P}_x^{\,2} \rangle = \frac{1}{\beta - \gamma} \left[w_o - (\alpha - \gamma) \langle \overline{P}_z^{\,2} \rangle - \gamma J(J+1) \right] .$$

Similarly

$$\langle \overline{P}_y^{\,2} \rangle = \frac{1}{\beta - \gamma} \left[w_o + (\alpha - \beta) \langle \overline{P}_z^{\,2} \rangle + \beta J(J+1) \right] .$$

Equations (17), (18), and (19) form the following set of simultaneous equations in three unknowns

$$<\bar{P}_x^4> + \frac{1}{2}<\bar{P}_y^2\bar{P}_x^2 + \bar{P}_x^2\bar{P}_y^2> = J(J+1)<\bar{P}_x^2> - \frac{1}{2}<\bar{P}_z^2\bar{P}_x^2 + \bar{P}_x^2\bar{P}_z^2>$$

$$<\bar{P}_y^4> + \frac{1}{2}<\bar{P}_y^2\bar{P}_x^2 + \bar{P}_x^2\bar{P}_y^2> = J(J+1)<\bar{P}_y^2> - \frac{1}{2}<\bar{P}_z^2\bar{P}_y^2 + \bar{P}_y^2\bar{P}_z^2>$$

$$\beta^2<\bar{P}_x^4> + \gamma^2<\bar{P}_y^4> + \beta\gamma<\bar{P}_y^2\bar{P}_x^2 + \bar{P}_x^2\bar{P}_y^2> = w_o^2 - \alpha^2<\bar{P}_z^4> - \alpha\beta<\bar{P}_z^2\bar{P}_x^2 + \bar{P}_x^2\bar{P}_z^2>$$

$$- \gamma\alpha<\bar{P}_z^2\bar{P}_y^2 + \bar{P}_y^2\bar{P}_z^2>$$

since all the terms to the right of the equality sign have been expressed in terms of the independent variables w_o, $<\bar{P}_z^2>$, α, β and γ. Solving this set of equations and substituting them along with Equation (15), Equation (24), and Equation (25) back into Equation (14) we have the desired expression

$$w = w_o + A_1 w_o^2 + A_2 w_o J(J+1) + A_3 J^2(J+1)^2 + A_4 J(J+1)<\bar{P}_z^2>$$

$$+ A_5<\bar{P}_z^4> + A_6 w_o<\bar{P}_z^2>$$

where

$$A_1 = \frac{1}{4(\beta-\gamma)^2}\left[\tau'_{xxxx} + \tau'_{yyyy} - 2\tau'_{xxyy}\right]$$

$$A_2 = \frac{1}{2(\beta-\gamma)^2}\left[-\gamma\tau'_{xxxx} - \beta\tau'_{yyyy} + (\beta+\gamma)\tau'_{xxyy}\right]$$

$$A_3 = \frac{1}{4(\beta-\gamma)^2}\left[\gamma^2\tau'_{xxxx} + \beta^2\tau'_{yyyy} - 2\beta\gamma\tau'_{xxyy}\right]$$

$$A_4 = \frac{1}{2(\beta-\gamma)^2}\left[\gamma(\alpha-\gamma)\tau'_{xxxx} + \beta(\alpha-\beta)\tau'_{yyyy} + (2\beta\gamma - \alpha\beta - \alpha\gamma)\tau'_{xxyy}\right.$$

$$\left. -\gamma(\beta-\gamma)\tau'_{zzxx} + \beta(\beta-\gamma)\tau'_{yyzz}\right]$$

$$A_5 = \frac{1}{4(\beta-\gamma)^2}\left[(\alpha-\gamma)^2\tau'_{xxxx} + (\alpha-\beta)^2\tau'_{yyyy} + (\beta-\gamma)^2\tau'_{zzzz}\right.$$

$$+2(\alpha-\gamma)(\beta-\gamma)\tau'_{xxyy} - 2(\alpha-\gamma)(\beta-\gamma)\tau'_{zzxx}$$

$$\left. +2(\alpha-\beta)(\beta-\gamma)\tau'_{yyzz}\right]$$

$$A_6 = \frac{1}{2(\beta - \gamma)^2}\left[-(\alpha - \gamma)\tau'_{xxxx} + (\beta - \gamma)\tau'_{yyyy} + (2\alpha - \beta - \gamma)\tau'_{xxyy} + (\beta - \gamma)\tau'_{zzxx} - (\beta - \gamma)\tau'_{yyzz}\right]$$

$\langle \overline{P}_z^2 \rangle$ and $\langle \overline{P}_z^4 \rangle$ may be evaluated by means of the following argument. $\overline{P}_z$ is diagonal in the limiting symmetric rotor basis, having the eigenvalue K. Then the n^{th} power of P_z will also be diagonal in this basis, having the eigenvalue K^n. Consider the operator

$$\overline{\lambda'(\kappa,q)} = \overline{\lambda(\kappa)} + \overline{q\,\pi}\,.$$

where $\overline{\lambda(\kappa)}$ is the operator associated with the rigid rotor reduced energy, $\overline{\pi}$ is an operator which is diagonal in the limiting symmetric rotor basis, and q is a variable, independent of the rotational quantum numbers.

Averaging and differentiating with respect to q,

$$\langle \overline{\pi} \rangle = \frac{\partial \langle \overline{\lambda'(\kappa,q)} \rangle}{\partial q}$$

At q=0, $\overline{\lambda'(\kappa,q)} = \overline{\lambda(\kappa)}$ so that the basis which diagonalizes $\overline{\lambda(\kappa)}$ also diagonalizes $\overline{\lambda'(\kappa,0)}$. Evaluating the derivative at q=0 and denoting the eigenvalue of $\overline{\lambda'(\kappa,q)}$ by λ'

$$\langle \overline{\pi} \rangle = \frac{\partial \lambda'}{\partial q}\bigg|_{q=0}.$$

The reduced matrices - that is the E ± and O ± matrices - are written in the limiting symmetric rotor basis. Since $\overline{\pi}$ is diagonal in this basis, the only differences between the $\overline{\lambda'(\kappa,q)}$ matrix and the $\overline{\lambda(\kappa)}$ matrix are the diagonal terms $q\pi_m$, the $\overline{\lambda'(\kappa,q)}$ matrix taking the form

$$\overline{\lambda'(\kappa,q)} = \begin{pmatrix} k_o + q\pi_o & 1 & 0 & \cdots & \cdots \\ b_1 & k_1 + q\pi_1 & 1 & \cdots & \cdots \\ 0 & b_2 & k_2 + q\pi_2 & \cdots & \cdots \\ \cdots & \cdots & \cdots & \cdots & \cdots \\ \cdots & \cdots & \cdots & \cdots & \cdots \end{pmatrix}$$

where the π_m is the mm element of $\overline{\pi}$ in this basis. The continued fraction solution of the associated secular will be identical with that for $\overline{\lambda(\kappa)}$ with the replacement of the k_m terms by $k_m + q\,\pi_m$. Then

$$\lambda' = k_m + q\,\pi_m - \cfrac{b_m}{k_{m-1} - \lambda' + q\,\pi_{m-1} - \cfrac{b_{m+1}}{k_{m-2} - \lambda' + q\,\pi_{m-2} - \cdots}}$$

$$- \cfrac{b_{m+1}}{k_{m+1} - \lambda' + q\,\pi_{m+1} - \cfrac{b_{m+1}}{k_{m+2} - \lambda' + q\,\pi_{m+2} - \cdots}}$$

differentiating with respect to q and setting q=0.

[Noting that $\lambda'(\kappa,o) = \lambda(\kappa)$]

$$\left.\frac{\partial\lambda'}{\partial q}\right|_{q=0} = \pi_m + \frac{b_m}{\left[k_{m-1} - \lambda - \cfrac{b_{m-1}}{k_{m-2} - \lambda \cdots}\right]^2}\left\{\pi_{m-1} - \left.\frac{\partial\lambda'}{\partial q}\right|_{q=0}\right.$$

$$+ \frac{b_{m-1}}{\left[k_{m-2} - \lambda - \cfrac{b_{m-2}}{k_{m-3} - \lambda \cdots}\right]^2}\left[\pi_{m-2} - \left.\frac{\partial\lambda'}{\partial q}\right|_{q=0} - \cdots\right]\Bigg\}$$

$$+ \frac{b_{m+1}}{\left[k_{m+1} - \lambda - \cfrac{b_{m+2}}{k_{m+2} - \lambda \cdots}\right]^2}\left\{\pi_{m+1} - \left.\frac{\partial\lambda'}{\partial q}\right|_{q=0}\right.$$

$$+ \frac{b_{m+2}}{\left[k_{m+2} - \lambda - \cfrac{b_{m+3}}{k_{m+3} - \lambda \cdots}\right]^2}\left[\pi_{m+2} - \left.\frac{\partial\lambda'}{\partial q}\right|_{q=0} - \cdots\right]\Bigg\}$$

$$\text{Defining } R_n = \frac{b_{n+1}}{\left[k_n - \lambda - \frac{b_n}{k_{n-1} - \lambda \ldots .}\right]^2}$$

$$R'_n = \frac{b_n}{\left[k_n - \lambda - \frac{b_{n+1}}{k_{n+1} - \lambda \ldots .}\right]^2}$$

$$\left.\frac{\partial \lambda'}{\partial q}\right|_{q=0} = \langle \bar{\pi} \rangle = \pi_m + R_{m-1}\left\{\pi_{m-1} - \langle \bar{\pi} \rangle + R_{m-2}\left[\pi_{m-2} - \langle \bar{\pi} \rangle + R_{m-3}(\ldots .)\right]\right\}$$

$$+ R'_{m+1}\left\{\pi_{m+1} - \langle \bar{\pi} \rangle + R'_{m+2}\left[\pi_{m+2} - \langle \bar{\pi} \rangle + R'_{m+3}(\ldots .)\right]\right\}$$

Solving for $\langle \bar{\pi} \rangle$

$$\langle \bar{\pi} \rangle = \frac{\pi_m + R_{m-1}\left[\pi_{m-1} + R_{m-2}(\ldots .)\right] + R'_{m+1}\left[\pi_{m+1} + R'_{m+2}(\ldots .)\right]}{1 + R_{m-1}\left[1 + R_{m-2}(1 + \ldots .)\right] + R'_{m+1}\left[1 + R'_{m+2}(1 + \ldots .)\right]} .$$

For the $\bar{P}_z^2$ reduced matrix $\pi_m = K^2$ and $\pi_{m+n} = (K \pm n)^2$ and for the $\langle \bar{P}_z^4 \rangle$ reduced matrix $\pi_m = K^4$ and $\pi_{m \pm 2} = (K \pm 2n)^4$. Then

$$\langle \bar{P}_z^2 \rangle = \frac{K^2 + R_{m-1}\left[(K-2)^2 + R_{m-2}(\ldots .)\right] + R'_{m+1}\left[(K+2)^2 + R'_{m+2}(\ldots .)\right]}{1 + R_{m-1}\left[1 + R_{m-2}(1 + \ldots .)\right] + R'_{m+1}\left[1 + R'_{m+2}(1 + \ldots .)\right]} .$$

$$\langle \bar{P}_z^4 \rangle = \frac{K^4 + R_{m-1}\left[(K-2)^4 + R_{m-2}(\ldots .)\right] + R'_{m+1}\left[(K+2)^4 + R'_{m+2}(\ldots .)\right]}{1 + R_{m-1}\left[1 + R_{m-2}(1 + \ldots .)\right] + R'_{m+1}\left[1 + R'_{m+2}(1 + \ldots .)\right]} .$$

The use of the computing program on molecules such as HDS or SO_2 produces excellent results. However, the results for H_2O are not as accurate because of the high degree of asymmetry. It is probable that the addition of the next term in the approximations $\langle \bar{P}_z^6 \rangle$ would improve this situation considerably. From the data computed, it is clear that the fit is best for low J values, but rapidly becomes poor for J values larger than 5.

The best constants obtained were:

$$A = 835710 \text{ MHz}$$

$$B = 434231$$

$$C = 278798$$

$$A_1 = -0.3477 \times 10^{-7}$$

$$A_2 = 0.2651 \times 10^{-1}$$

$$A_3 = -0.3289 \times 10^{4}$$

$$A_4 = -0.2524 \times 10^{4}$$

$$A_5 = 0.1467 \times 10^{4}$$

$$A_6 = -0.3743 \times 10^{-2}$$

VIII. ABSORPTION BY WATER VAPOR

The formulas for absorption by water vapor take the form

$$\alpha = \left[10^6 \log_{10} e \frac{8\pi^2}{3hc}\right] N\Sigma \left[\frac{\left\{\frac{3}{1}\right\} e^{-E_\ell/kT} - \left\{\frac{3}{1}\right\} e^{-E_u/kT}}{G}\right] \left[\mu^2 S_{\ell u}\right]$$

$$\times \begin{cases} \nu_{\ell u} \nu^2 \left[\dfrac{4\Delta\nu_{\ell u}}{\left[\nu_{\ell u}^2 - \nu^2\right]^2 + 4\nu^2 \Delta\nu_{\ell u}^2}\right] & (ZN) \\ \dfrac{\nu^2}{\nu_{\ell u}} \left[\dfrac{\Delta\nu_{\ell u}}{(\nu_{\ell u} - \nu)^2 + \Delta\nu_{\ell u}^2}\right] + \left[\dfrac{\Delta\nu_{\ell u}}{(\nu_{\ell u} + \nu)^2 + \Delta\nu_{\ell u}^2}\right] & (VVW) \end{cases}$$

where Z N indicates the Zhevakin and Naumov form of the shape factor and V V W indicates the Van Vleck-Weisskopf form (both have an additional factor of ν from the common part of the formula and the factor π has been absorbed in the numerical factor). The symbols have been explained in section II. The summation is overall transitions which materially contribute at the frequency ν being considered. We will consider each group of factors.

The constant contains factors $10^6 \log_{10} e$ which give the absorption in units of dB/km. If these factors are left out, the units are in cm^{-1}. If N is stated in terms of ρ, the mass density, we may divide each side by ρ, and state the attenuation as α/ρ in units of dB/km per gm/cm^3 of water vapor. Often the units are changed to state ρ in terms of gm/m^3.

The quantity N is the number of H_2O molecules per cc. By use of the gas law it may be written, since $N = n N_0/V$ where n = number of gm-moles and N_0 = Avogadro's number, as $N = p N_0/RT$. If p[dynes/cm^2], V[cm^3], n[gm-mole], T[°K], then R = 8.31 x 10^7 erg/mole °K. If p[atm], V[liters], n[gm-moles], T[°K], then R = 0.08207 liters atm/mole °K. Since $R = p_0 V_0/T$, where the p_0 = standard pressure, T_0 = standard temperature and V_0 = molar volume, we may write $N = p N_0 T_0/p_0 V_0 T$. The molar volume is $V_0 = V/n$.

The number of moles is n = m/n, where m = mass of the gas, M = molecular weight, and ρ = m/V is the density. Thus $N = 10^{-6} N_o \rho/M$ when ρ is in gm/m^3 ($N = 6.025 \times 10^{23}$).

It is sometimes convenient to state the conditions on water content of the atmosphere in terms of the total water content of the path. The total absorption is then independent of the length of the path. If the total path has x gm/cm^2 of precipitable water vapor, then considering that the path is of one cm^2 cross-section, of length 1, then the density of water vapor considered spread evenly throughout the volume is x $gm/10^5$ cc or 10 x gm/m^3. If α is then stated in dB/km per gm/m^3 of H_2O, then 10 (α/ρ) x is the attenuation for 1 kilometer, and hence for any distance containing a total of x gm/cm^2 of precipitable water.

The Boltzmann factor has included the nuclear degeneracy $\begin{Bmatrix} 3 \\ 1 \end{Bmatrix}$ in the numerator as well as in

$$G = \sum_{J=o}^{\infty} \sum_{\tau=-J}^{J} \left[2 - (-1)^{|\tau|} \right] (2J + 1)\, e^{-E(J,\tau)/kT}$$

Zhevakin and Naumov (Reference 3) show this degeneracy in G, but do not show it in the numerator, since they, like Van Vleck (Reference 41) include it in the factor $|\mu_{ij}|^2$. This factor arises because the nuclei forming the H_2O molecule have a non-zero spin, producing symmetric and antisymmetric states with different statistical weights. The H_2O molecule has a ratio of statistical weights of 3 to 1 for antisymmetric and symmetric states. For any other molecule the braces in the Boltzmann factor and the brackets in G may be replaced by the appropriate statistical weight. This statistical weight is in addition to the Zeeman degeneracy. The value of G is taken to be 170, for T = 295°.

The matrix element of the dipole moment $|\mu_{ij}|^2$ which enters the expression for the absorption coefficient is $|(a|P|b)|^2$ where P is the dipole moment operator $\Sigma_1 e \underline{r}_i$, where sum is over the electrons. Here a,b refer to specific states, i.e., components of a level. The total absorption due to all the components is found by summing over a,b; i.e., $|\mu_{ij}|^2 = \sum_{a,b} |(a|P|b)|^2$. This quantity is called the line strength:

$$S_{J \to J'} = \sum_{a,b} |(a|P|b)|^2 \ .$$

Thus if the intensity of a line is

$$I(J,J') = N(j) \frac{h\nu}{3h\lambda^3} \frac{64\pi^4}{} \sum_{a,b} |(a|P|b)|^2 ,$$

the quantity N(j) is the number of molecules in one component, and

$$N(j) = \frac{e^{-W_j/kT} N}{G}$$

where N is the number of molecules per cc. It is not necessary to enter a factor of 2J+1 to account for the degeneracy of the level, since all possible transitions are accounted for in the summation producing the line strength. On the other hand, if the quantity N(J), the number of molecules in the level, are used, N(J) = (2J+1) N(j) and the intensity may be written

$$I(J,J') = N(J)\, h\nu \frac{64\pi^4}{3h\lambda^3} \frac{S(J,J')}{(2J+1)} .$$

Further, the dipole moment is frequently broken up into factors containing the square magnitude of the moment, μ^2, and direction cosine factors. Therefore the line strength is often seen in the form $\mu^2 S_{JJ'}$ where $S_{JJ'}$ is called the transition strength by authors Townes and Schawlow (Reference 7) or again the line strength by King, Hainer and Cross (Reference 31). Thus it is necessary to verify the definitions when using tables. The tables of line strength being used in this report are those of West and Mizushima (Reference 33); it is necessary, in order to obtain the dipole moment matrix element to calculate:

$$|\mu_{ij}|^2 = \frac{\mu^2 S_{JJ'}}{2J+1}$$

where μ is the dipole moment in debye. However, it should be noted that when the $|\mu_{ij}|^2$ is used in this form, as in Townes and Schawlow (Reference 7), in intensity type formulas it must be used in conjunction with (2J+1)N(j) as a multiplier, so that the factors (2J+1) cancel and the Zeeman degeneracy is borne by the transition or line strength $S_{JJ'}$. The line strengths are included in Table IV. In this report the number of molecules in a given component of the level is $N\, e^{-W(J)/kT}$ without multiplying by (2J+1) and we take account of the $|\mu_{ij}|^2$ by using it as $\mu^2\, S_{JJ'}$, without dividing by (2J+1). However, note the next paragraph.

Due to the nuclear spins one other degeneracy arises. The states functions of water are divided into symmetric and asymmetric states. States of one symmetry only combine with other states of the same symmetry.

The linewidths of the various transitions in the form factors vary depending on the particular levels involved. A calculation of the linewidths in H_2O-N_2 collisions has been made by Benedict and Kaplan (Reference 4). These values were adjusted to give precisely the results obtained from accurate measurements on the $5_{-1} \rightarrow 6_{-5}$ microwave line (Reference 39). The half-width of the line as given by Benedict and Kaplan is

$$\Delta_{ij} = \left(\frac{nv}{2c}\right)\left[\sum_{J_2} \rho_{J_2} (b_{ij,\, J_2})^2\right]\left[cm^{-1}\ atmos^{-1}\right]$$

where

- n = number of colliding molecules per cm^3 at one atmosphere
- v = mean collision velocity
- ρ_{J_2} = fraction of molecules in the state J_2, from Boltzman distribution
- $b_{ij,\, J_2}$ = partial collision diameter.

The quantity b_{ij,J_2} is obtained from a quantum mechanical calculation of the rate at which the combined effects of all the intermolecular forces induce a simultaneous transition in the radiating and colliding molecule.

The variation of the linewidth with pressure has been well established over wide ranges to be $\Delta_{ij} \propto \rho$ and this has been assumed for this report. However, the variation with temperature is more complicated. An exponential law $(T/300)^{-n_{ij}}$ re-presents the results calculated by Benedict and Kaplan quite well if n is allowed to vary from line to line. Their results correspond to constant pressure, the variation at constant density is $\lambda \propto T^{(1-n)}$. The values of n may range from -0.045 to 0.756. Values of n are listed in Table IV for the lines of interest.

The linewidths at T = 295°K, p = 1 atm are listed in Table IV. One column lists the widths calculated by Benedict and Kaplan; the adjacent column lists the observed values. The constants used in the final calculation of the H_2O absorption spectrum are the observed values where known, and the calculated values otherwise.

The frequencies $\nu_{\ell u}$ are the observed frequencies when known, otherwise they are taken from Clough and Benedict. Both observed and computed frequencies are shown in Table IV.

Ideally, the computation of the absorption should be done by performing the summation. However, although there are only ten important lines in the regions of interest the absorption there is affected by all the lines, to some extent; in the case of water this amounts to almost 900 lines in rotational states. Many of these are of low strength, and poorly populated since the J values are high. However, their combined effect may be considerable. Van Vleck (References 40 and 41) has introduced a method of computing a residual term approximating the effect of the other lines, or background. This method was followed in the first report (Reference 1) on this program but was not carried out here because of the desire to see the influence of the two form factors of Van Vleck-Weisskopf and Zhevakin-Naumov. Accordingly, the results presented here are obtained by summing over the transitions below 1000 GHz and as many lines as contribute significantly from the infrared into the band 1000 GHz. These lines contributing to a residual term were determined by dividing the lines in tables assembled by Benedict* into sets depending on their strengths and rotational quantum numbers and by multiplying an average contribution of each group by the number of lines in each group. Using these sums an approximate curve of residual contributions may be drawn through the region 100 to 1000 GHz and added to the contributions from all the lines in this region. The results agree well with the Zhevakin-Naumov results.

The results of this computation differ from Zhevakin and Naumov because a slightly different value of the width of the 183 GHz line is used and because more accurate values of the line center frequencies are used. The values of the line strength used here are probably more accurate than those previously employed.

Four graphs are presented in Figures 23 through 26. The conditions of the computation are shown on each graph. The residual effect of the infrared lines are contained in the graphs, estimated as described above. It can be seen that the Zhevakin-Naumov shape factor gives larger values in the valleys which are consistent with the conclusions of the first report on this task (Reference 1).

Figure 27 is a graph of atmospheric absorption over the range from microwaves to 10 microns wavelength reconstructed from several sources, chiefly Zhevakin and Naumov (Reference 3) and Yates and Taylor (Reference 46).

*Private communication from Benedict to L. Frenkel

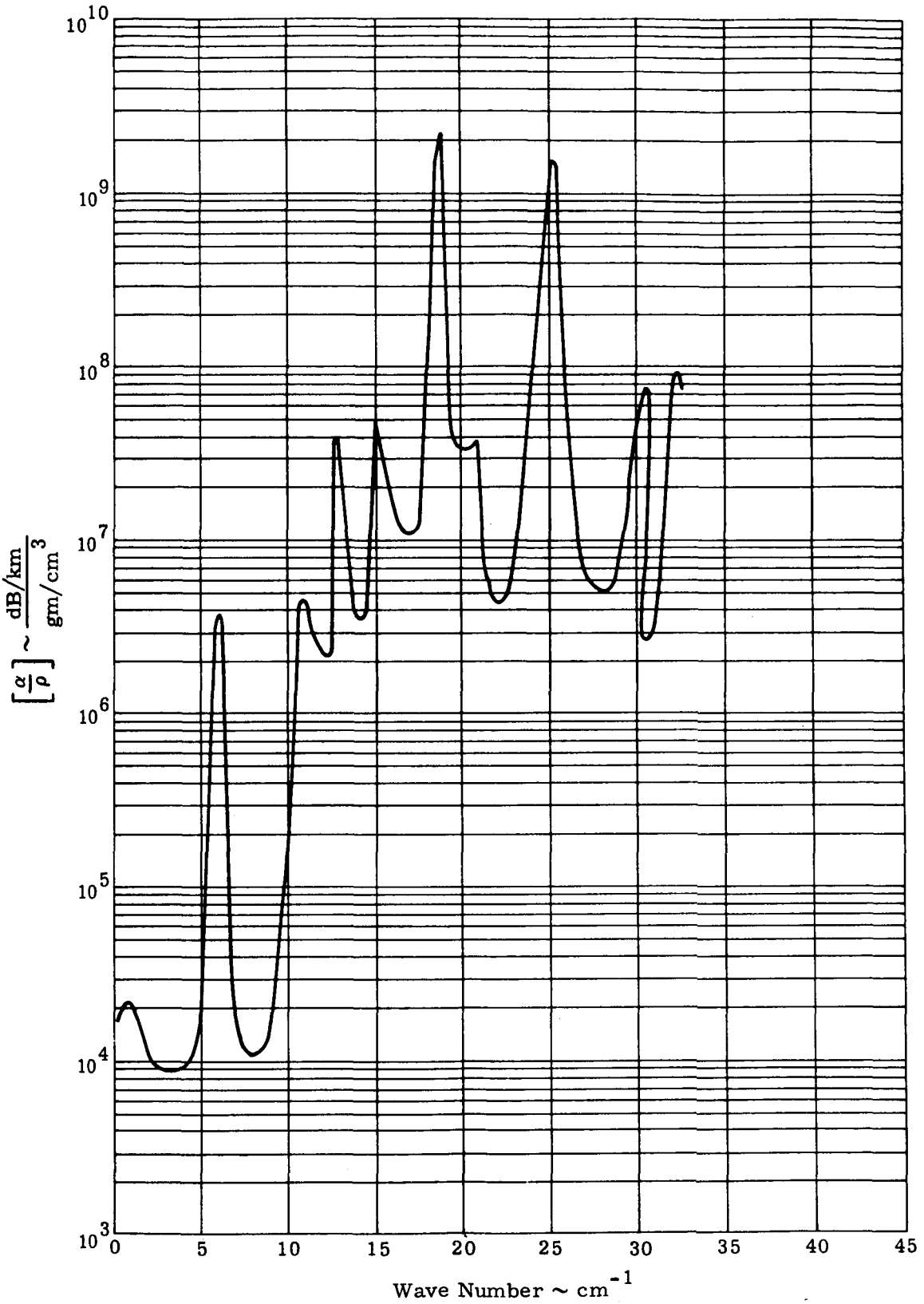

Figure 23. Absorption by Water Vapor at 1 Atmosphere Pressure - Shape: Van Vleck-Weisskopf

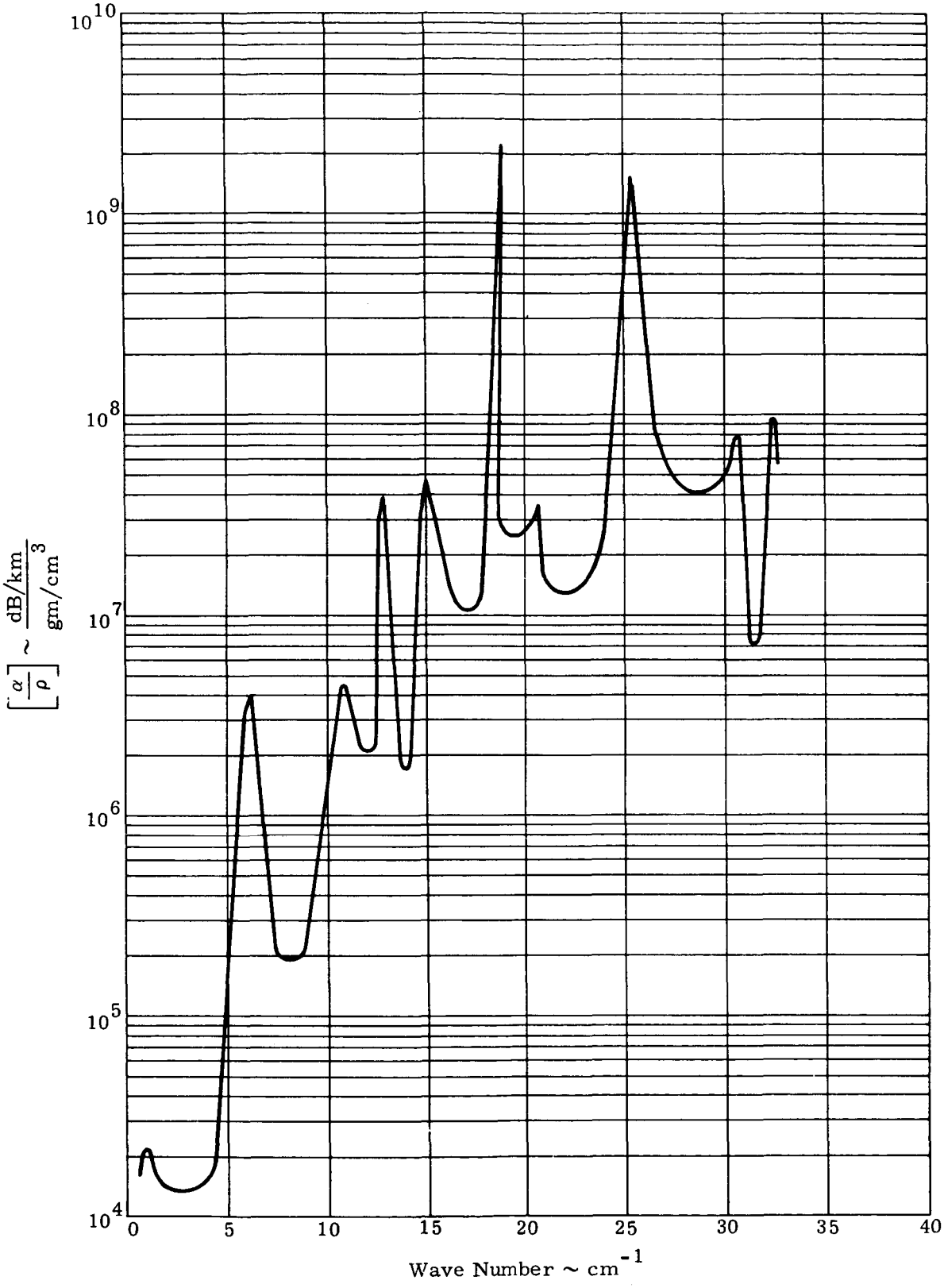

Figure 24. Absorption by Water Vapor at 1 Atmosphere Pressure - Shape: Zhevakin-Naumov

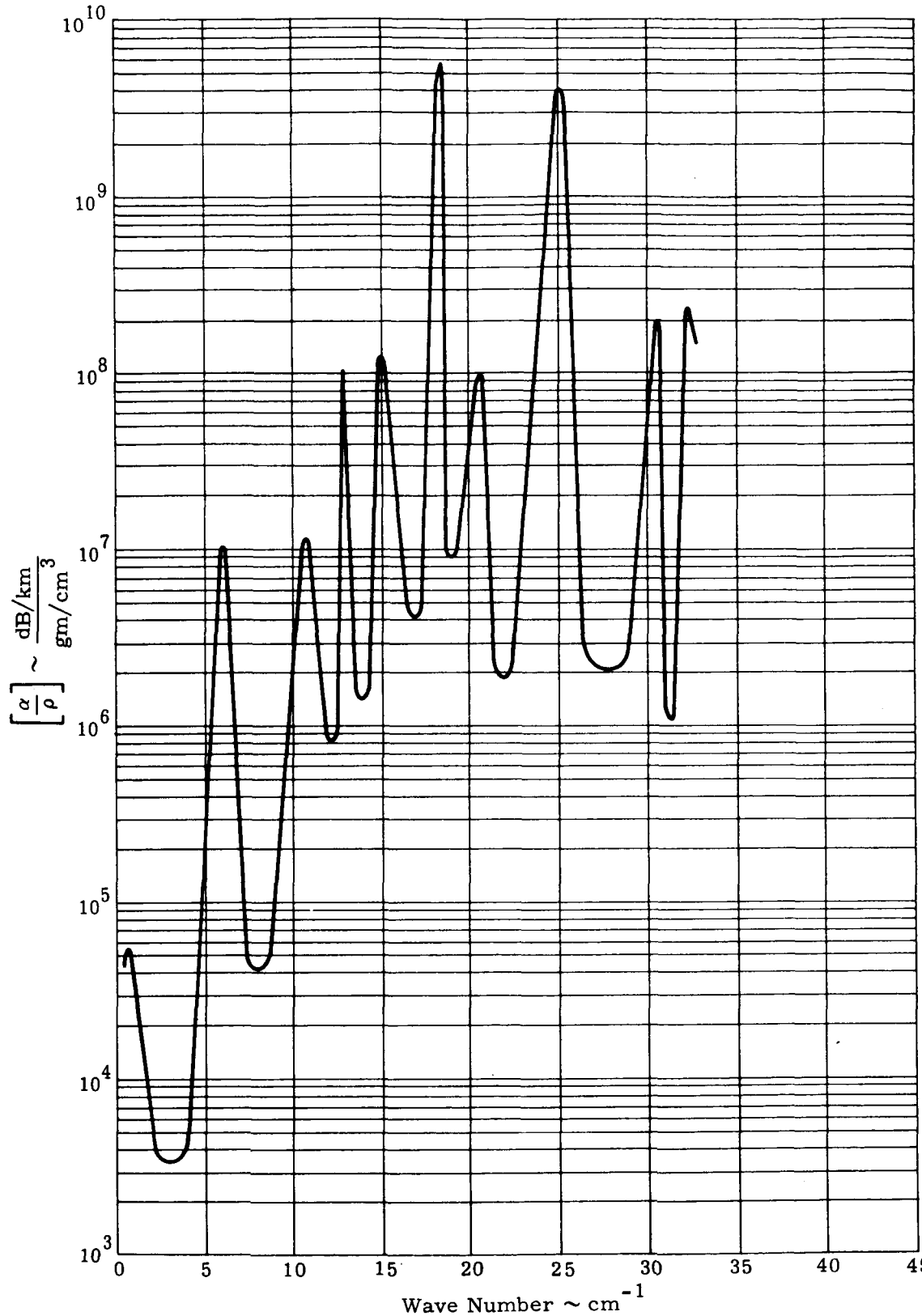

Figure 25. Absorption by Water Vapor at 0.39 Atmosphere Pressure - Shape: Van Vleck-Weisskopf

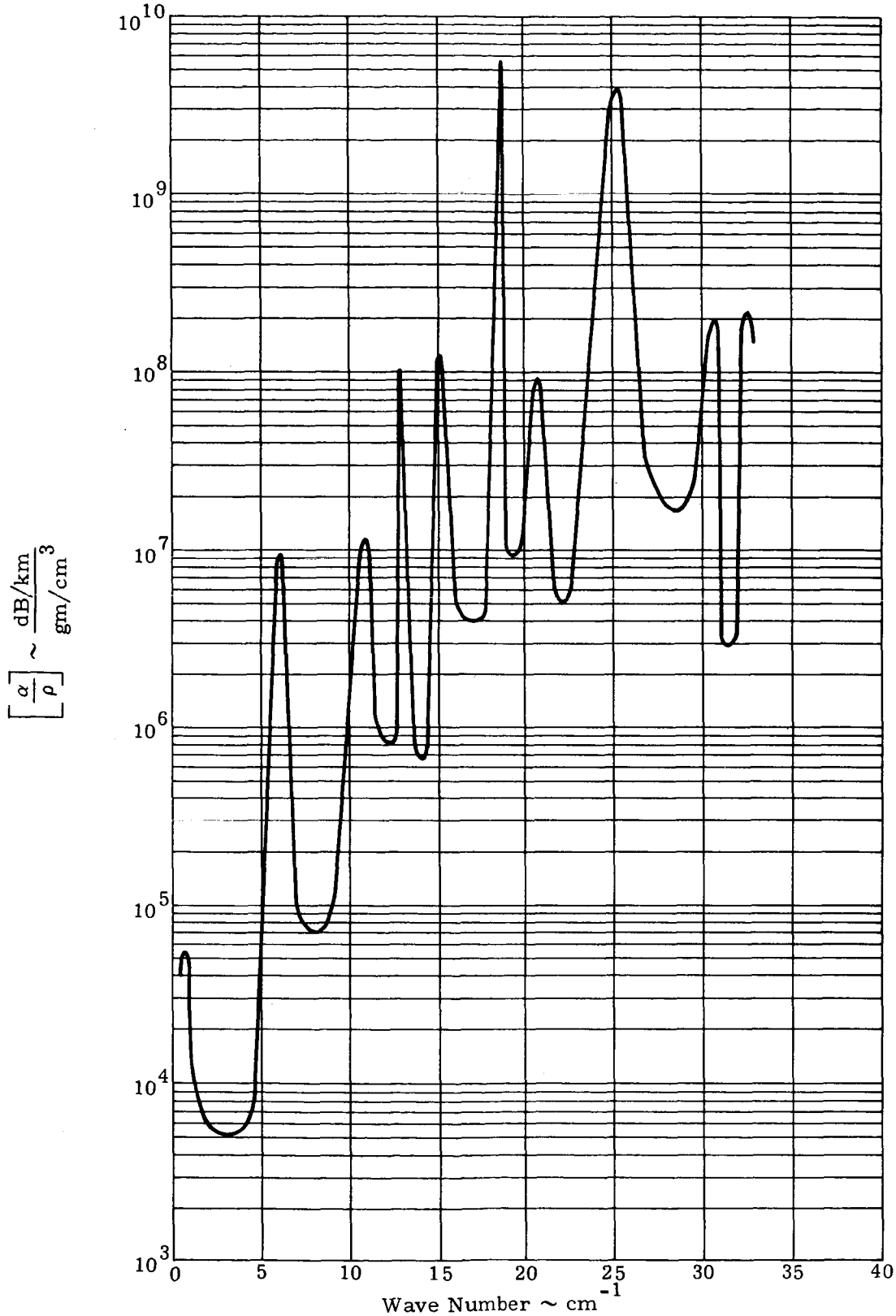

Figure 26. Absorption by Water Vapor at 0.39 Atmosphere Pressure - Shape: Zhevakin-Naumov

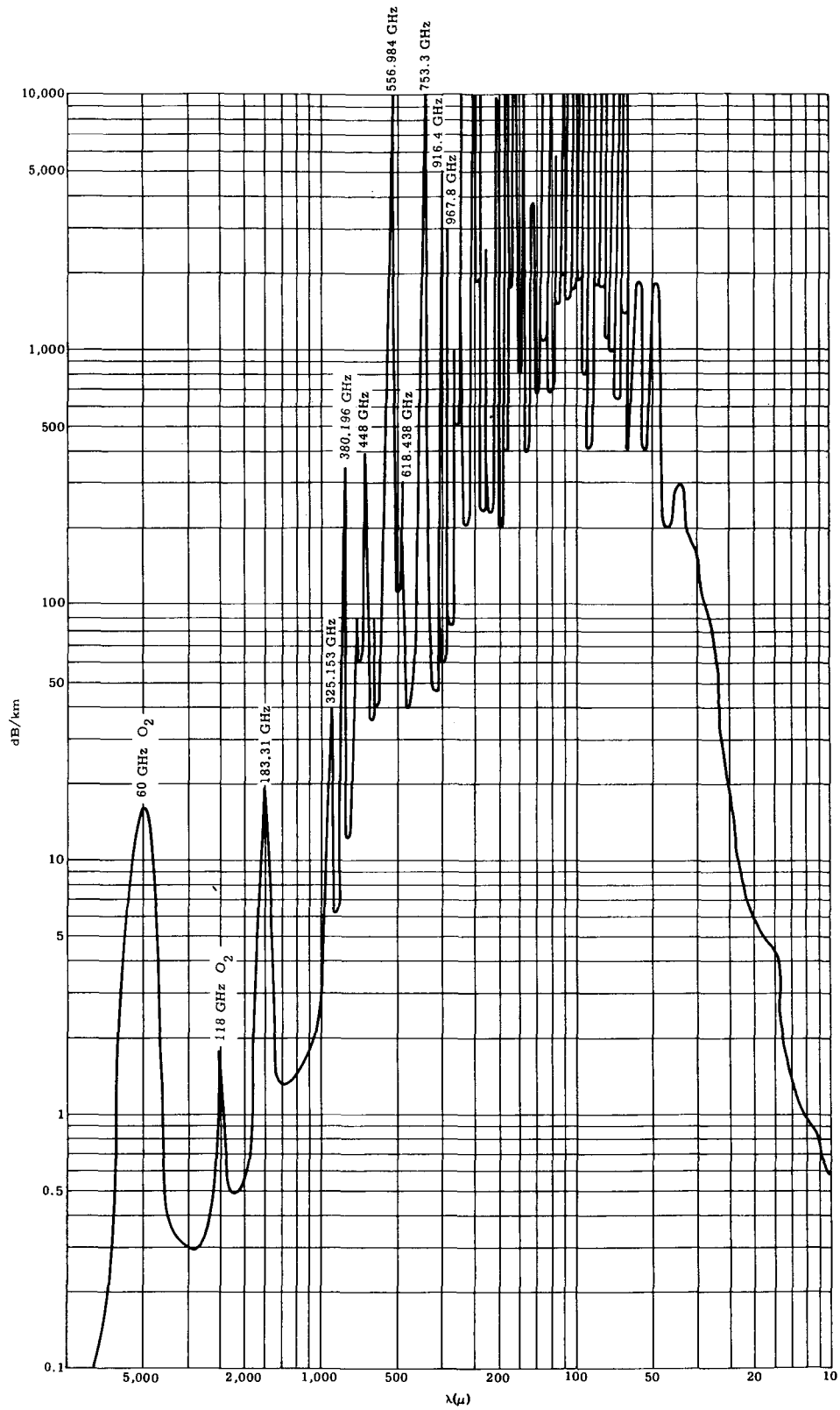

Figure 27. Absorption from 10 to 5000 Microns at 1 Atmosphere Pressure, 293°K, and Absolute Humidity ρ = 7.5 gm/m^3 - Shape: Zhevakin-Naumov

IX. CONCLUSIONS

A large effort during the contract period was expended on the development of methods and equipment to perform measurements above 600 GHz. Although it has been possible to observe spectral lines above 600 GHz, there is a major difference between observation and performing accurate measurements. A signal-to-noise ratio of at least 10:1 is required in order to measure absorptions as low as 50 dB/km and higher ratios are needed for less absorption. With single harmonic generation and with video detection, the signal-to-noise ratio is nearly 1:1 at 618 GHz. An additional increase by a factor of 20 dB is required in order to overcome the insertion loss of the Fabry-Perot interferometer. In order to solve this problem, a new, broad-band, harmonic generator was designed and built and a high gain traveling-wave tube amplifier was assembled. An increase of a least 12:1 in signal-to-noise ratio was obtained by this superheterodyne receiver. The new harmonic generator is also the best mixer and best detector of all that have been tested at Martin Company. Further increase in signal-to-noise ratio can come about by the use of integrating procedures. These require stable sources; stability of the various klystrons is sufficient, but the carcinotron power supply would require major revision. Since the cost of carcinotrons above 600 GHz is prohibitive, other sources have been sought. Lasers appear to be a partial solution, although the narrow tuning range would require lasers with many lines in the output or several different gases. Water lasers have been operated and a cyanide laser was completed but not tested as the task terminated. These equipment developments, used cooperatively, appear to solve the problem of measurement above 600 GHz, at least to the extent that the present coupling to the Fabry-Perot remains efficient.

Because of the insufficient power available, development of the theory of line broadening and the theory of asymmetric top molecules was a major effort. A study of the broadening in CO_2 and a contribution to the theory of orientation relaxation have been made. The application of Kivelson-Wilson distortion theory to several asymmetric top molecules was made and a computer program was prepared by which constants of the molecule could be determined by a best squares fit. This program used only terms through $\langle \overline{P}_z^4 \rangle$ and this limitation allows good fit of the data only to the lower levels, those for small J values, in molecules which are very assymmetrical. In the case of water, where distortion is large, it is clear that the

addition of the $\langle \overline{P}_z^6 \rangle$ terms is necessary in order to have an expression useful for prediction of transition frequencies. The addition of this term to the computation is not complicated.

A compression of the shape factors of Van Vleck-Weisskopf and of Zhevakin and Naumov has shown that with the limited data available on water, the fit of the latter is better in the valleys of the absorption curve in the microwave-millimeter region. Zhevakin and Naumov point out that the high frequency tails of the Van Vleck-Weisskopf expression remove windows at 10μ which actually exist. The comparison of these expressions for other gases must be done before the entire significance of the different line shapes is understood.

The small absorption of oxygen has prevented detection above 118 GHz by coherent or incoherent methods. In the presence of appreciable quantities of water vapor the oxygen absorption is negligible and the frequencies of the lines have been calculated; they can thus be avoided in the design of communication or other equipment.

X. RECOMMENDATIONS

The present task was part of an extented program* recommended by Martin Company to NASA on the radiation propagation characteristics, absorption scattering and dispersion of gases, smokes and dusts of the earth and the other planets. Because of internal changes in programs and funding, the sponsoring agency is not continuing this aspect of the work at Martin Company although participation in some field experiments, transmission of microwaves between earth and satellite for NASA-Goddard, is beginning as this task ends. It is in terms of the more ambitious program that these recommendations for future work are made.

The problems of space communication and the electromagnetic exploration of space either from the earth or from space vehicles depends on the characteristics of the media through which radiation must travel or from which it must reflect, or from which, due to black body or other excitation, it must emit. The characteristics of the planetary atmospheric gases are least known in the region from microwave to infrared frequencies.

The laboratory phase of such studies would include the absorption spectra with identification of levels by Stark and Zeemann effects, the absolute absorption, the effects of pressure and temperature on line broadening, and the effects of mixtures of gases.

The theoretical studies include the further development of molecular theory, particularly collision effects and the theory of the temperature dependence of linewidth. An investigation should be made of the importance of spontaneous emission and scattering processes. The theory of linewidth is still not complete, particularly for mixtures, although unexplained effects are still found in self-broadening.

The gases to be studied should include N_2, O_2, NO, NO_2, O_3, H_2O, CO_2 from the earth's atmosphere as well as CO, N_2O, CH_4, C_2H_4, NH_3, SO_2 as possible components of other atmospheres. In addition, free radicals and molecular ions found in the ionosphere should be studied as these are of potential importance to the planetary heat balance.

*An Outline of the Problems Associated with Deep Space Communications, Martin Company Report OR 6046, June 1964.

It is of course necessary to develop sources and detectors for the millimeter and far infrared regions. The gas laser and the solid state mixing and parametric oscillator and amplifier are the most likely devices to possess sufficient power and stability. A necessary concomitant must be the development of oversize waveguide and power coupling methods.

It will not be necessary to investigate every spectral line of every gas; it is sufficient to verify a developing theory to the point where confidence in calculations may enable the system designer to obtain enough data to produce a device which can perform its mission.

This confidence will be completed when the necessary field tests to verify the theoretical and laboratory predictions have been performed.

Of the required information for system design probably only the knowledge of water and oxygen in the range 100 to 1000 GHz is sufficient at this time.

REFERENCES

1. Martin Company OR 6607, "Propagation of Millimeter and Submillimeter Waves (Final Report)," Contract NASw-963, Martin Marietta Corporation, Orlando, Florida, NASA-ERC, July 1965

2. Van Vleck, J. H. and Weisskopf, V. F., Rev Mod Phys, 17, 227 (1945)

3. Zhevakin, S. A. and Naumov, A. P., "Microwave Spectroscopy," McGraw-Hill, N. Y., 1955

4. Benedict, W. S. and Kaplan, L. D., Journ Chem Phys, 30, 388 (1959)

5. Gebbie, H. A., Phys Rev, 107, 1194 (1957)

6. Heitler, W., "Quantum Theory of Radiation," Oxford Press, Third Ed, London, 1960

7. Townes, C. H. and Schawlow, A. L., "Microwave Spectroscopy," McGraw-Hill, N. Y., 1955

8. Pauling, L. and Wilson, E. B., "Introduction to Quantum Mechanics," McGraw-Hill Book Co., N. Y. 1935

9. Uhlenbeck, G. E. and Wang Chang, C. S., "Symp on Transport Processes in Statistical Mechanics," Brussels, August 1956, Interscience Publishers, 1958

10. Bleaney, B. and Penrose, R. P., The Inversion Spectrum of Ammonia at Centrimetric Wavelengths, Proc Roy Soc, Vol A189, p 358, 1947

11. Weidner, R. T., Microwave Spectrum of Iodine Monochloride at 4.5 Centimeters Wavelength, Phys Rev Vol 72, p 1268, 1947

12. Gordy, W., Microwave Spectroscopy, Rev Mod Phys Vol 20, No. 4, October 1948

13. Culshaw, W., "High Resolution Millimeter Wave Fabry-Perot Interferometer," IRE Trans on Microwave Theory and Techniques, Vol MTT-8, No 2, pp 182-189, March 1960

14. Culshaw, W., "Resonators for Millimeter and Submillimeter Wavelengths," IRE Trans on Microwave Theory and Techniques, Vol MTT-9, No. 2, pp 135-144, March 1961

15. Culshaw, W., "Further Considerations on Fabry-Perot Type Resonators," IRE Trans on Microwave Theory and Techniques, Vol MTT-10, No. 5, pp 331-339, Sept 1962

16. Zimmerer, R. W., "Spherical Mirror Fabry-Perot Resonators," IRE Trans on Microwave Theory and Techniques, Vol MTT-11, No. 5, pp 371-379, September 1963

17. Lichtenstein, M., Gallagher, J. J. and Cupp, R. E., "Millimeter Spectrometer Using a Fabry-Perot Interferometer," Rev Sci Instr Vol 34, No. 8, August 1963

18. Fox, A. G. and Li, T., "Resonant Modes in a Maser Interferometer," Bell Sys Tech J., March 1961

19. Boyd, G. D. and Gordon, J. P., "Confocal Multimode Resonator for Millimeter Through Optical Wavelength Masers," Bell Sys Tech J., March 1961

20. Boyd, G. D. and Kogelnik, H., "Generalized Confocal Resonator Theory," Bell Sys Tech J., July 1962

21. Jenkins, F. A. and White, H. E., "Fundamentals of Optics," McGraw-Hill, N. Y., p 258

22. Renk, K. F. and Genzel, L., "Interference Filters and Fabry-Perot Interferometers for the Far Infrared," J. Appl Opt, Vol 1, p 643, September 1962

23. Miller, S. L. and Townes, C. H., Phys Rev, 90, 537 (1953)

24. Mizushima, M. and Hill, R. M., Phys Rev, 93, 745 (1954)

25. Mizushima, M., "Final Report on Microwave Spectrum of the O_2 Molecule," U.S. Army Signal Res and Dev Lab, Fort Monmouth, N. J. Contract No. DA-30-039-SC-78137, 31 July 1960

26. Burkhalter, J. H., Anderson, R S., Smith, W. V., and Gordy, W., Phys Rev Ltrs to Ed, 23 November 1949

27. Birnbaum, G. and Chattergee, S. K., Journ Appl Phys, 23, 220 (1952)

28. Golden, S., Wentink, T., Hillger, R., and Strandbert, M. W. P., Phys Rev, 73, 92 (1948)

29. Lichtenstein, M., Derr, V. E., and Gallagher, J. J., Jour Mol Spectroscopy, August 1966, "Millimeter Wave Rotational Transitions and the Stark Effect of the Water Molecule."

30. Randall, H. M., Dennison, D. M., Ginsburg, N., and Weber, L. R., Phys Rev, 52, 160 (1937)

31. King, W., Hainer, R. M., and Cross, P. C., Phys Rev, 71, 433 (1947)

32. Benedict, W. S., Claassen, H. H., and Shaw, J. H., "Absorption Spectrum of Water Vapor Between 4.5 and 13 Microns," Journ Res NRS, 49, 91 (1952)

33. West, B. and Mizushima, M., "Table of Rotational Transition Strengths for Asymmetric Rotations," Supp A, Quar Prog Rpt No. 2, U.S. Army Signal Supply Agency, University of Colorado, Boulder, Colorado, Contract No. DA-36-039-SC-87277, 11 September 1962

34. Frenkel, L., Journ Chem Phys, 45, 416 (1966)

35. Birnbaum, G., Journ Chem Phys, 27, 360 (1957)

36. Frenkel, L. and Woods, D., Journ Chem Phys, 44, 2219 (1966)

37. Maryott, A. A. and Birnbaum, G., Journ Chem Phys

38. Gebbie, H. A. and Stone, W. B., Proc Phys Soc, (London) 82, 543 (1963)

39. Becker, G. E. and Autler, S. H., Phys Rev, 70, 300 (1945)

40. Van Vleck, J. H., Phys Rev, 71, 413 (1947)

41. Van Vleck, J. H., Phys Rev, 71, 425 (1947)

42. Knapp, P. H. and Martin, D. H., Proc IEEE 54, 528 (1966)

43. King, G. W., Hanier, R. M., and Cross, P. C., "The Assymmetric Rotor. I. Calculation and Symmetry Classification of Energy Levels," J. Chem Phys 11, 27 (1943)

44. Wilson, E. B., Jr., and Howard, J. B., "The Vibration-Rotation Energy Levels of Polyatomic Molecules," Journ Chem Phys 4, 260 (1936)

45. Kivelson, D. and Wilson, E. B., Jr., "Approximate Treatment of the Effect of Centrifugal Distortion on the Rotational Energy Levels of Assymmetric-Rotor Molecules," Journ Chem Phys 20, 1575 (1952)

46. Yates, H. W., and Taylor, J. H., "Infrared Transmission of the Atmosphere," U.S. Naval Research Laboratory, Washington, D.C., NRL Report 5453, 8 June 1960

47. Marshall, J. Weber, Phys Rev, 105, 1502 (1957)

APPENDIX A

SUMMARY OF DATA FROM PREVIOUS REPORT (CONTRACT NASw-963)

The present program is the continuation of a previous one year contract. In order to make this final report self-contained the most important data from the previous report "Propagation of Millimeter and Submillimeter Waves" Contract NASw-963, Martin Marietta Corporation, OR 6607, July 1965, are summarized in this appendix.

The data often graphs tan δ instead of $\alpha = \frac{2\pi}{\lambda} \tan \delta$. p_1 = partial pressure of H_2O and p_2 is the partial pressure of the foreign gas.

Figures 28 and 29 show some data taken for the determination of k_{11}^{w} and k_{11}^{o}, respectively. Using Equation (17b, Reference 1) at various frequencies, k_{11}^{o} was found to be 22 MHz/mm and k_{11}^{w} about 200 MHz/mm. Other data taken supported this large value but the precision of the measurement of k_{11}^{w} is subject to a number of systematic errors which are hard to detect.

Figure 30 gives a plot of tan δ for fixed values of p_1 and p_2 as a function of frequency. Using Equation (16, Reference 1), k_{12}^{w} could be determined to be 18 MHz/mm.

Two groups of data were taken for the determination of k_{12}^{o} with N_2 in order to detect any deviations from the assumed shape factor. One group of measurements was made at fixed frequencies approximately 100 to 200 MHz from the center of the line at 183.31 GHz using values of p_1 of 1 to 2 mm and up to 300 mm of the foreign gas. In these data tan δ_{max} was used to determine the exact pressure of H_2O by means of Equation (18a, Reference 1) since this way of determining small pressures was found preferable to the Dubrovin gauge. Using the attenuation by pure H_2O measured as the first point of each set of measurements in this group, k_{11}^{o} was carefully determined as well as k_{12}^{o} which is independent of p_1. Figure 31 shows typical curves of tan δ versus the $\log_{10}$ of p_0'.

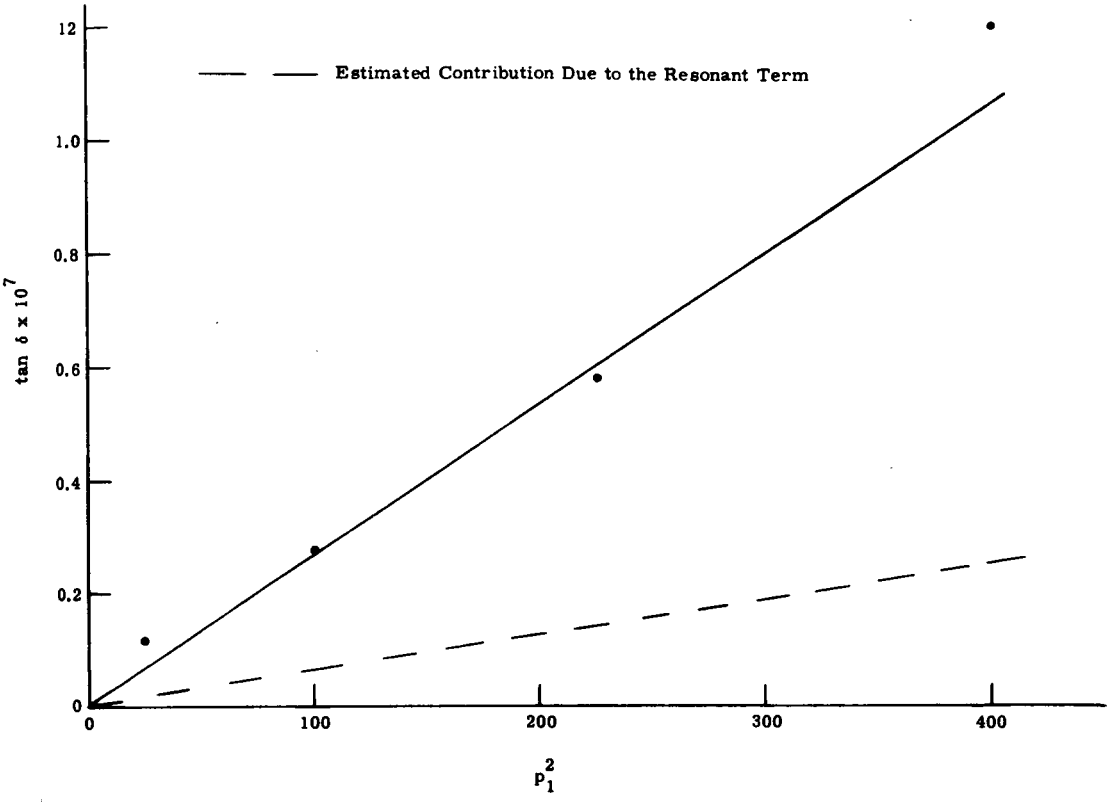

Figure 28. Tan δ versus p_1^2, ν = 169.794 MHz

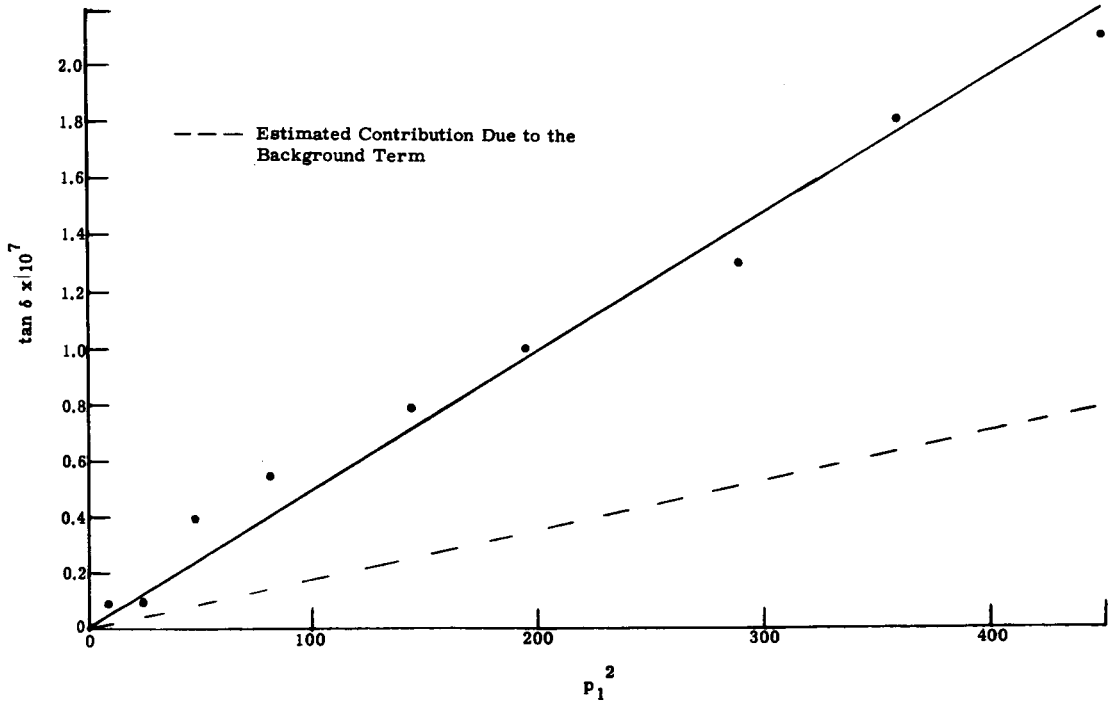

Figure 29. Tan δ versus p_1^2, ν = 190.000 GHz

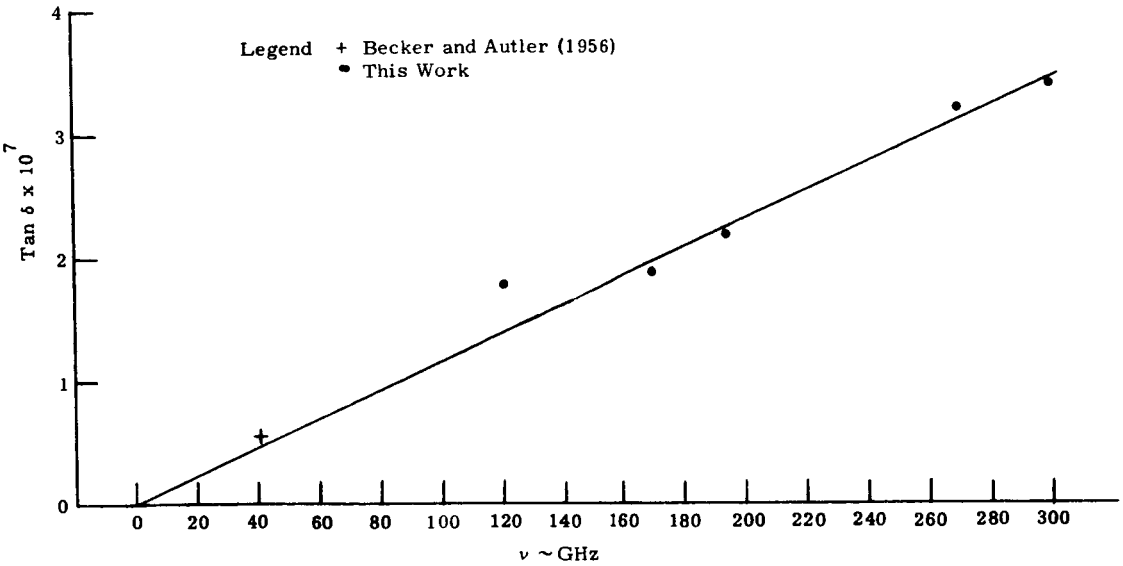

Figure 30. Tan δ' versus ν, p_1 = 15 mm, p_2 = 800 mm N_2

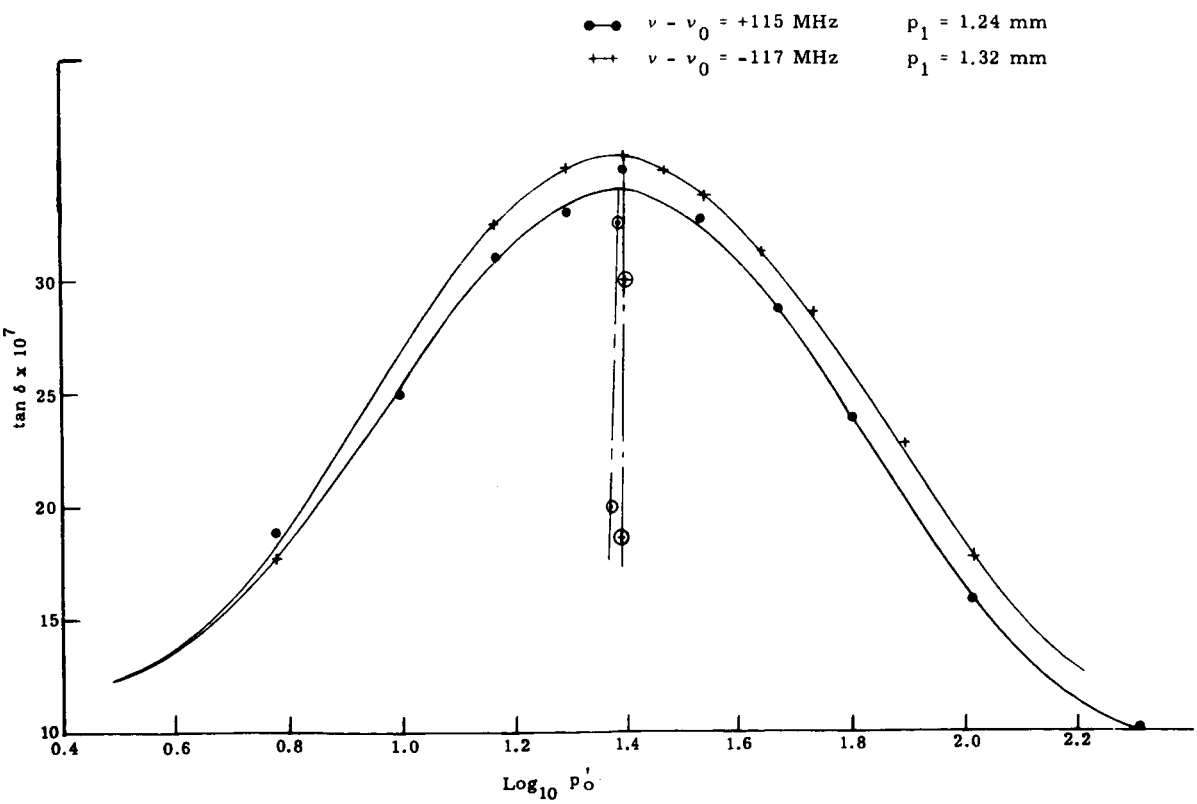

Figure 31. Tan δ versus Log p' for N_2, T = 300°K

The second group of measurements was made at frequencies between 1 and 3 GHz from line center and here corrections for the background were necessary. On the other hand, the partial pressures of H_2O used in this region (15 mm) could be determined accurately and the line strength could be compared to theory. Figure 32 shows a set of data together with the background corrections.

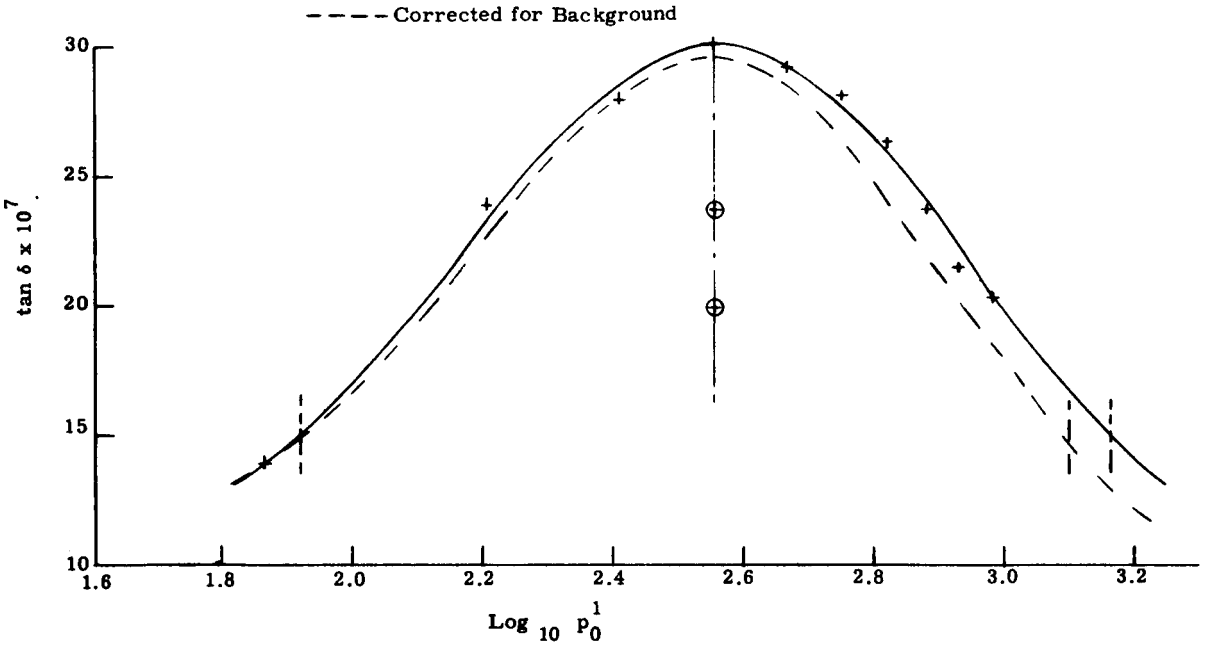

Figure 32. Tan δ versus Log p' for N_2, $\nu - \nu_0$ = 1.5 GHz, T = 300°K, p_1 = 15 mm

Tables VIIa and VIIb give summaries of results in these two groups:

TABLE VIIa

Results for Group 1 Measurements
(100 to 200 MHz from the Line Center at 183.31 GHz)

$\nu_{GH_z}-\nu_{01}$	p_1 (mm/Hg)	k^o_{12} MHz/mm	k^o_{11} MHz/mm	k^o_{11}/k^o_{12} MHz/mm	tan δ_{max} Percent	$\Delta\frac{1}{2}$ log (p'_0)*
+0.310	2	4.7	21	4.5		1.23
+0.180	1	4.8	30	6.2		1.17
+0.110	½	(4.3)	24	(5.6)		1.20
+0.110	1	(4.6)	25	(5.0)		1.20
+0.115	1	4.6	24	5.2		1.21
+0.115	1	(4.7)	25	(5.3)		1.18
-0.210	1	4.7	24	5.1		1.15
-0.170	2	4.7	19	4.0		1.00
-0.182	2	(4.3)	28	(6.5)		1.30
-0.117	1	4.7	22	4.7		1.25
<		4.7	24	5.0		>

TABLE VIIb

Results for Group 2 Measurements
(1 to 3 GHz from the Line Center at 183.31 GHz)

-2.7	10	4.0	21.0	5.2	97	1.14
-2.7	16	4.1	24.5	6.0	91	1.00
+2.3	10	(4.3)	(17)	(4.0)	98	1.04
+2.3	15	4.3	24	5.6	98	1.00
+3.0	18	4.3	19	4.4	119	0.9
+1.5	14	3.9	21.7	5.6	100	1.02
<		4.1	22.0	5.4	100	1.02 >

* This column gives the 1/2 amplitude width of the tan δ versus $\log_{10}p$ curves in units of $\log_{10}p$.

The sixth column gives the value of tan δ_{max} in terms of a percent value compared to theory. In Table VIIa this column is left blank since 100 percent agreement was assumed. The values in parentheses were adjusted on the basis of the corrections that had to be applied to p_1 and are not counted in the averages in the bottom rows.

It is not possible to ascribe the difference between k^o_{12} as measured in group 1 and group 2 experiments definitely to the lineshape since an experimental error of ±5 percent cannot be excluded. For the present these values will be averaged in the overall results in Table VIII.

TABLE VIII

Linewidth Parameters in MHz/mm

	H_2O	N_2	CO_2	O_2
k^o_{11}	22 ± 2	-	-	-
k^w_{11}	200 ± 40	-	-	-
k^o_{12}	-	4.4 ± 0.2	6 ± 0.3	2.7 ± 0.2
k^w_{12}	-	19 ± 2	65 ± 7.0	-

Figure 33 gives the absorption calculated by Equation (1b, Reference 1) using these values over the range from 10 to 300 GHz. Figure 34 gives absorption coefficient α for various gases.

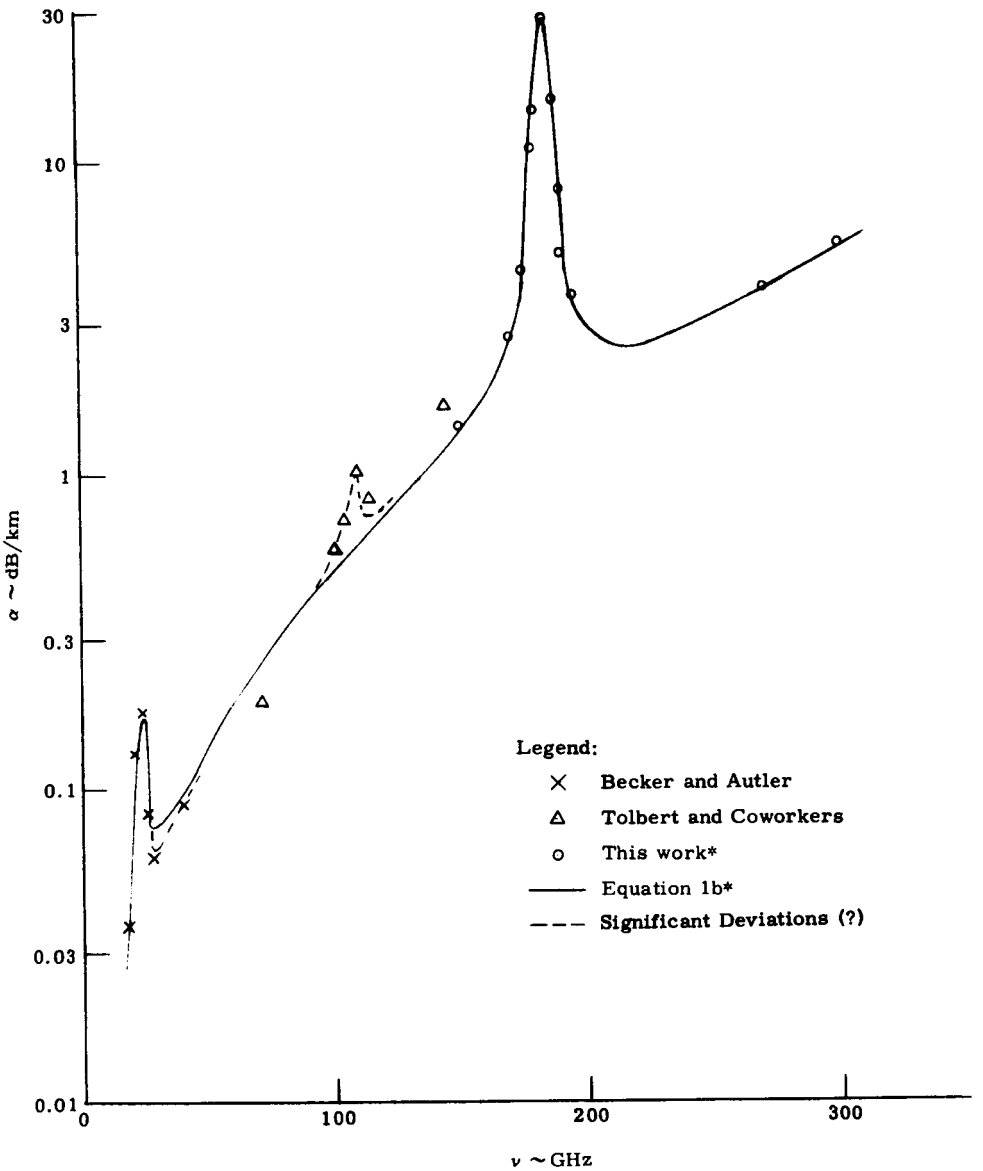

Figure 33. Absorption Coefficient α Due to 7.5 mm of H_2O in 750 mm of N_2 versus Frequency ν

* See Reference 1.

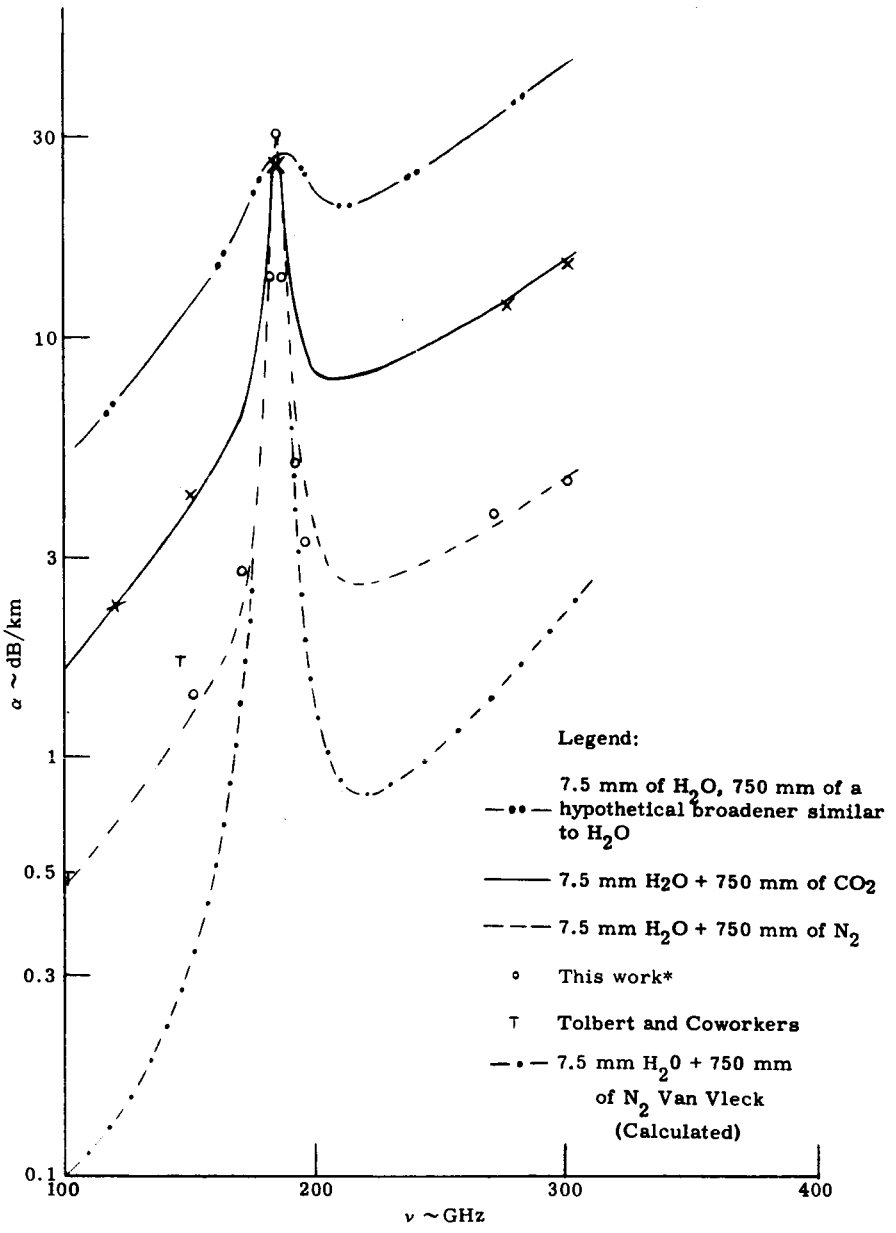

Figure 34. Absorption Coefficient α for Various Gas Systems, p_1 = 15 mm, p_2 = 750 mm

The coefficients k are the multipliers of pressure to obtain the broadening $\Delta\nu$: $\Delta\nu = kp$. The subscripts indicate either self-broadening k_{11} or foreign gas broadening k_{12}. $k_{12}{}^{W}$ is the broadening, caused by foreign gases, in the residual broadening term or background term.

* See Reference 1.

There have been indications in the literature that anomalies observed in the atmospheric absorption between 110 to 140 GHz may be due to an interaction of H_2O on O_2 near the oxygen absorption line at 118.75 GHz. At present, the capabilities of the resonant cavity do not permit measurements in the wing region of this line but an anomalously large effect in the wings should also result in an excessive broadening near the line center where the sensitivity of the cavity is adequate.

In these experiments another technique was found expedient which permitted the evaluation of the effect of H_2O on O_2 in terms of that of N_2 and of the self-broadening of O_2.

The cavity was tuned to 118.760 GHz and the attenuator adjusted for a full response on the oscilloscope screen. Ten millimeters of O_2 were then admitted into the cavity and the amplitudes of the attenuator were read. Ten millimeters of H_2O, N_2, or O_2 were then added and the amplitudes were again read. Using Equation (18, Reference 1) at $(\nu - \nu_0) \approx 0$ gives

$$\tan\delta = p_1 C_{01}^{t} \frac{\nu_0}{p_0' k_{12}^{o}}$$

where the subscript 1 refers to O_2

For pure O_2, $k_{12}^{o} = k_{11}^{o}$ and $p_0' = p_1$ so that,

$$\tan\delta = C_{01}^{t} \frac{\nu_0}{k_{11}^{o}}$$

This is independent of pressure so that the amplitude does not change. This step was used to check on the instrument's performance in this series of tests. For N_2, it has been shown that $k_{11}^{o} \approx k_{12}^{o}$ so that from Equation (12a, Reference 1)

$$p_0' \approx p_1 + p_2$$

and therefore, on adding 10 mm of N_2 to 10 mm of O_2

$$\tan\delta = C_{01}^{t} \frac{\nu_0}{2 k_{11}^{o}}$$

so that the loss now is cut in half. This, too, was used as a check.

When 10 mm of H_2O were added to 10 mm of O_2, the amplitude dropped by the same amount, indicating that the cross section for H_2O collisions with O_2 is not significantly larger than that for the other two gases.

As pointed out in Chapter III, section C (Reference 1), the O_2 molecule has no electric dipole and its spectrum in the millimeter region consists primarily of transitions in which the electronic spin alignment with respect to the total orbital angular momentum changes by one unit. These transitions lie in a band about 60 GHz except for one line at 118.75 GHz and have been extensively studied.

Because of the perturbation of the wave functions of O_2 by the electron spin, the orbital angular momentum N of the molecule is not a good quantum number and $\Delta N = 2$ transitions between the levels usually denoted by N+, o, - are possible. Mizushima has predicted three such transitions (Table IX).

TABLE IX

Rotational Transitions Predicted in O_2

Transition	Frequency in MHz	Relative Strength
$1_0 \rightarrow 3_-$	368,447	0.55
$1_+ \rightarrow 3_-$	424,613	9.12
$1_+ \rightarrow 3_0$	487,199	7.94

The intensity of the strongest one of these lines ($1_+ \rightarrow 3_-$) is given by him as roughly 10 times the intensity of the ($1_+ \rightarrow 1_0$) line in the magnetic spectrum. This would still make it a relatively weak line* and in view of the small amount of power available at that frequency, special efforts must be made in the search for it. For one thing it is advantageous to cool the cell; secondly, since the O_2 molecule is magnetic, Zeeman modulation and synchronous detection may be employed. The search for this line was, therefore, made in an existing absorption cell which had provisions for cooling and Zeeman modulation. A number of problems developed partic-

* The absorption at the peak of these lines would be comparable to the losses in the gaps between the H_2O absorption lines.

ularly in connection with cooling, such as condensation on the windows and an inconveniently high consumption of coolant. These difficulties made the use of this particular cell very tedious. In addition, calculations showed that the predicted strength of the line would make a longer cell desirable.

Since the effort on O_2 competed for men and materials with more important and promising investigations on H_2O, it was decided to postpone this phase of the work until a new cell could be made available.

The NO_2 molecule is an asymmetric top with one unpaired electron. The unpaired electron spin interacts with the nuclear spin on (N^{14}) to give a hyperfine structure. NO_2 is found in the upper atmosphere and is, therefore, of some interest. A number of lines not previously reported in the literature were found but no final assignments have been made. This work is progressing as a continuing effort and will require further experimental and theoretical study. To date the following series of lines have been cross checked from two different fundamental frequencies (Table X).

TABLE X

Transition Tentatively Assigned to NO_2

235,055.5 MHz	215,269.8 MHz
235,030.6 MHz	215,262.9 MHz
235,077.6 MHz	215,255.5 MHz
235,510.2 MHz	215,246.6 MHz
	215,243.3 MHz
	215,236.4 MHz
	215,075.7 MHz

APPENDIX B

PUBLICATIONS ARISING FROM THE PROGRAM

This list includes talks and articles published by personnel working on the contract or on which work was performed during either of the two contract periods.

1. Valkenburg, E. P. and Derr, V. E., "A High-Q Fabry-Perot Interferometer for Water Vapor Measurements in the 100 Gc/s to 300 Gc/s Frequency Range," Proc IEEE, 54, 493 (1966). Also presented at Boulder Mm Wave Conf (Sept 1965)

2. Frenkel, L. and Woods, D., "The Microwave Absorption by H_2O Vapor and its Mixtures with Other Gases Between 100 and 300 Gc/s," Proceedings IEEE 54, 498 (1966). Also presented at Boulder Mm Wave Conf (Sept 1965)

3. Frenkel, L., "Orientation Relaxation in Symmetrical-Top Gases and Binary Gas Mixtures," Jour Chem Phys, 45, 416 (1966)

4. Frenkel, L., Kryder, S. J. and Maryott, A. A., "Debye Relaxation in Symmetric-Top-Foreign-Gas Mixtures; Temperature Dependence of Collision Cross Sections," Journ Chem Phys 44, 2610 (1966). (Based on thesis of L. Frenkel, Univ of Maryland 1964)

5. Frenkel, L. and Woods, D., "Microwave Absorption in Compressed CO_2." Jour Chem Phys 44, 2219 (1966)

6. Woods, D. and Strauch, R., "Submillimeter Wave Harmonic Mixers," Proc IEEE, April 1966

7. Frenkel, L., Gallagher, J. J., and Smith, W. T., "Dipole Moment of $FClO_3$, Jour Chem Phys 45, 2251 (1966)

8. Frenkel, L., "Precision Absolute Measurements in the Millimeter Region," Talk, Society for Applied Spectroscopy, Chicago, 16 June 1966

9. Frenkel, L., "Bulletin American Physical Society for Mexico City Meeting," Orientation Relaxation, Abstract, 1966

10. Frenkel, L., "Symmetric Top Molecules in Collision Broadening," Talk, American Physical Society Meeting, Washington, D. C., March 1966

11. Lichtenstein, M., Derr, V. E., and Gallagher, J. J., "Millimeter Wave Rotational Transitions and the Stark Effect of the Water Molecule," Jour Mol Spectroscopy, August 1966

APPENDIX C

UTILIZATION REPORT FOR TRANSITION CALCULATIONS (Problem No. ZØ127)

ORIGIN OF PROBLEM

The need to calculate the rotation energies of asymmetric molecules measured by microwave spectroscopy.

PROGRAM DESCRIPTION

For a molecule selected the program computes the rigid rotor energy and the semi-rigid rotor energy and their respective transitions in megahertz. Given constants a, b and c for some molecule and the six coefficients of the Kivelson-Wilson equation, the program computes the proper transitions based on the maximum J value and selection rules input. Given a, b and c and laboratory observed transitions, the program will compute the six Kivelson-Wilson coefficients and fit these coefficients to the transitions input.

If only transitions are available as data, the program will compute a, b, c and the six Kivelson-Wilson coefficients and fit these values to the transitions input. It is possible to load in the data in two blocks such that the first block is very accurate. From this accurate data the a, b, c and six Kivelson-Wilson coefficients can be obtained. Then these accurate values can operate on the second less accurate blocks of data to compute transitions. This option is available with or without starting values for a, b, c.

RESTRICTIONS AND SPECIAL CONSIDERATIONS

In the least squares portion of the program there are three error messages. One of these indicates a singular matrix was encountered in the fitting process. The second error message indicates that in ten passes the fitting process did not converge. The third error message indicates a, b, c were not determined correctly. The message most likely to be encountered is that the system did not converge after ten passes. If this happen the data is possibly at fault. If the data proves to be correct then the incre-

ments used to take the derivatives in the "LEAST" subroutine may be too small. These increments can be changed by changing the factor on cards corresponding to internal statement numbers 103 and 145 of the listing for "LEAST". The factor chosen was determined by trial and error and inspection of the computation arrays. If the increments are made cruder there is a higher probability of convergence, however the results will be cruder, and it is doubted if they will be of use. It has been noted that even if part of the input is accurate it is possible the resulting a, b, c will provide useful transition calculations. The "lighter" molecules seem to give the most problems in this area (H_2O, HDS). If more accurate results are necessary for heavier molecules then it is recommended that the afore mentioned increments be reduced to three ten thousandths of a percent. The problem is optimizing the size of the derivative taking increment such that the system will just converge.

The external sort has an upper limit of three thousand energy levels. If more than 3000 energy levels are to be sorted, they are sorted into groups of 3000.

The selection rules will not permit a J value greater than 12.

TIMING

Program execution time is a function of the number of energy levels requested and input versus calculated coefficients. The program should not run more than ten minutes unless an unusually large amount of data is input. Most of the runs will take about 5 minutes. A ten minute time card is recommended with all runs.

DESCRIPTION OF OUTPUT

All of the output is identification labeled and it includes the six a input coefficients, the inertial constants a, b and c along the principal axes, the rigid rotor energy for each level, the rigid rotor transition energy, the transitions with the distortion factors added and the input transitions.

The energy levels are written on a scratch data file and reprinted after a second pass sort.

DESCRIPTION OF INPUT

Numerical input data must be divided into two forms: the real number data and integer data. Real number data must contain a decimal point and it may be placed anywhere in its input field. Integer data contains no decimal point and it must be right adjusted in its input field.

There are several options available in the program which are selected via input cards. Card A of the input deck is a title card. Card B of the input deck is the option card. The four options are listed below:

OPTION 1: Read in a, b, c, a1, . . . , a6, maximum J value and symmetry indicators. The correct energy levels are computed and the transitions between them are computed.

OPTION 2: Read in a, b, c, a1, . . . , a6, J, Tau, J, Tau and Nu. The rigid rotor and semi-rigid rotor transitions are computed.

OPTION 3: Read in a, b, c, J, Tau, J, Tau and Nu. This option assumes an accurate a, b, c, a1, . . . , a6 are computed by least squares, then the rigid rotor and the semi-rigid rotor transitions are computed.

OPTION 4: Read in J, Tau, J, Tau and Nu. a, b, c are determined from a sub-routine, and the program proceeds the same as option three.

FLOW OF PROGRAM UNDER EACH OPTION

IN = 1

Z$\emptyset$127 → SELECT → CALTRN → CALCON → REDUCE → SUBRED → TRIX

IN = 2

Z$\emptyset$127 → CALTRN → CALCON → REDUCE → SUBRED → TRIX

IN = 3

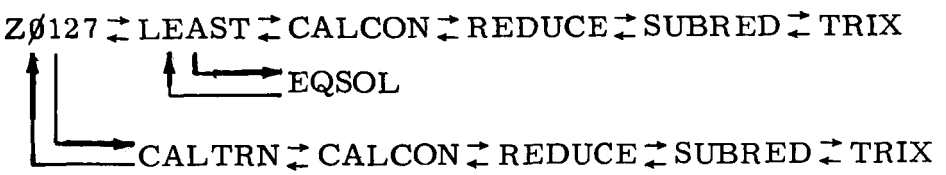

IN = 4

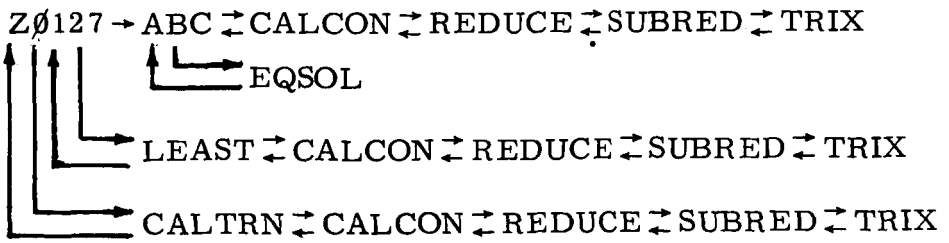

DESCRIPTION OF EACH ROUTINE

ZØ127: This is the control program. It senses the option selected and channels the input of data to the correct subroutines. It terminates the computation when control is returned to it by the subroutines.

SELECT: Up to a maximum J value of 12, "SELECT" computes the correct $J(K_{-1}, K_1)$ for the types of symmetry input.

LEAST: Chooses the best set of a1, . . . , a6 based on a, b, c input or a, b, c computed by "ABC". It modifies a, b, c and fits the a1, . . . , a6 to the data again and repeats this a maximum of ten times. When convergence is obtained the data calculated is printed.

ABC: If a, b, c are not input, this routine calculates these variables based on data input.

EQSOL: This is a double precision equation solving routine. It solves n x n + 1 systems of equations and returns an error indication if the coefficient matrix is singular.

CALTRN: This routine calculates rigid rotor transitions and semi-rigid rotor transitions.

CALCON: Calculates the terms which multiply a1, . . . , a6 in the Kivelson-Wilson equation.

REDUCE: Forms and solves the reduced energy matrix for the current approximations of a, b, c and the transitions input. It forms the terms of the continued fractions used to calculate the PZ2 and PZ4 terms of the Kivelson-Wilson equation.

SUBRED: Solves one term of a tri-diagonal reduced energy matrix specified by "REDUCE".

TRIX: Calculates a single term of the continued fraction sequence formed by "REDUCE".

DESCRIPTION OF INPUT VALUES

These inputs are real numbers and their units are described below:

a, b, c are in megahertz

a1 is in reciprocal megahertz

a2 is unitless

a3, . . . , a5 are in megahertz

a6 is unitless

Nu is in megahertz

Conversion factor:

1 wave number = 29977.6 megahertz

The other inputs are described in the next section.

The following is a detailed description of the input deck under all options.

Cards A and B of the input deck have the same format for all options.

Card	Columns	Variable Name	Program Variable Name	Description
A	1 - 72		TIT(I)	Appropriate title
B	1 - 5		IN(1)	IN(1) and LP are integers and must be right adjusted in their fields. IN(1) is option signal and is 1,2,3, or 4.
	6 - 70	Blanks		
	71 - 72		LP	If convergence is not obtained after 10 iteractions under option 3 or 4, a 1 placed in column 71 and a 3 placed in column 72 will cause the arrays computed by "LEAST" to be printed out after each iteration. By examining these array values, it can be determined whether convergence is likely with the data being used.

A	1	Data for XXXX Molecule Option X Apr 15, 1999 72
B	5 2	6 71 72 1 3

IN = 1

Card	Columns	Variable Name	Program Variable Name	Description
C	1 - 10	a	A(7)	Inertial constants a, b, c are real number inputs. They must have a decimal point. The numbers may be punched anywhere in their fields.
	11 - 20	b	A(8)	
	21 - 30	c	A(9)	
	31 - 72	Blanks		
D	1 - 10	a1	A(1)	a1, . . . , a6 are the six coefficients in the Kivelson-Wilson equation. They are real numbers and must have decimal point. The numbers may be punched anywhere in their field. They are 0.0 if only the rigid rotor energy is desired.
	11 - 20	a2	A(2)	
	21 - 30	a3	A(3)	
	31 - 40	a4	A(4)	
	41 - 50	a5	A(5)	
	51 - 60	a6	A(6)	
	61 - 72	Blanks		
E	1 - 5	J	IEXTRA (12)	These four variables are integers and must be right adjusted in their five col field if IEXTRA(13) = 1, A type symmetry, if 0, no A type symmetry. If IEXTRA(14) = 1, B type symmetry, if 0, no B type symmetry. If IEXTRA (15) = 1, C type symmetry, if 0, no C type symmetry.
	6 - 10		IEXTRA (13)	
	11 - 15		IEXTRA (14)	
	16 - 20		IEXTRA (15)	
	21 - 72	Blanks		

Examples:

	1 - 10	11 - 20	21 - 30	31 - 72
C	123000.0	.124E06	125000.0	

	1 - 10	11 - 20	21 - 30	31 - 40	41 - 50	51 - 60	61 - 72
D	12300.0	12.4	.125E-5	.126E02	12700.	1280.	

	1 - 5	6 - 10	11 - 15	16 - 20	21 - 72
E	8	1	0	1	

IN = 2

Card	Columns	Variable Name	Program Variable Name	Description
	1 - 10	a	A(7)	Inertial constants a, b, c are real number inputs. They must have a decimal point. The numbers may be punched anywhere in their fields.
	11 - 20	b	A(8)	
	21 - 30	c	A(9)	
C	31 - 72	Blanks		
	1 - 10	a1	A(1)	a1, . . . , a6 are the six coefficients in the Kivelson-Wilson equation. They are real numbers and must have a decimal point. The numbers may be punched anywhere in its field.
	11 - 20	a2	A(2)	
	21 - 30	a3	A(3)	
	31 - 40	a4	A(4)	
	41 - 50	a5	A(5)	
	51 - 60	a6	A(6)	
D	61 - 72	Blanks		
	1 - 10	Blanks		J and Tau are integers and must be right adjusted in their fields. Nu is a real number and must have a decimal point. Nu may be punched anywhere in its field.
	11 - 20	J	XJA(1,1)	
	21 - 30	Tau	TAUA(1,1)	
	31 - 40	J	XJA(1,2)	
	41 - 50	Tau	TAUA(1,2)	
	51 - 60	Nu	XNU(1)	
E	61 - 72	Blanks		
	1 - 5		LL	LL is the integer 11111 and signals the end of data.
F	6 - 72	Blanks		

Examples:

	1 10	11 20	21 30	31 72
C	.123E06	12400.0	125000.0	

	1 10	11 20	21 30	31 40	41 50	51 60	61 72
D	.1234	.124E-3	.125	126.0	12.7	1.28	

	1 10	11 20	21 30	31 40	41 50	51 60	61 72
E		7	3	6	-5		

	1 5	6 72
F	11111	

IN = 3

Card	Columns	Variable Name	Program Variable Name	Description
C	1 - 10	a	A(7)	Inertial constants a, b, c are real number inputs. They must have a decimal point. The numbers may be punched anywhere in their fields.
	11 - 20	b	A(8)	
	21 - 30	c	A(9)	
	31 - 72	Blanks		
D	1 - 10	Blanks		J and Tau are integers and must be right adjusted in their fields. Nu is a real number and must have a decimal point. Nu may be punched anywhere in its field.
	11 - 20	J	XJA(I,1)	
	21 - 30	Tau	TAUA(I,1)	
	31 - 40	J	XJA(I,2)	
	41 - 50	Tau	TAUA(I,2)	
	51 - 60	Nu	XNU(I)	
	61 - 72	Blanks		
E	1 - 5		LL	LL is the integer 11111 and signals the end of the first block of data.
	6 - 72	Blanks		
F	1 - 10	Blanks		J and Tau are integers and must be right adjusted in their fields. Nu is a real number and must have a decimal point. Nu may be punched anywhere in its field. This data is to be used to compute transitions based on the constants found using the input just prior on D cards. The D card input is assumed as accurate as possible.
	11 - 20	J	XJA(1,1)	
	21 - 30	Tau	TAUA(1,1)	
	31 - 40	J	XJA(1,2)	
	41 - 50	Tau	TAUA(1,2)	
	51 - 60	Nu	XNU(1)	
	61 - 72	Blanks		
G	1 - 5		LL	LL is the integer 11111 and signals the end of the second block of data, and must present even if no F cards are input.
	6 - 72	Blanks		

Note: D, E and G cards are always present when using option 3. F cards may or may not be present.

Examples:

	1 10	11 20	21 30	31 72
C	12300.0	.124E06	125000.0	

	1 10	11 20	21 30	31 40	41 50	51 60	61 72
D		7	5	6	-3	99900.00	

	1 5	6 72
E	11111	

	1 10	11 20	21 30	31 40	41 50	51 60	61 72
F		2	-2	1	1	999900.0	

	1 5	6 72
G	11111	

IN = 4

Card	Columns	Variable Name	Program Variable Name	Description
C	1 - 10	Blanks		J and Tau are integers and must be right adjusted in their fields. Nu is a real number and must have a decimal point. Nu may be punched anywhere in its field.
	11 - 20	J	XJA(I,1)	
	21 - 30	Tau	TAUA(I,1)	
	31 - 40	J	XJA(I,2)	
	41 - 50	Tau	TAUA(I,2)	
	51 - 60	Nu	XNU(I)	
	61 - 72	Blanks		
D	1 - 5		LL	LL is the integer 11111 and signals the end of the first block of data.
	6 - 72	Blanks		
E	1 - 10	Blanks		J and Tau are integers and must be right adjusted in their fields. Nu is a real number and must have a decimal point. Nu may be punched anywhere in its field. This data is to be used to compute transitions based on the constants found using the input just prior on C cards. The C card input is assumed as accurate as possible.
	11 - 20	J	XJA(1,1)	
	21 - 30	Tau	TAUA(1,1)	
	31 - 40	J	XJA(1,2)	
	41 - 50	Tau	TAUA(1,2)	
	51 - 60	Nu	XNU(1)	
	61 - 72	Blanks		
F	1 - 5		LL	LL is the integer 11111 and signals the end of the second block of data, and must be present even if no E cards are input.
	6 - 72	Blanks		

Note: C, D and F cards are always present when using option 4. E cards may or may not be present.

Examples:

C

1 10	11 20	21 30	31 40	41 50	51 60	61 72
	3	-2	2	1	444.E3	

D

1	72
11111 5 6	

E

1 10	11 20	21 30	31 40	41 50	51 60	61 72
	10	-5	10	-8	671000.0	

F

1 5	6	72
11111		

NASA-Langley, 1967 —— 7 CR-863